Universal Bounds on Efficiency and Power of Heat Engines with Broken Time-Reversal Symmetry

Von der Fakultät Mathematik und Physik der Universität Stuttgart
zur Erlangung der Würde eines Doktors der
Naturwissenschaften (Dr. rer. nat.) genehmigte Abhandlung

Vorgelegt von

Kay Brandner

aus Bad Schlema

Hauptberichter:	Prof. Dr. Udo Seifert
Erster Mitberichter:	Prof. Dr. Siegfried Dietrich
Zweiter Mitberichter:	Prof. Dr. Eric Lutz

Tag der Einreichung:	3. Juni 2015
Tag der mündlichen Prüfung:	21. Juli 2015

II. Institut für Theoretische Physik der Universität Stuttgart

2015

Contents

List of Figures

Important Symbols

Natural Constants

Symbol	Description
k_B	Boltzmann's constant
h, $\hbar$	Planck's constant
c	Speed of light

Irreversible Thermodynamics

Symbol	Description	Definition
T_c, T_h, T_α	Temperature of the cold reservoir, the hot reservoir, the reservoir α	–
μ_c, μ_h, μ_α	Chemical potential of the cold reservoir, the hot reservoir, the reservoir α	–
J_q, J_q^α	Heat current leaving the hot reservoir, the reservoir α	–
J_ρ, J_ρ^α	Particle current leaving the hot reservoir, the reservoir α	–
ΔT, ΔT_α	Gradient in temperature	$\Delta T \equiv T_\mathrm{h} - T_\mathrm{c}$, $\Delta T_\alpha \equiv T_\alpha - T_\mathrm{c}$
$\Delta\mu$, $\Delta\mu_\alpha$	Gradient in chemical potential	$\Delta\mu \equiv \mu_\mathrm{h} - \mu_\mathrm{c}$, $\Delta\mu_\alpha \equiv \mu_\alpha - \mu_\mathrm{c}$
$\mathcal{F}_q$, $\mathcal{F}_q^\alpha$	Entropic conjugate affinity to J_q, J_q^α	$\mathcal{F}_q \equiv 1/T_\mathrm{h} - 1/T_\mathrm{c} \overset{\mathrm{LR}}{=} \Delta T/T_\mathrm{c}^2$ [1], $\mathcal{F}_q^\alpha \equiv 1/T_\alpha - 1/T_\mathrm{c} \overset{\mathrm{LR}}{=} \Delta T_\alpha/T_\mathrm{c}^2$
$\mathcal{F}_\rho$, $\mathcal{F}_\rho^\alpha$	Entropic conjugate affinity to J_ρ, J_ρ^α	$\mathcal{F}_\rho \equiv \Delta\mu/T_\mathrm{c}$, $\mathcal{F}_\rho^\alpha \equiv \Delta\mu_\alpha/T_\mathrm{c}$
L_{ik}	Kinetic coefficients relating the affinity $\mathcal{F}_k$ to the current J_i	$L_{ik} \equiv \partial J_i/\partial\mathcal{F}_k\vert_{\mathcal{F}=0}$, $i,k = \rho, q$
$\dot{S}$	Total rate of entropy production	–

[1] The notation $\overset{\mathrm{LR}}{=}$ indicates equality in the linear response regime.

Multi-Terminal Model and Nernst Engine

Symbol	Description	Definition
$\mathbb{L}^n$	Matrix of primary kinetic coefficients for the n-terminal model	Eqs. (3.5), (3.2), (3.26)
$\mathbb{L}^n_{\alpha\beta}$	Subunits of $\mathbb{L}^n$	Eqs. (3.5), (3.21)
$\mathbb{L}$	Matrix of effective kinetic coefficients for the multi-terminal model	Eq. (3.10)
$\mathbb{M}^{\mathrm{NE4}}$	Extended matrix of primary kinetic coefficients for the Nernst engine	Eq. (3.117)
$\mathbb{L}^{\mathrm{NE4}}$	Matrix of primary kinetic coefficients for the Nernst engine	Eq. (3.118)
$\mathbb{L}^{\mathrm{NE}}$	Matrix of effective kinetic coefficients for the Nernst engine	Eq. (3.128)
L^{NE}_{ik}	Effective kinetic coefficients for the Nernst engine	$L^{\mathrm{NE}}_{ik} \equiv (\mathbb{L}^{\mathrm{NE}})_{ik}$
$S_{\alpha\beta}$	Scattering amplitude corresponding to the transition from lead β to lead α	–
$\mathbb{S}$	Scattering matrix	$(\mathbb{S})_{\alpha\beta} \equiv S_{\alpha\beta}$
$T_{\alpha\beta}$	Quantum transmission coefficient corresponding to the transition for the from lead β to lead α	$T_{\alpha\beta} \equiv \lvert S_{\alpha\beta}\rvert^2$
$\tilde{T}_{\alpha\beta}$	Classical transmission coefficient corresponding to the transition from reservoir β to reservoir α	Eq. (3.112)
$\mathbb{T}$	Quantum transmission matrix	$(\mathbb{T})_{\alpha\beta} \equiv T_{\alpha\beta}$
$\tilde{\mathbb{T}}$	Classical transmission matrix	$(\tilde{\mathbb{T}})_{\alpha\beta} \equiv \tilde{T}_{\alpha\beta}$
f	Rescaled derivative of the Fermi distribution	Eq. (3.22)
u	Modified Maxwell-Boltzmann distribution	Eq. (3.119)
N_{ik}	Normalization constants for kinetic coefficients	Eqs. (3.68), (4.52)

Cyclic Heat Engines

Symbol	Description	Definition
H	Time-dependent Hamiltonian	–
H_0, ΔH, g_w	Unperturbed Hamiltonian, strength of the time-dependent perturbation, driving protocol	$H \equiv H_0 + \Delta H g_w$
T, T_{h}, T_{c}	Time-dependent, maximal, minimal temperature	–
ΔT	Temporal gradient in temperature	$\Delta T \equiv T_{\mathrm{h}} - T_{\mathrm{c}}$
γ_q, g_q	Protocol for the time-dependent temperature	$T \equiv T_{\mathrm{c}} T_{\mathrm{h}} / (T_{\mathrm{h}} - \Delta T \gamma_q)$ $g_q \equiv -H_0 \gamma_q$
p^{c}	Periodic limit of the time-dependent phase-space distribution	–

J_w	Work flux	Eq. (4.12)
J_q	Heat flux	Eq. (4.13)
$\mathcal{F}_w$	Generalized affinity	$\mathcal{F}_w \equiv \Delta H/T_\mathrm{c}$
$\mathcal{F}_q$	Generalized affinity	$\mathcal{F}_q \equiv 1/T_\mathrm{h} - 1/T_\mathrm{c} \overset{\mathrm{LR}}{=} \Delta T/T_\mathrm{c}^2$
$L_{\alpha\beta}$	Generalized kinetic coefficients	$L_{\alpha\beta} \equiv \partial J_\alpha/\partial\mathcal{F}_\beta\vert_{\mathcal{F}=0}$, $\alpha,\beta = w,q$
$L_{\alpha\beta}^\mathrm{ad}$	Adiabatic generalized kinetic coefficients	Eq. (4.24)
p^eq	Equilibrium distribution	$p^\mathrm{eq} \equiv \exp\left(-H_0/(k_\mathrm{B}T_\mathrm{c})\right)/Z_0$
Z_0	Canonical partition function	$Z_0 \equiv \int d^n\mathbf{x}\, \exp\left(-H_0/(k_\mathrm{B}T_\mathrm{c})\right)$
L	Time-dependent Fokker-Planck operator	Eq. (4.30)
L_0	Unperturbed Fokker-Planck operator	Eq. (4.37)
L^H, L^T	Time-dependent perturbation of the Fokker-Planck operator	Eq. (4.37)
$\langle\bullet\rangle$	Ensemble average with respect to p^eq	Eq. (4.25)
$\langle\!\langle\bullet\rangle\!\rangle$	Combined ensemble and cycle average with respect to p^eq	Eq. (4.25)
$\langle\!\langle\bullet;\bullet\rangle\!\rangle$	Equilibrium correlation function	Eq. (4.40)
δA	Equilibrium fluctuation of the quantity A	$\delta A \equiv A - \langle A\rangle$
N_{qq}	Normalization constant for L_{qq}	$N_{qq} \equiv -\langle\!\langle \delta g_q \mathsf{L}^{0\dagger} \delta g_q\rangle\!\rangle/k_\mathrm{B}$

Performance Figures

Symbol	**Description**	**Definition**
ZT	Thermoelectric figure of merit	$ZT \equiv L_{\rho q}^2/(L_{\rho\rho}L_{qq} - L_{\rho q}^2)$
$\mathcal{Z}T$	Thermomagnetic figure of merit	$\mathcal{Z}T \equiv (L_{\rho q}^\mathrm{NE})^2/\left(L_{\rho\rho}^\mathrm{NE}L_{qq}^\mathrm{NE} - (L_{\rho q}^\mathrm{NE})^2\right)$
x	Asymmetry parameter	$x \equiv L_{\rho q}/L_{q\rho}$, $x \equiv L_{wq}/L_{qw}$
y	Generalized figure of merit	$y \equiv L_{\rho q}L_{q\rho}/(L_{\rho\rho}L_{qq} - L_{\rho q}L_{q\rho})$, $y \equiv L_{wq}L_{qw}/(L_{ww}L_{qq} - L_{wq}L_{qw})$
h	Universal bound on y following from the second law	$h(x) \equiv 4x/(x-1)^2$
h_n	Detailed bound on y in the n-terminal model	$h_n(x) \equiv 4x\cos^2(\pi/n)/(x-1)^2$
η	Thermodynamic efficiency	$\eta \equiv P/J_q$
η_max	Maximum efficiency with respect to $\mathcal{F}_\rho$, $\mathcal{F}_w$	–
η^*	Efficiency at maximum power with respect to $\mathcal{F}_\rho$, $\mathcal{F}_w$	–
η_C	Carnot efficiency	$\eta_\mathrm{C} \equiv 1 - T_\mathrm{c}/T_\mathrm{h} \overset{\mathrm{LR}}{=} \Delta T/T_\mathrm{c}$
η_CA	Curzon-Ahlborn efficiency	$\eta_\mathrm{CA} \equiv 1 - \sqrt{T_\mathrm{c}/T_\mathrm{h}} \overset{\mathrm{LR}}{=} \eta_\mathrm{C}/2$
$\bar{\eta}$	Normalized efficiency	$\bar{\eta} \equiv \eta/\eta_\mathrm{C}$
$\bar{\eta}_\mathrm{max}$	Normalized maximum efficiency	$\bar{\eta}_\mathrm{max} \equiv \eta_\mathrm{max}/\eta_\mathrm{C}$
P	Power output of thermoelectric, cyclic heat engines	$P \equiv -\Delta\mu J_\rho$, $P \equiv -\Delta H J_w$
P_max	Maximum power with respect to $\mathcal{F}_\rho$, $\mathcal{F}_w$	–
P^*	Power at maximum efficiency with respect to $\mathcal{F}_\rho$, $\mathcal{F}_w$	–
$\hat{P}^*$	Upper bound on power at maximum efficiency obtained by estimating L_{qq}	–

P_+	Maximum power at given efficiency obtained by fixing η using $\mathcal{F}_\rho$, $\mathcal{F}_w$	–
P_-	Minimum power at given efficiency obtained by fixing η using $\mathcal{F}_\rho$, $\mathcal{F}_w$	–
$\hat{P}$	Upper bound on power obtained by estimating L_{qq}	–
$\hat{P}_{\max}$	Upper bound on power obtained by estimating L_{qq} and maximizing the result with respect to y	–
P_0, $\bar{P}_0$	Standard power	$P_0 \equiv T_c\mathcal{F}_q^2 L_{qq}/4$, $\bar{P}_0 \equiv T_c\mathcal{F}_q^2 N_{qq}/4$

Mathematical Notations

Notation	**Description**
δ_{ik}, δ	Kronecker delta symbol, Dirac delta function
$\mathbb{R}$, $\mathbb{C}$	Field of real, complex numbers
$\mathbb{R}^m$, $\mathbb{C}^m$	Space of m-dimensional real, complex column vectors
$\mathbb{R}^{m\times m}$, $\mathbb{C}^{m\times m}$	Space of m-dimensional real, complex square matrices
$\mathbb{1}$	Identity matrix
$\mathbb{O}$	Zero matrix
$\mathbf{0}$	Column vector filled with zeros
$\mathbb{X}_{\{A\}}$	Principal submatrix of the square matrix $\mathbb{X}$ obtained by taking the rows and columns indexed by A
$\mathbb{X}_{\{\{A\}\}}$	Principal submatrix of the even-dimensional square matrix $\mathbb{X}$ obtained by taking all 2×2-subunits indexed by A, i.e., the rows and columns $a_1, a_1+1, \ldots, a_k, a_k+1$ for $A \equiv \{a_1, \ldots, a_k\}$
$\mathbb{X}_{[A]}$	Principal submatrix of the square matrix $\mathbb{X}$ obtained by deleting the rows and columns indexed by A
$\mathbb{X}_{[[A]]}$	Principal submatrix of the even-dimensional square matrix $\mathbb{X}$ obtained by deleting all 2×2-subunits indexed by A, i.e., the rows and columns $a_1, a_1+1, \ldots, a_k, a_k+1$ for $A \equiv \{a_1, \ldots, a_k\}$
$\mathcal{S}$	Asymmetry index, see (3.38)
$\dot{X}$	Time-derivative of the quantity X
$\mathsf{X}^\dagger$	Adjoint of the operator X

Publications

Parts of this thesis have been published in:

- Brandner K., Saito, K. and Seifert, U., Strong Bounds on Onsager Coefficients and Efficiency for Three-Terminal Thermoelectric Transport in a Magnetic Field, *Phys. Rev. Lett.* **110**, 070603 (2013), DOI: 10.1103/PhysRevLett.110.070603.

- Brandner K. and Seifert U., Multi-Terminal Thermoelectric Transport in a Magnetic Field: Bounds on Onsager Coefficients and Efficiency, *New J. Phys.* **15**, 105003 (2013), DOI: 10.1088/1367-2630/15/10/105003.

- Stark J., Brandner K., Saito K. and Seifert U., Classical Nernst Engine, *Phys. Rev. Lett* **112**, 140601 (2014), DOI: 10.1103/PhysRevLett.112.140601.

- Brandner K. and Seifert U., Bound on thermoelectric power in a magnetic field within linear response, *Phys. Rev. E* **91**, 012121 (2015), DOI: 10.1103/PhysRevE.91.012121.

- Brandner K., Saito K. and Seifert U., Thermodynamics of Micro- and Nano-Systems Driven by Periodic Temperature Variations, to appear in *Phys. Rev. X*, `arXiv:1505.07771`.

Zusammenfassung

Einleitung

Mehr als zwei Jahrhunderte nach James Watts bahnbrechender Erfindung sind die technologischen Nachfahren seiner Dampfmaschine in unserem modernen Alltagsleben unverzichtbar geworden. Wir nutzen sie beispielsweise zum Antrieb von Fahrzeugen oder elektrischen Generatoren in Kraftwerken. Das grundlegende Funktionsprinzip dieser Maschinen hat sich dabei seit den frühen Tagen der industriellen Revolution nicht geändert. Ein Arbeitsmedium, welches sich abwechselnd in Kontakt mit einem heißen und einem kalten Wärmebad befindet, wird mit Hilfe eines beweglichen Kolbens periodisch komprimiert und expandiert. Aufgrund des Druckunterschieds zwischen dem heißen und dem kalten Medium kann hierbei ein Nettogewinn an mechanischer Arbeit erzielt werden.

Thermoelektrische Generatoren, die im Gegensatz zu ihren zyklisch arbeitenden Verwandten ohne bewegliche Teile auskommen, stellen eine zweite wichtige Klasse von Wärmekraftmaschinen dar. Ein Minimalmodell für ein solches Bauelement besteht aus zwei Teilchenreservoiren unterschiedlicher Temperatur, die statisch durch einen Leiter verbunden sind. Aufgrund des Seebeck-Effekts kann der in diesem Aufbau entstehende Wärmestrom einen Teilchenstrom gegen ein äußeres Feld oder einen chemischen Potentialgradienten treiben und so elektrische Energie erzeugen. Obwohl dieses Arbeitsprinzip erhebliche Vorteile mit sich bringt, beschränkt sich der Anwendungsbereich von thermoelektrischen Elementen derzeit auf Spezialgebiete wie Raumfahrt und Labortechnik, was insbesondere der Tatsache geschuldet ist, dass ihr Wirkungsgrad in praxi deutlich niedriger ist als der von zyklischen Wärmekraftmaschinen.

Die Güte einer Wärmekraftmaschine wird typischerweise anhand der beiden Parameter Wirkungsgrad und Leistung beurteilt. Die erste dieser beiden Kennzahlen ist als direkte Folge des zweiten Hauptsatzes universell durch den Carnot-Faktor $\eta_C = 1 - T_c/T_h$ beschränkt, wobei T_h und T_c die Temperaturen des heißen beziehungsweise kalten Reservoirs bezeichnen. Eine ähnliche Schranke an die Leistung kann nicht aus den Hauptsätzen der Thermodynamik abgeleitet werden, da diese keinerlei Zeitskalen beinhalten.

Sowohl zyklische als auch thermoelektrische Wärmekraftmaschinen können die Carnot-Schranke asymptotisch erreichen. Die jeweiligen Grenzfälle zeichnen sich durch einen unendlich langsam bewegten Kolben beziehungsweise perfekte energetische Filterung der zwischen den Reservoiren ausgetauschten Teilchen aus. Beide Szenarien führen jedoch unweigerlich zu verschwindender Leistung. Aus diesem Grund ist der maximale Wirkungsgrad einer Wärmekraftmaschine im Allgemeinen nur von geringem praktischen Interesse.

Eine nützlichere Kenngröße ist durch die Effizienz bei maximaler Leistung gegeben. Für diesen Parameter fanden Curzon und Ahlborn den bemerkenswert einfachen Ausdruck $\eta_{CA} = 1 - \sqrt{T_c/T_h}$ unter Verwendung eines elementaren Modells, welches als endoreversible

Maschine bekannt ist [1]. Dieses Resultat führte zu einem beachtlichen wissenschaftlichen Interesse an der Frage, inwieweit η_{CA} - ähnlich wie η_{C} - eine universelle Schranke darstellen könnte. Mittlerweile hat sich herausgestellt, dass das Konzept von Effizienz bei maximaler Leistung kritisch an die zur Verfügung stehenden Variationsparameter gebunden ist. Nichtsdestotrotz lassen sich innerhalb bestimmten Modellklassen universelle Resultate gewinnen. Im Allgemeinen zeigt sich jedoch, dass die Maximierung der Leistung zu einem erheblich niedrigeren Wirkungsgrad als η_{C} führt. Dieser Befund bestätigt die allgemeine Vermutung, dass Effizienz und Leistung einer Wärmekraftmaschine nicht gleichzeitig optimiert werden können [4].

Für thermoelektrische Generatoren im linearen Regime kann dieses Dilemma quantitativ formuliert werden. Innerhalb des theoretischen Rahmens der irreversiblen Thermodynamik lässt sich zeigen, dass die Leistung einer solchen Maschine durch eine quadratische Funktion ihres Wirkungsgrades beschränkt ist, die bei η_{C} verschwindet und bei η_{CA} ihr lokales Maximum erreicht. Dieses Ergebnis beruht sowohl auf dem zweiten Hauptsatz als auch auf den Onsagersche Reziprozitätsbeziehungen. Letztere lassen sich wiederum auf die Invarianz der mikroskopischen Bewegungsgleichungen unter Zeitumkehr zurückführen. Wie von Benenti *et al.* festgestellt wurde, führt das lokale Brechen dieser Symmetrie durch Anwendung eines äußeren Magnetfeldes zu einem Abschwächen effizienzabhängigen Schranke an die Leistung. Insbesondere scheint es dadurch möglich zu sein, den Carnot-Wirkungsgrad bei endlicher Leistung zu erreichen.

Diese verblüffende Beobachtung stellt den Ausgangspunkt der vorliegenden Arbeit dar. Unser erstes Kernziel ist die Suche nach zusätzlichen Prinzipien jenseits des zweiten Hauptsatzes und der Reziprozitätsrelationen, welche die Leistung von thermoelektrischen Wärmekraftmaschinen mit gebrochener Zeitumkehrsymmetrie bestimmen. Weiterhin sollen konkrete Modellsysteme betrachtet werden, um ein besseres Verständnis der mikroskopischen Mechanismen thermoelektrischer Energieumwandlung in Gegenwart eines Magnetfeldes zu gewinnen.

Mit Hinblick auf unseren Ausgangspunkt stellt sich die natürliche Frage, inwieweit die Resultate von Benenti *et al.* auch auf zyklische Maschinen angewandt werden können. Das Finden entsprechender Analogien erscheint zunächst schwierig, weil zyklisch arbeitende Wärmekraftmaschinen nicht innerhalb des Rahmens der irreversiblen Thermodynamik modelliert werden können. Diese Theorie wurde ursprünglich nur zur Beschreibung stationärer Nichtgleichgeweichtszustände entwickelt. Es ist daher ein weiteres Anliegen dieser Arbeit, die Konzepte der irreversiblen Thermodynamik auf periodisch getriebene Systeme zu erweitern. Das Ziel dieser Überlegungen soll ein universeller Rahmen sein, innerhalb dessen untersucht werden kann, welche Rolle die mikroskopische Zeitumkehrsymmetrie für Effizienz und Leistung zyklischer Wärmekraftmaschinen spielt.

Thermodynamik Thermoelektrischer Maschinen

Wir führen zunächst die phänomenologischen Konzepte der irreversiblen Thermodynamik als Grundlage für die Beschreibung thermoelektrischer Wärmekraftmaschinen ein. Innerhalb dieses Zugangs werden stationäre Nichtgleichgewichtszustände mit einer universellen thermodynamischen Struktur aus Strömen und Affinitäten versehen. Wichtig ist dabei, dass die Rate der totalen Entropieproduktion auch bei starken Abweichungen vom thermodynamischen Gleichgewicht eine bilineare Funktion dieser Größen ist.

Sind die Temperatur- und Potentialgradienten innerhalb des betrachteten Systems klein bezogen auf die jeweiligen Referenzwerte, genügt es die stationären Ströme in linearer Ordnung bezüglich der Affinitäten zu betrachten. Die in dieser Entwicklung auftretenden kinetischen Koeffizienten werden durch zwei fundamentale Prinzipien beschränkt. Der zweite Hauptsatz verlangt, dass die Rate der totalen Entropieproduktion, welche nach Linearisierung der Ströme eine quadratische Funktion der Affinitäten ist, stets positiv oder Null ist. Die Reversibilität der mikroskopischen Dynamik führt zu einer Reziprozitätsrelation, als Folge derer die indirekten kinetischen Koeffizienten in zeitumkehrsymmetrischen Systemen identisch sein müssen. Diese Symmetrie ist jedoch in Gegenwart eines Magnetfeldes typischerweise gebrochen.

Nach dem Bereitstellen der allgemeinen Grundlagen widmen wir uns zunächst zeitumkehrsymmetrischen, thermoelektrischen Generatoren. Wir zeigen, dass die drei wahrscheinlich wichtigsten Kenngrößen maximale Effizienz, Effizienz bei maximaler Leistung und Leistung bei gegebener Effizienz im linearen Regime durch einen einzigen dimensionslosen Parameter bestimmt werden, der seinerseits eine Funktion der kinetischen Koeffizienten ist. Weiterhin leiten wir eine universelle Schranke an die Leistung her, welche eine quadratische Funktion des Wirkungsgrades ist.

Anschließend wenden wir uns Systemen mit gebrochener Zeitumkehrsymmetrie zu. Wir rekapitulieren die Analyse von Benenti *et al.*, innerhalb welcher die oben eingeführten Kenngrößen durch zwei dimensionslose Parameter ausgedrückt werden. Der erste hiervon stellt eine Verallgemeinerung der konventionellen thermoelektrischen Gütezahl[1] dar, der zweite ein quantitatives Maß für die durch das äußere Magnetfeld erzeugte Asymmetrie der kinetischen Koeffizienten. Reversiblen Transports wird dann möglich, wenn dieser Parameter von seinem symmetrischen Wert 1 abweicht. Schließlich zeigen wir, dass sich dieses faszinierende Phänomen auf unbeschränkte, reversible Ströme zurückführen lässt, die nicht zur totalen Entropieproduktion beitragen.

Multi-Terminal Systeme

Auf der Größenskala von Nanometern kann thermoelektrischer Transport als quantenmechanischer Streuprozess beschrieben werden. Diese bahnbrechende Idee geht ursprünglich auf Landauer zurück [35]. Sein Formalismus wurde später insbesondere in den Arbeiten von Büttiker weiter entwickelt [36–41]. Im Allgemeinen betrachtet man n Teilchenreservoire (Terminals), die durch perfekte, halbunendliche Leiter mit einer zentralen Streuregion verbunden sind, die einem externen Magnetfeld ausgesetzt werden kann. Nimmt man zusätzlich nicht wechselwirkende Teilchen an, die in kohärenten Streuprozessen zwischen den Reservoiren ausgetauscht werden, so lassen sich die kinetischen Koeffizienten, welche den stationären Transportprozess in dieser Geometrie beschreiben, durch quantenmechanische Übergangswahrscheinlichkeiten ausdrücken.

Für das einfachste Modell dieser Klasse, welches aus nur zwei Terminals besteht, lässt sich zeigen, dass die Vernachlässigung von Wechselwirkungen und inkohärenten Prozessen auch in Gegenwart eines Magnetfeldes stets zu symmetrischen kinetischen Koeffizienten führt [39, 42]. Um diese Symmetrie zu brechen, müssen inelastische Streuprozesse

[1] Engl. *figure of merit*. In Abwesenheit äußerer Magnetfelder sind maximale Effizienz und Effizienz bei maximaler Leistung eines thermoelektrischen Generators eindeutig durch diese Kennzahl festgelegt [15, 27].

berücksichtigt werden. Innerhalb des Landauer-Büttiker-Formalismus ist dies auf einer phänomenologischen Ebene durch das Einführen zusätzlicher Reservoire möglich, deren Temperatur und chemisches Potential so gewählt werden, dass im Mittel weder Teilchen noch Wärme mit dem restlichen System ausgetauscht werden. Solche fiktiven Terminals tragen nicht zum eigentlichen Transportprozess bei, sondern simulieren lediglich inelastische Streuprozesse.

In einem ersten Schritt untersuchen wir den einfachsten Fall von nur drei Terminals. Für dieses System beweisen wir eine universelle Schranke an die kinetischen Koeffizienten. Als Konsequenz dieser Schranke muss die Rate der totalen Entropieproduktion strikt positiv sein, wann immer die indirekten kinetischen Koeffizienten nicht identisch sind. Hierdurch wird insbesondere die Option dissipationsfreien, nur auf reversiblen Strömen beruhenden Transports ausgeschlossen. Dieses Ergebnis lässt sich weder aus den Hauptsätzen der Thermodynamik noch aus den Onsagerschen Reziprozitätsrelationen gewinnen, sondern folgt letztlich aus dem fundamentalen Gesetz der Stromerhaltung.

Der nächste logische Schritt unserer Analyse besteht in der Betrachtung allgemeinerer Systeme mit einer beliebigen Zahl von Terminals. In Analogie zu unseren vorherigen Überlegungen beweisen wir innerhalb dieser Modellklasse eine allgemeine Schranke an die kinetischen Koeffizienten, die nur von der Gesamtzahl n der Terminals abhängt. Diese geht für $n = 3$ in das bereits bekannte Ergebnis über und wird mit wachsendem n sukzessive schwächer. Im Limes $n \to \infty$ reduziert sie sich schließlich auf jene Bedingung, die bereits vom zweiten Hauptsatz verlangt wird. Folglich liefert unsere verallgemeinerte Schranke an die kinetischen Koeffizienten zwar für jedes endliche n eine Schranke an die Effizienz, die das Erreichen des Carnot-Wirkungsgrades bei endlicher Leistung ausschließt, im Grenzfall $n \to \infty$ führt sie jedoch nicht zu zusätzlichen Einschränkungen.

Wir widmen uns nun der Frage, ob sich nicht nur die Effizienz, sondern auch die Leistung innerhalb des Multi-Terminal-Modells beschränken lässt. Hierzu führen wir zunächst geeignete Normierungskonstanten ein, um dimensionslose kinetische Koeffizienten zu erhalten. Anschließend zeigen wir, dass diese einer zusätzlichen Zwangsbedingung unterworfen sind, die ebenfalls aus dem Gesetz der Stromerhaltung folgt und unabhängig von der Zahl der involvierten Terminals ist. Diese neue Bedingung erlaubt es die Leistung des Multi-Terminal-Modells als thermoelektrische Wärmekraftmaschine allgemein durch eine quadratische Funktion seines Wirkungsgrades zu beschränken, die bis auf einen Skalierungsfaktor mit jener identisch ist, die sich in zeitumkehrsymmetrischen Systemen aus der Reziprozitätsrelation ergibt. Folglich zeigt unser Resultat, dass der Carnot-Wirkungsgrad innerhalb eines jeden Systems, welches sich durch ein Multi-Terminal-Modell beschreiben lässt, nicht bei endlicher Leistung erreicht werden kann.

Auf Grundlage starker numerischer Evidenz gelangen wir anschließend zu der Vermutung, dass die oben beschriebene Schranke in Systemen mit nur wenigen Terminals noch verstärkt werden kann. Unsere numerischen Ergebnisse legen nahe, dass die Leistung des Multi-Terminal-Generators bereits bei Erreichen der jeweils maximalen Effizienz für festes n verschwindet. Dieser Wert ist für endliches n und nicht symmetrische kinetische Koeffizienten strikt kleiner als η_C. Im Grenzfall $n \to \infty$ reduziert sich diese detaillierte Schranke auf die zuvor exakt bewiesene, von n unabhängige Schranke.

Nachdem wir uns bis zu diesem Punkt ausschließlich mit allgemeinen Schranken an Wirkungsgrad und Leistung beschäftigt haben, werden wir im letzten Teil dieses Kapitels ein konkretes Modell für eine thermoelektrische Wärmekraftmaschine diskutieren, welches

von J. Stark in seiner Masterarbeit untersucht wurde. Hierzu führen wir zunächst ein zweidimensionales, klassisches Analogon zum bisher verwendeten, quantenmechanischen Multi-Terminal-Modell ein. Dabei konzentrieren wir uns auf einen einfachen Spezialfall mit vier Terminals [62]. Durch ein äußeres Magnetfeld, sowie geeignete Randbedingungen kann in dieser Geometrie ein Teilchenstrom erzeugt werden, der von einem Wärmestrom senkrecht zu seiner eigenen Flussrichtung getrieben wird. Dieses Phänomen ist als Nernst-Effekt bekannt. Eine allgemeine Überlegung basierend auf dem Satz von Liouville zeigt, dass die maximale Effizienz und die Effizienz bei maximaler Leistung dieses klassischen Nernst-Generators durch $(3-2\sqrt{2})\eta_{\mathrm{C}} \simeq 0.172\eta_{\mathrm{C}}$ beziehungsweise $\eta_{\mathrm{C}}/6$ beschränkt sind. Diese Schranken können für ein starkes äußeres Magnetfeld und kleine Teilchendichten in den Reservoiren saturiert werden.

Periodische Thermodynamik auf Kleinen Größenskalen

Bisher haben wir uns ausschließlich mit thermoelektrischen Wärmekraftmaschinen beschäftigt. Um unser Bild zu komplettieren, wenden wir uns in diesem Kapitel der Untersuchung zyklischer Maschinen zu. Hierfür entwickeln wir zunächst eine allgemeine Theorie zur Beschreibung von Systemen, die sowohl durch eine zeitlich alternierende Umgebungstemperatur, als auch durch periodisch zeitabhängige Kontrollparameter in ihrer Hamiltonfunktion getrieben werden. Anhand einer einfachen Überlegung identifizieren wir die Stärke der zeitabhängigen Störung der Hamiltonfunktion und die Oszillationsamplitude der inversen Badtemperatur als geeignete Affinitäten. Die zugehörigen Ströme stellen zeitlich gemittelte und damit konstante Größen dar. Nichtsdestotrotz ist die Zyklendauer als fundamentale Zeitskala in unserem Formalismus enthalten, sodass dieser insbesondere auch die Untersuchung von Größen wie der mittleren Leistung erlaubt. Darüber hinaus lässt sich in unserem Zugang - in perfekter Analogie zur irreversiblen Thermodynamik - die mittlere Entropieproduktion pro Zyklus auch für große Auslenkungen aus dem thermodynamischen Gleichgewicht als bilineare Form von Strömen und Affinitäten darstellen.

Im linearen Regime liefert unser Ansatz eine konsistente Definition kinetischer Koeffizienten. Indem wir zur Beschreibung der mikroskopischen Dynamik eine allgemeine Fokker-Planck-Gleichung verwenden, zeigen wir dass sich diese Koeffizienten aus einem adiabatischen Beitrag und einer Korrelationsfunktion zusammensetzen. Der zweite Beitrag erinnert dabei an die von den Green-Kubo-Relationen bekannten Ausdrücke für lineare Transportkoeffizienten. Weiterhin zeigen wir, dass die verallgemeinerten kinetischen Koeffizienten eine Reziprozitätsrelation erfüllen, die sich auf die Zeitumkehrsymmetrie der Mikrodynamik zurückführen lässt. Bemerkenswerterweise sind die indirekten Koeffizienten hierbei im Allgemeinen nur identisch, falls sowohl die Badtemperatur als auch die externen Kontrollparameter symmetrische Funktionen der Zeit sind. Dieses Resultat gilt unabhängig von der zusätzlichen Anwesenheit eines Magnetfeldes.

Nachdem unsere Theorie exakt dieselbe Struktur besitzt wie die lineare irreversible Thermodynamik, können die Überlegungen von Benenti *et al.* nun direkt auf zyklische Wärmekraftmaschinen übertragen werden. Dies bedeutet insbesondere, dass weder der zweite Hauptsatz noch die mikroskopische Zeitumkehrsymmetrie ausschließen, dass solche Maschinen den Carnot-Wirkungsgrad bei endlicher Leistung erreichen können. In Analogie zu unseren Ergebnissen für thermoelektrische Systeme können wir allerdings eine zusätzliche Schranke an die verallgemeinerten kinetischen Koeffizienten beweisen. Diese

ist bis auf einen Skalierungsfaktor identisch mit jener, die innerhalb des Multi-Terminal-Modells auf eine universelle Schranke an die Leistung geführt hatte. Die hierbei verwendete Herleitung stützt sich auf einige natürliche Eigenschaften des Fokker-Planck-Operators wie beispielsweise die Invarianz der Boltzmann-Verteilung im Gleichgewicht. Sie ist jedoch unabhängig von spezifischen Eigenschaften des jeweiligen Modells. Folglich können wir zeigen, dass die Leistung von zyklischen Wärmekraftmaschinen, die durch eine Fokker-Planck-Dynamik beschrieben werden können, wenigstens linear verschwindet, wenn sich deren Effizienz dem Carnot-Wirkungsgrad annähert. Schließlich vervollständigen wir unsere Analyse, indem wir das konkrete Beispiel einer stochastischen Wärmekraftmaschine, deren Arbeitsmedium nur aus einem kolloidalen Teilchen in einer harmonischen Falle besteht, ausarbeiten. Innerhalb dieser Modellstudie zeigen wir insbesondere, dass unsere neue Schranke an die Leistung zyklischer Wärmekraftmaschinen asymptotisch saturiert werden kann.

Allgemeine Schranken an die Asymmetrie Positiv Semidefiniter Matrizen

In diesem Kapitel entwickeln wir eine abgeschlossene mathematische Theorie zur die Asymmetrie positiv semidefiniter Matrizen. Den Ideen von Crouzeix und Gutan [56] folgend definieren wir zunächst ein quantitatives Maß für diese Eigenschaft, welches für symmetrische Matrizen verschwindet und für antisymmetrische Matrizen divergiert. Anschließend beschäftigen wir uns mit einer speziellen Klasse von Matrizen, die in der Form $\mathbb{D} - \mathbb{T} \in \mathbb{R}^{m\times m}$ parametrisiert werden kann. Hierbei ist die Matrix $\mathbb{T}$ entweder doppelt stochastisch, doppelt substochastisch oder summensymmetrisch und $\mathbb{D}$ in den ersten beiden Fällen die Einheitsmatrix, sowie im letzten Fall eine Diagonalmatrix, welche die geordneten Spaltengewichte von $\mathbb{T}$ enthält. Unter Ausnutzung des Birkhoff-von-Neumann-Theorems und seiner Verallgemeinerungen beweisen wir, dass der Asymmetrieindex in der ersten und letzten Klasse durch $\cot(\pi/m)$ beschränkt ist, während für die zweite Klasse die Schranke $\cot(\pi/(m+1))$ gilt.

Diese Studien sind durch unsere Untersuchungen des Multi-Terminal-Modells motiviert. Die hier untersuchten Typen von Matrizen treten typischerweise innerhalb des Landauer-Büttiker-Formalismus auf, den wir zur Beschreibung dieses Modells verwenden. Tatsächlich können die von uns bewiesenen Schranken an den Asymmetrieindex bestimmter Matrizen dazu verwendet werden, den Wirkungsgrad des Multi-Terminal-Systems als thermoelektrische Wärmekraftmaschine zu beschränken. Unabhängig von dieser wichtigen Anwendung stellen die Resultate dieses Kapitels einen neuartigen Beitrag zum mathematischen Gebiet der Matrix-Analysis dar, der auch über die Themen dieser Arbeit hinaus von Interesse sein könnte.

Summary

Introduction

More than two centuries after James Watt's pioneering invention, the highly developed technological descendants of his steam engine have become indispensable in our modern daily life. The mechanical power they provide is used, for example, to propel vehicles or electrical generators in power plants. Still, the basic working principle of such machines is the same as in the early days of the industrial revolution. A reciprocating piston is used to periodically compress and expand a working fluid, which is alternately coupled to a hot and a cold thermal reservoir. Due to the pressure gradient between the hot and the cold state of the fluid, a net gain in mechanical work is obtained.

Thermoelectric generators form a second important class of heat engines. In contrast to their cyclic counterparts, such devices work in a steady state without any moving parts. Specifically, they consist of two thermochemical reservoirs of different temperature and chemical potential that are permanently connected via a conductor. Due to the Seebeck effect, the heat current arising in this setup can drive a particle current uphill against the gradient in chemical potential thus generating electrical power. Although this working principle provides some considerable advantages, thermoelectric heat engines are outperformed by cyclic ones in most situations. Therefore, they are currently used only in niche applications like deep space missions.

The performance of heat engines is typically assessed in terms of two key figures. The first one, efficiency, is universally bounded by the Carnot value $\eta_{\mathrm{C}} = 1 - T_{\mathrm{c}}/T_{\mathrm{h}}$ as a direct consequence of the first and the second law, where T_{h} and $T_{\mathrm{c}} < T_{\mathrm{h}}$ denote the temperature of the hot and the cold reservoir, respectively. A similar bound on power, the second one, is, however, not available by now since this quantity is out of reach for the laws of thermodynamics, which do not invoke any time scale.

Both, cyclic and thermoelectric heat engines, can, in principle, saturate the Carnot bound. The corresponding limits are characterized by an infinitely slow-moving piston and a conductor acting as a perfect energy filter, respectively. In both cases, however, the power output vanishes as the Carnot efficiency is approached. Consequently, maximum efficiency is only of minor practical importance as a performance benchmark. A more useful alternative is provided by efficiency at maximum power. For this figure, Curzon and Ahlborn found the surprisingly simple value $\eta_{\mathrm{CA}} = 1 - \sqrt{T_{\mathrm{c}}/T_{\mathrm{h}}}$ using an elementary model known as endoreversible engine [1]. Their result has spurred considerable research interest concerning the putative universality of efficiency at maximum power. Meanwhile, it has become clear that this concept crucially depends on the parameter space, within which the power output is maximized. Nevertheless, semi-universal results are available within various classes of models for which natural choices of variational parameters exist.

It turns out that, generally, the optimization of power leads to an efficiency substantially smaller than η_C. These findings confirm the general expectation that high efficiency and large power output mutually exclude each other [4].

For thermoelectric heat engines in the linear response regime, this dilemma can be formulated quantitatively by virtue of a straightforward analysis within the phenomenological framework linear irreversible thermodynamics. Specifically, it can be shown that power is bounded by a quadratic function of efficiency, which vanishes at the Carnot value and attains its maximum at the Curzon-Ahlborn efficiency. This result follows by simultaneously exploiting the second law and Onsager's reciprocity relation. The latter constraint ultimately relies microscopic reversibility. Therefore, it becomes effectively meaningless if this symmetry is locally broken by an external magnetic field as recently pointed out by Benenti *et al.* [27]. In fact, once the microscopic time-reversal symmetry broken, the efficiency-dependent bound on power is lifted such that the Carnot efficiency might be reached at finite power.

The intriguing observation of Benenti *et al.* constitute the starting point for this thesis. Our first main objective is the search for additional principles beyond the second law and the reciprocity relations that govern the performance of thermoelectric heat engines with broken time-reversal symmetry in the linear response regime. Furthermore, as our second main objective, we will look for specific models, within which the microscopic mechanisms determining the performance of thermoelectric generators in the presence of a magnetic field can be studied.

Coming back to our starting point, the natural question arises whether the results of Benenti *et al.* might also apply to cyclic heat engines. Investigations in this direction appear *a priori* difficult, since cyclic engines can not be described using the concepts of linear irreversible thermodynamics. Therefore, our third main objective is to extend this theory, which was originally designed for the thermodynamics description of non-equilibrium steady states, to periodically driven systems. The aim of this endeavor is to obtain a universal framework, within which the role of time-reversal symmetry for the performance of cyclic heat engines can be studied on a general level.

Thermodynamics of Thermoelectrics

We begin by introducing the phenomenological but powerful framework of irreversible thermodynamics as a toolkit for the description of thermoelectric heat engines. Within this theory, the non-equilibrium steady state underlying the thermoelectric transport process is furnished with a universal thermodynamic structure built from currents and affinities corresponding to gradients in temperature and chemical potential. The key point here is that the total rate of entropy production becomes a bilinear form in these quantities, even in the non-linear regime.

If the gradients are small compared to their respective reference values, the currents can be linearized with respect to the affinities. The kinetic coefficients showing up in this expansion are constrained by two fundamental principles. First, the second law requires the total rate of entropy, which becomes a quadratic form in the affinities through the linearization of the currents, to be non-negative. Second, microscopic reversibility leads to a reciprocal relation, which renders the off-diagonal kinetic coefficients identical in time-reversal symmetric systems. This symmetry is, however, typically broken in the presence

of a magnetic field. In this situation, the second law is effectively the only constraint.

After setting the general stage, we first focus on time-reversal symmetric thermoelectric engines in linear response. We find that the three arguably most important key figures in this context, maximum efficiency, efficiency at maximum power and power at given efficiency, can be expressed in terms of a single dimensionless parameter, the thermoelectric figure of merit, which is a function of the kinetic coefficients. Furthermore, by exploiting the reciprocal relation, we derive the aforementioned efficiency-dependent bound on power.

We then turn to systems with broken time-reversal symmetry. Recapping the analysis of Benenti *et al.*, we express the previously introduced key figures in terms of two dimensionless parameters. The first one hereof generalizes the thermoelectric figure of merit, the second one quantifies the magnetic-field induced asymmetry between the off-diagonal kinetic coefficients. The option of reversible transport arises if this parameter deviates from its symmetric value 1. Finally, we show that this intriguing phenomenon can be traced back to reversible currents, which do not contribute to the total rate of entropy production and thus are unconstrained by the second law.

Multi-Terminal Systems

A promising platform for investigations of putative constraints on the kinetic coefficients beyond the second law is provided by thermoelectric nano-devices, which can be modeled using the scattering approach to quantum transport. The basic idea behind this method, which goes back to the pioneering work of Landauer [35] and was later substantially refined by Büttiker [36–40], is to connect a set of n electronic reservoirs (terminals) via perfect, semi-infinite leads to a central region, where a magnetic field can be applied. By assuming non-interacting particles, which are transferred coherently between the reservoirs, the kinetic coefficients describing the transport process in this multi-terminal geometry can be expressed in terms of quantum-mechanical transmission probabilities.

In a minimalistic two-terminal setup, the neglect of interactions and dephasing leads to identical off-diagonal kinetic coefficients, even in the presence of an external magnetic field [39,42]. Therefore, such phenomena must be taken into account in order to investigate the effect of non-symmetric kinetic coefficients. In the Landauer-Büttiker formalism, they can be included on a phenomenological level. To this end, fictitious terminals are introduced, whose temperature and chemical potential are adjusted such that they, on average, do not exchange any heat or particles with the real terminals. Consequently, these probe terminals do not contribute to the physical transport process but rather mimic inelastic scattering.

In a first step, we investigate the paradigmatic and arguably most simple case of three terminals. On the basis of the multi-terminal Landauer-formula, we derive a universal bound on the kinetic coefficients, which is independent of model-specific details like the potential landscape inside the central region or the strength of the magnetic field. This constraint implies that, whenever the symmetry between the off-diagonal kinetic coefficients is broken, the total rate of entropy production must be strictly larger than zero. It thus rules out the option of dissipationless transport generated solely by reversible currents. We emphasize that this result can be obtained neither from Onsager's principle of micro-reversibility nor from purely thermodynamic arguments involving only the second

law. Rather it ultimately follows from the law of current conservation, which should be regarded as the fundamental physical principle underlying our new bounds.

As the next logical step in our investigation, we consider more general models involving an arbitrary number of probe terminals. By extending the concepts of our previous analysis, we prove a generalized constraint on the kinetic coefficients, which depends only on the total number of terminals n. For the special case $n = 3$ this constraint reduces to the result obtained previously for the three-terminal model. As n increases, it becomes successively weaker. In the limit $n \to \infty$, it reduces to the same relation as required by the bare second law. Consequently, for any finite n, the generalized constraint leads to a bound on efficiency, which is stronger than the one imposed by the second law. In particular, it prevents the option of reversible transport. In the limit $n \to \infty$, however, we are back at the situation originally discussed by Benenti *et al.*.

This result prompts the question, whether not only efficiency, but also power can be bounded. Since power carries a physical dimension, such an endeavor can be expected to be harder and, *a priori*, less universal, than searching a bound for dimensionless efficiency. Within the multi-terminal setup, we overcome this obstacle by identifying proper normalization factors for the kinetic coefficients, which are independent of model-specific details. We then derive a further constraint on the effective kinetic coefficients, which, in contrast to the relations involved in our previous discussion of efficiency, does not depend on the number of terminals. The new constraint allows to establish an upper bound on power, which is a quadratic function of efficiency and vanishes at the Carnot value. Consequently, this result finally rules out the option of Carnot efficiency at finite power for the entire class of multi-terminal models. Remarkably, the bound on power relies on the same physical principle like the bounds on efficiency discussed before, i.e., current conservation.

Strong numerical evidence leads us to the conjecture that this bound can still be strengthened for any finite number of terminals. Specifically, our numerical results suggest a detailed constraint on the kinetic coefficients, which forces power to vanish not only at the Carnot efficiency, but already at the maximum efficiency corresponding to a fixed number of terminals and a fixed asymmetry parameter x. For $n \to \infty$, this detailed bound reduces to the weaker one, which we have proven exactly foregoing analysis.

A key topic one naturally encounters in the context thermoelectric heat engines with broken time-reversal symmetry is provided by the thermomagnetic effects. These phenomena describe a coupling between a heat and a particle current transversing an isotropic conductor perpendicular to each other, which is induced by a constant magnetic perpendicular to both fluxes. The Nernst effect refers to the special situation, where the heat current drives the particle current. Like the Seebeck effect, for which the two currents are parallel, it can be utilized for power generation. Moreover, heat engines based on the Nernst effect provide ideal candidates to study thermodynamic aspects like power and efficiency of coupled heat and matter transport in the presence of a magnetic field. Here, we discuss a simple setup based on classical mechanics, within which such a device can be realized. This system was studied by J. Stark in his master thesis [62]. For a microscopic model invoking four terminals, the kinetic coefficients could be obtained exactly from a geometric approach exploiting that the Lorentz force leads to circular single-particle trajectories. Moreover, a general consideration based on Liouville's theorem shows that ratio between the maximum efficiency of this classical Nernst engine and the Carnot efficiency

is universally bounded by $3 - 2\sqrt{2} \simeq 0.172$. It turns out that this bound, as the slightly lower one 1/6 for efficiency at maximum power, can indeed be saturated for a strong magnetic field and small fugacities in the thermochemical baths.

Periodic Thermodynamics on the Micro- and Nano-Scale

So far our discussion has focused only on thermoelectric heat engines. In order to obtain a complete picture, in this chapter we study the influence of broken time-reversal symmetry on cyclic engines. To this end, we first develop a general framework for the description of systems driven by periodically changing the temperature of their environment as well as certain control parameters determining their internal energy. A straightforward analysis using the first law as a starting point allows us to identify the strength of the time-dependent perturbation of the Hamiltonian and the the amplitude of the oscillating inverse temperature of the heat bath as proper affinities. The corresponding currents are defined on the level of cycle averages and thus time-independent. Nevertheless, since the the cycle duration is incorporated in our formalism as a fundamental time-scale, finite-time quantities like power are perfectly captured by this approach. Moreover, without making a linear response assumption, we recover the bilinear expression of the total rate of entropy production in terms of currents and affinities, which is a cornerstone of irreversible thermodynamics.

In the linear response regime, our formalism provides consistent definitions for generalized kinetic coefficients. Specializing to a Fokker-Planck type stochastic dynamics, we show that these coefficients can be expressed as a sum of an adiabatic contribution and one reminiscent to a Green-Kubo expressions that contains deviations from adiabaticity. Furthermore, we show that the generalized kinetic coefficients fulfill an Onsager type reciprocal relation tracing back to microscopic reversibility. Remarkably, we find that the off-diagonal kinetic coefficients are typically not identical, even in absence of magnetic fields. Specifically, symmetric kinetic coefficients are obtained only if the driving protocols are invariant under time-reversal.

Since our theory is structurally identical with linear irreversible thermodynamics, the analysis of Benenti *et al.* can now be repeated line by line for cyclic heat engines. This analogy in particular implies that, even if the constraints imposed by the laws of thermodynamics and microscopic reversibility are fully considered, cyclic heat engines operating at Carnot efficiency with finite power output might still be possible.

By borrowing from our results obtained for the multi-terminal model, we then prove a constraint on the kinetic coefficients of periodically driven systems, which is beyond these principles. This derivation exploits some natural properties of the Fokker-Planck operator generating the microscopic dynamics, e.g. preservation of the Boltzmann distribution, but is independent of model-specific details. The resulting bound on the kinetic coefficients is, up to a the normalization factor, identical to the one which lead to a universal bound on power for in the multi-terminal setup. As a consequence, we can prove that the power of cyclic micro- and nano-heat engines vanishes at least linearly when their efficiency comes close to the Carnot value. Finally, we complete our analysis by working out the paradigmatic case of a Brownian heat engine, whose working fluid consists only of a single

colloidal particle confined in a time-dependent harmonic trap. Within this case study, we prove that our new bound on power is asymptotically tight.

Bounding the Asymmetry of Positive Semidefinite Matrices

This chapter is devoted to the development of a self-contained mathematical theory on the asymmetry of positive semi-definite matrices. In the spirit of Crouzeix and Gutan [56], we define an asymmetry index as quantitative measure for this property, which is zero for a symmetric matrix and diverges for an antisymmetric one. We then consider a special type of matrices, which can be parametrized as $\mathbb{D} - \mathbb{T} \in \mathbb{R}^{m\times m}$. Three particularly interesting classes are obtained by following choices. First, the matrix $\mathbb{T}$ is assumed to be doubly stochastic and $\mathbb{D} = \mathbb{1}$, second, $\mathbb{T}$ is chosen doubly substochastic and $\mathbb{D} = \mathbb{1}$, third, $\mathbb{T}$ is chosen as a sum-symmetric matrix and $\mathbb{D}$ as the diagonal matrix filled with the ordered row-weights of $\mathbb{T}$. Within an increasingly involved analysis, which relies on the Birkhoff-von Neumann theorem and its generalizations, we prove that the asymmetry index of the first and the third type of matrices is bounded from above by $\cot(\pi/m)$, while for the second type the bound $\cot(\pi/(m+1))$ applies.

These studies are motivated by our investigations of the multi-terminal model. Indeed, since the sort of matrices investigated here is typical for the scattering approach to transport, the constraints derived in this chapter can be used to bound the efficiency of multi-terminal thermoelectric generators. However, apart from this important application, our results constitute an independent and original piece of linear algebra, which might be useful beyond the scope of this thesis.

Chapter 1

Introduction

1.1 Quantifying Performance: Efficiency vs Power

James Watt's steam engine, a pioneering invention, which triggered enormous technological progress during the early days of the industrial revolution, was one of the first practical devices that allowed the continuous conversion of heat into useful work. Ever since, the urge to explore the fundamental principles governing the performance of such machines was one of the major quests in thermodynamics. Within this powerful theory, any heat engine can be described by the general scheme shown in Fig. 1.1, which suggests two particularly important key figures. The first one, efficiency, is defined as the ratio of the delivered work and the heat uptake from the hot bath. As a direct consequence of the second law, this parameter is universally bounded by the Carnot value $\eta_C \equiv 1 - T_c/T_h$. The second one, power, which is given by the average work generated per unit time, is, however, out of reach for the laws of thermodynamics due to their notorious lack of time scales. Therefore, no fundamental bound on this figure is known by now. Nevertheless, it is generally expected that, under realistic conditions, the Carnot bound can be approached only in the quasi-static limit, which is useless from a practical point of view, since it comes with minuscule power. On the other hand, heat engines, which have been optimized in terms of power output, e.g. to be used in cars or power plants, typically operate at an efficiency much lower than the Carnot value [1–3]. It thus appears to be a general rule that high efficiency and large power mutually exclude each other [4].

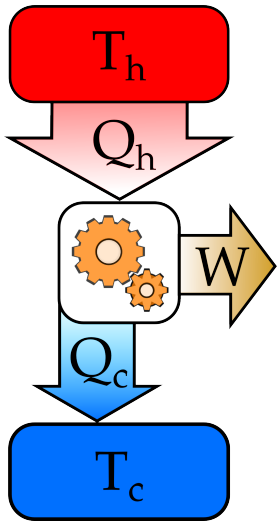

Figure 1.1: Thermodynamic scheme of a general heat engine. The machine operates between two reservoirs of respective temperature T_h and $T_c < T_h$. The heat Q_h supplied by the hot reservoir is partly converted into work W and partly passed on to the cold reservoir as waste heat Q_c.

For this reason, maximum efficiency is only of minor practical importance as a benchmark parameter. A possible alternative is provided by efficiency at maximum power, which can be studied within a simple but sound model proposed by Curzon and Ahlborn [1]. By implementing linear heat conduction [5] between two reservoirs and a heat engine

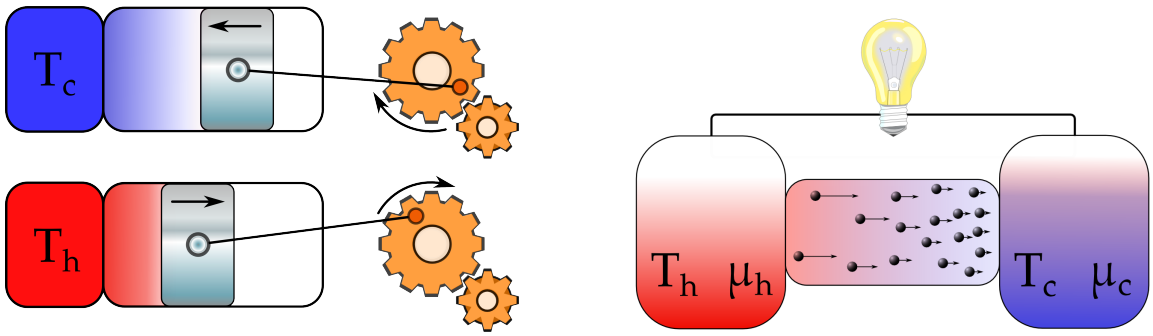

Figure 1.2: Two different kinds of heat engines. The left panel shows two snapshots of the operation cycle of a mechanical heat engine. The reciprocating piston extracts mechanical work from the pressure difference between the cold and the hot fluid and converts it into rotary motion. In the right panel, a thermoelectric heat engine is shown. Here, the temperature difference between the reservoirs leads to a constant electrical current from the low chemical potential μ_h to the higher one μ_c, which supplies power to an external load.

operating at Carnot efficiency, they obtained an endoreversible engine, whose efficiency at maximum power was found to be $\eta_{CA} \equiv 1-\sqrt{T_c/T_h}$. Quite surprisingly, this value, which is nowadays commonly known as Curzon-Ahlborn efficiency, is independent of the thermal conductivities characterizing the heat transport between the reservoirs and the machine. Therefore, one might assume that η_{CA} is valid beyond the endoreversible setup or even constitutes a universal upper bound similar to η_C. This issue was actively investigated during the last decade, see for example [3, 6–10]. Meanwhile, it has become clear that the concept of efficiency at maximum power is well-defined only in combination with a fixed space of variational parameters [10]. Nevertheless, universal results can be obtained within various classes of models, where a generic choice for these parameters exists [7,8].

1.2 Two Classes

According to their working principle, heat engines can be divided into two classes [11], which are illustrated in Fig. 1.2. Cyclic engines, like the steam engine, utilize a certain working, which is alternately coupled to a hot and a cold reservoir. By periodically compressing the fluid in the cold state, where the pressure is low, and expanding it in the hot state, which comes with a higher pressure, a net gain of mechanical work is obtained. Thermoelectric engines consist of two heat and particle reservoirs, which are permanently coupled by conductor. Due to the Seebeck effect [5], the heat current flowing naturally in this setup from the hot to the cold reservoir can drive a particle in the same direction. Hence, if the chemical potential of the cold reservoir is higher than the chemical potential of the hot one, this current generates electrical power, which can be extracted by closing the circuit via an external load.

While, today, cyclic heat engines are omnipresent in our everyday life, for example in cars, thermoelectric devices are so far reserved for special applications like deep space missions or laboratory equipment. This imbalance is surprising at first sight, since, due to their ability to work in a steady state without any moving parts, thermoelectric engines provide a lot of advantages compared to their mechanical counterparts. Unique benefits

are for example their small size, a quiet mode of operation, robustness and reliability, especially in demanding environments. These promising features and the associated potential applications, like waste heat recovery in vehicles [12], have triggered a great amount of scientific interest during the last decades as reviewed in [13–18]. Indeed, it has been shown theoretically that proper energy filtering leads to highly efficient thermoelectric engines [19], which, in principle, might even reach the Carnot bound [20, 21]. Nevertheless, no competitive devices that come even close to this limit are currently available. This major drawback has so far prevented a wide-ranging applicability of thermoelectrics.

An elementary and well established framework for the theoretical description of thermoelectric energy converters is provided by irreversible thermodynamics. The basic concepts of this phenomenological but powerful approach can be understood with the help of the setup shown in the right panel of Fig. 1.2. Two reservoirs, which are effectively inexhaustible and locally in thermal equilibrium, are put in contact such that, after a certain relaxation time, constant heat and particle currents J_q and J_ρ are established. In the linear response regime, these currents are related to the gradients $\Delta T \equiv T_\mathrm{h} - T_\mathrm{c}$ and $\Delta\mu \equiv \mu_\mathrm{h} - \mu_\mathrm{c}$ by a set of four kinetic coefficients $L_{\rho\rho}$, $L_{\rho q}$, $L_{q\rho}$ and L_{qq}. As we will detail in the next section, the crucial point here is that these coefficients are subject to a universal constraint, which is beyond the laws of thermodynamics and leads to profound consequences for the performance of thermoelectric heat engines.

In principle, the concepts of irreversible thermodynamics can be transferred to periodically driven systems as some studies have shown [22–24]. These results are, however, crucially tied to specific models and require rather involved and nonintuitive definitions for currents and gradients. In fact, despite the clear conceptual similarities, no universal framework that allows to describe cyclic heat engines on an equal footing with thermoelectric ones is currently available.

1.3 The Role of Time-Reversal Symmetry

The microscopic equations of motion governing the time evolution of an isolated system of particles, i.e., Hamilton's equations in the classical and Schrödinger's equation in the quantum realm, are invariant under a simultaneous reversal of time and momenta. This symmetry leads to a remarkable constraint on the phenomenological laws describing coupled transport processes on the macroscopic scale, which is established by Onsager's theorem. In the context of thermoelectricity, it states that the off-diagonal kinetic coefficients $L_{\rho q}$ and $L_{q\rho}$ respectively relating a temperature gradient to a particle current and a chemical potential gradient to a heat current must be identical.

Ever since its discovery, this reciprocal relation has turned out to be extremely useful for a plethora of applications. In particular, it lead to a unified theory, which allows to treat the various thermoelectric effects such as the Peltier, the Seebeck or the Thomson effect on an equal footing thus revealing their interdependencies [5, 25, 26]. Moreover, it can be used to establish a quantitative relation between the efficiency and power output of thermoelectric heat engines. Specifically, it can be shown that, at least in the linear regime, power is bounded by a quadratic function of efficiency, which vanishes at the Carnot value η_C and attains its maximum at the Curzon-Ahlborn value being $\eta_\mathrm{CA} = \eta_\mathrm{C}/2$ up to higher orders in ΔT.

This result must, however, be reassessed in the presence of an external magnetic field

B, which, as illustrated in Fig. 1.3, breaks the microscopic time-reversal symmetry and thus inhibits the reciprocal relation between the kinetic coefficients $L_{\rho q}$ and $L_{q\rho}$. We emphasize that, here, we adopt a local standpoint, where **B** enters the microscopic equations of motion as a fixed parameter. Indeed, in an extended system, which comprises the sources of the magnetic field, time-reversal symmetry is of course not broken such that the reciprocal relation can be recovered as $L_{\rho q}(\mathbf{B}) = L_{q\rho}(-\mathbf{B})$. This relation is, however, practically useless, since it involves the kinetic coefficients of two distinct setups, which differ in the direction of the magnetic field. In fact, for fixed **B**, besides the second law, no general restrictions on the kinetic coefficients are known.

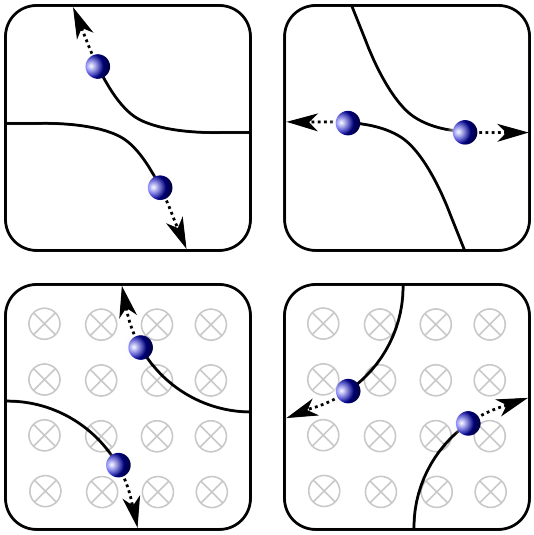

Figure 1.3: Illustration of the time-reversal symmetry breaking effect of a magnetic field. The upper left panel shows the collision of two identically charged particles in absence of external fields. As shown in the upper right panel, the particles trace back their original trajectories if their momenta are reversed after the scattering event, i.e., the process appears as running backwards in time. In the presence of a magnetic field, indicated by the symbol ⊗, the particles move on circles due to the Lorentz force (lower left panel). This force changes its direction as the momenta of the particles are reversed such that they depart from their original trajectories (lower right panel). Consequently, the magnetic field breaks the symmetry between the two directions of time.

Recently, in an intriguing paper, Benenti *et al.* pointed out that this additional freedom might allow to enhance the performance of thermoelectric engines in such a significant way that, in principle, even devices delivering finite power at Carnot efficiency seem to be achievable [27]. Such a spectacular result has two immediate implications. First, it serves us a new, so far unexplored, avenue to improve the efficiency of thermoelectric devices in practice. Second, from a conceptual point of view, it constitutes the first concrete option to overcome longstanding dilemma between high efficiency and large power output. The scrutiny of these aspects as well as the search for microscopic realizations are the major aims of this thesis.

The discoveries of Benenti *et al.* naturally raise the question whether a magnetic field might have similarly striking effects on the performance of cyclic heat engines. Systematic investigations of this issue require a general framework for the thermodynamic description of systems driven by periodic variations of certain control parameters, e.g. an external force or the temperature of their environment, rather than static gradients. Such a theory should in particular allow the definition of a linear response regime and, moreover, provide an appropriate generalization of Onsager's reciprocity relations for periodically driven systems. By now, none of these objectives has been accomplished on a general level beyond the trivial quasi-static limit, within which finite-time quantities like power can not be studied. Finding a proper way to overcome this limitation will be the subject of the second part of this thesis.

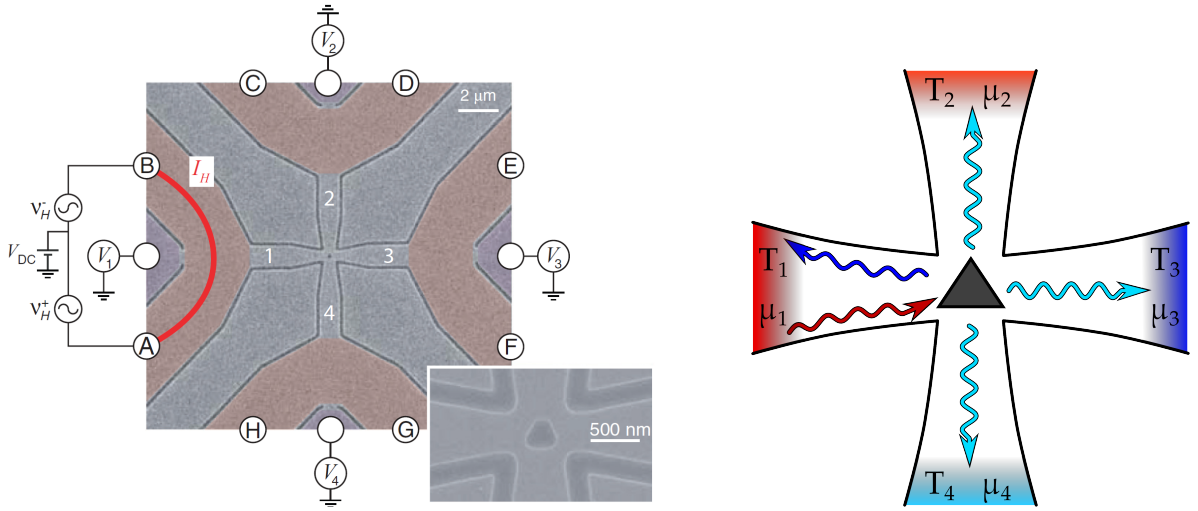

Figure 1.4: Thermoelectric nano-device. Four heat and particle reservoirs, whose temperatures $T_1, \ldots, T_4$ and chemical potentials $\mu_1, \ldots, \mu_4$ can be externally controlled, are connected to a central scattering region. The left panel shows the snapshot of an experimental realization as semiconductor heterostructure. Reprinted figure with permission from [28]. Copyright (2014) by the American Physical Society. The right panel illustrates the theoretical description of the device within the scattering approach. An incoming wave (red) in terminal 1 is partly reflected (dark blue) by the triangular scatterer and partly transmitted (light blue) to the other terminals.

1.4 On Small Scales

Nowadays, technological progress has paved the way for experiments on the micro- and nano-scale, within which thermodynamic processes can be scrutinized under the microscope by virtue of precise measurements of characteristic quantities like applied work or exchanged heat [28–34]. Due to their conceptual simplicity, such systems provide promising starting points for further investigations of the fundamental principles governing the relation between efficiency and power of thermoelectric and cyclic heat engines.

Thermoelectric nano-devices, like the one shown in Fig. 1.4, are particularly interesting subjects in this context. Two unique features facilitate their theoretical description significantly. First, interactions between charge carriers in these systems can typically be neglected such that a single particle picture applies. Second, the phase relaxation length of the charge carriers, which is the characteristic distance they can travel before their phase information is lost, is typically of the same order as the dimensions of device, i.e., several hundred nanometers. For this reason, incoherent effects such as dephasing or dissipation can be relegated to the reservoirs and do not have to be considered for the dynamics of the charge carriers, which, in fact, is fully captured by Schrödinger's equation.

These properties permit to describe thermoelectric transport in terms of a coherent quantum scattering process as illustrated in the right panel of Fig. 1.4. This idea was originally spawned by Landauer almost six decades ago [35]. In his pioneering work, considering a system of non-interacting particles sandwiched between two reservoirs, he derived a relation between the quantum mechanical reflection coefficient of a point scatterer and the electrical resistance of the corresponding sample. Building on his results,

a quite general formalism was developed, which allows to describe multiple electronic reservoirs (terminals) as well as coupled heat and matter transport [36–41]. In particular, this approach provides a rather simple and physically transparent formula relating kinetic coefficients to quantum mechanical transmission probabilities. Inelastic scattering events can be reintroduced into the formalism on a phenomenological level using fictitious heat and particle reservoirs (terminals), whose temperature and chemical potential are chosen such that they, on average, do not exchange any heat or particles with the real terminals. Such probe terminals are crucial for our purposes, since it is well known that for a pure two-terminal setup the matrix of kinetic coefficients is always symmetric, even in the presence of a magnetic field [39, 42]. We note that the original derivations of Landauer's formula and its subsequent generalizations utilize some plausible but heuristic arguments. Substantial research efforts on the basis of the Green-Kubo relations [43] have, however, shown that the crucial relation between kinetic coefficients and scattering amplitudes can be derived from first principles [44–51].

Like their thermoelectric counterparts, cyclic heat engines have meanwhile been downscaled to micrometers [29, 30]. A particular landmark was achieved by Blickle and Bechinger, who realized the theoretical proposal [7] of a minimalistic Stirling engine, whose working fluid consists only of a single colloidal particle [30]. Remarkably, both, efficiency and power, were accurately measured in this experiment.

The theoretical description of such systems requires a stochastic approach to take into account thermal fluctuations, which play an important role on small length and energy scales. A suitable dynamical principle is provided by the Fokker-Planck equation [52], which has proven to be a valuable tool within the emerging field of stochastic thermodynamics, see [10] for a comprehensive review. Although this approach has so far been mainly applied in the overdamped limit, where the dynamics of the system is dominated by strong friction forces, it can be easily extended to the underdamped regime, which is necessary to study the influence of a magnetic field [52, 53]. Moreover, periodically changing external forces [54] as well as environments with time-dependent temperature can be incorporated into the Fokker-Planck operator in a straightforward and thermodynamically consistent manner. It thus serves us an ideal theoretical basis to investigate the relation between power and efficiency in cyclic micro-engines with broken time-reversal symmetry.

Chapter 2

Thermodynamics of Thermoelectrics

In this chapter, we introduce the framework of linear irreversible thermodynamics as a basic tool for the description of thermoelectric devices. Focusing first on time-reversal symmetric systems, we briefly review the standard analysis, which leads to universal bounds on the efficiency and power of thermoelectric heat engines. We then explore how these bounds are affected by an external magnetic field. By summarizing the work of Benenti *et al.* [27], we show how the option of Carnot efficiency at finite power arises from broken time reversal symmetry.

2.1 Framework

Thermoelectric transport can conveniently be discussed within the setup sketched in Fig. 2.1. Two particle reservoirs of respective temperature T_c and $T_\mathrm{h} > T_\mathrm{c}$ and chemical potential μ_c and $\mu_\mathrm{h} < \mu_\mathrm{c}$ are connected by a conductor, which allows for the exchange of heat and particles. Consequently, as soon as the steady state is reached, constant heat and particle currents, J_q and J_ρ, flow from the hot to the cold reservoir. Time-reversal symmetry can be broken in this setup by applying a constant magnetic field $\mathbf{B}$ to the conductor.

We now assume that both, the temperature difference $\Delta T \equiv T_\mathrm{h} - T_\mathrm{c} > 0$ and the chemical potential difference $\Delta\mu \equiv \mu_\mathrm{h} - \mu_\mathrm{c} < 0$ are small compared to their respective reference values, which we chose to be T_c and μ_c. In this linear response regime, the currents J_ρ and J_q are related to the affinities

$$\mathcal{F}_\rho \equiv \Delta\mu/T_\mathrm{c} \quad \text{and} \quad \mathcal{F}_q \equiv \Delta T/T_\mathrm{c}^2 \tag{2.1}$$

via the phenomenological equations [5]

$$J_\rho = L_{\rho\rho}\mathcal{F}_\rho + L_{\rho q}\mathcal{F}_q \quad \text{and} \quad J_q = L_{q\rho}\mathcal{F}_\rho + L_{qq}\mathcal{F}_q. \tag{2.2}$$

The constant rate of entropy production accompanying this transport process reads

$$\dot{S} = \mathcal{F}_\rho J_\rho + \mathcal{F}_q J_q = L_{\rho\rho}\mathcal{F}_\rho^2 + L_{qq}\mathcal{F}_q^2 + (L_{\rho q} + L_{q\rho})\mathcal{F}_\rho\mathcal{F}_q. \tag{2.3}$$

Clearly, the crucial quantities of this formalism are the kinetic coefficients L_{ik} $(i, k = \rho, q)$, which are subject to two fundamental constraints. First the second law requires $\dot{S} \geq 0$, which is equivalent to the conditions

$$L_{\rho\rho}, L_{qq} \geq 0 \quad \text{and} \quad L_{\rho\rho}L_{qq} - (L_{\rho q} + L_{q\rho})^2/4 \geq 0. \tag{2.4}$$

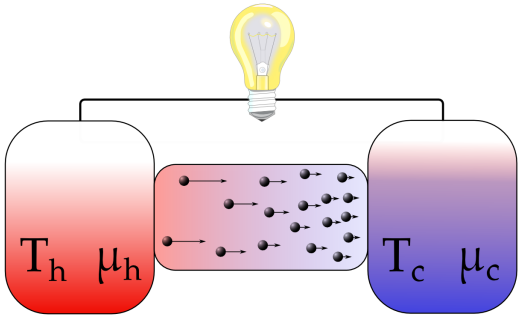

Figure 2.1: Operation principle of a thermoelectric heat engine. Two inexhaustible reservoirs of respective temperature T_h and $T_\mathrm{c} < T_\mathrm{h}$ and chemical potential μ_h and $\mu_\mathrm{c} > \mu_\mathrm{h}$ are coupled via a conductor, which accommodates constant heat and particle currents J_q and J_ρ. For $J_\rho > 0$, the device delivers the power $P = (\mu_\mathrm{c} - \mu_\mathrm{h})J_\rho$.

Second, Onsager's theorem implies the reciprocal relation

$$L_{\rho q}(\mathbf{B}) = L_{q\rho}(-\mathbf{B}). \tag{2.5}$$

Here, we have reintroduced the external magnetic field $\mathbf{B}$, which, for convenience, is notationally suppressed throughout the thesis whenever there is no need to indicate it explicitly. We emphasize that, besides (2.4) and (2.5), no further general relations between the off-diagonal kinetic coefficients $L_{\rho q}$ and $L_{q\rho}$ are known.

Choosing the affinities $\mathcal{F}_\rho$ and $\mathcal{F}_q$ such that $J_\rho > 0$ turns the general setup discussed so far into a proper heat engine, which is characterized by the power output

$$P \equiv -\Delta\mu J_\rho = -T_\mathrm{c}\mathcal{F}_\rho J_\rho = -T_\mathrm{c}\mathcal{F}_\rho(L_{\rho\rho}\mathcal{F}_\rho + L_{\rho q}\mathcal{F}_q) \tag{2.6}$$

and the efficiency

$$\eta \equiv \frac{P}{J_q} = -\frac{T_\mathrm{c}\mathcal{F}_\rho J_\rho}{J_q} = -\frac{T_\mathrm{c}\mathcal{F}_\rho(L_{\rho\rho}\mathcal{F}_\rho + L_{\rho q}\mathcal{F}_q)}{L_{q\rho}\mathcal{F}_\rho + L_{qq}\mathcal{F}_q}. \tag{2.7}$$

Here, we used the phenomenological equations (2.2) to express currents in terms of affinities. By recalling the rate of entropy production (2.3) and invoking the second law $\dot{S} \geq 0$, it is now straightforward to verify that η is universally bounded by the Carnot efficiency $\eta_\mathrm{C} \equiv 1 - T_\mathrm{c}/T_\mathrm{h}$, which becomes $\eta_\mathrm{C} = \Delta T/T_\mathrm{c} + \mathcal{O}(\Delta T^2) = T_\mathrm{c}\mathcal{F}_q + \mathcal{O}(\Delta T^2)$ in the linear response regime.

2.2 Time-Reversal Symmetric Engines: Bounds on Efficiency and Power

In the absence of a magnetic field, the reciprocal relation (2.5) becomes

$$L_{\rho q} = L_{q\rho}. \tag{2.8}$$

Due to this symmetry, the features of a time-reversal symmetric thermoelectric heat engine are completely determined by three kinetic coefficients $L_{\rho\rho}, L_{\rho q}$ and L_{qq}. The performance of such a device can be quantified in terms of a single dimensionless parameter. A convenient choice is given by the thermoelectric figure of merit [15, 27]

$$ZT \equiv \frac{L_{\rho q}^2}{L_{\rho\rho}L_{qq} - L_{\rho q}^2}, \tag{2.9}$$

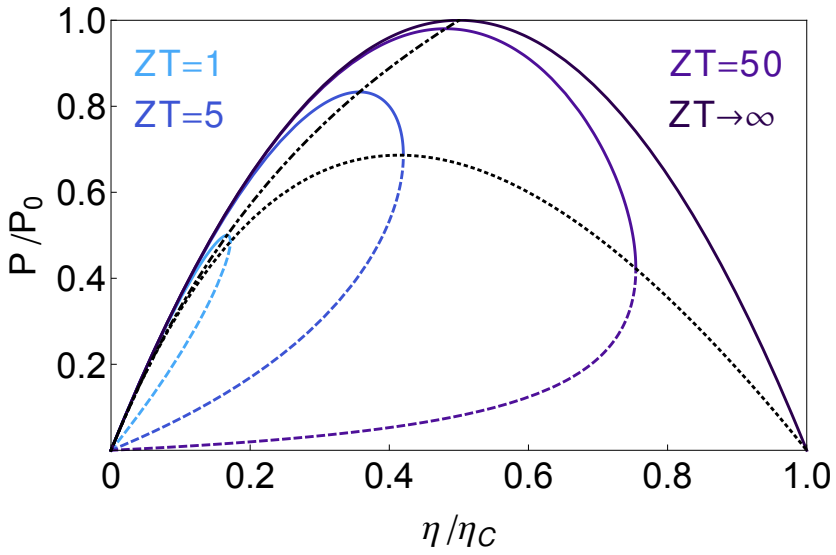

Figure 2.2: Plots of normalized power at given efficiency (2.14) as a function of the efficiency η in units of η_C for different values of ZT. The solid lines correspond to $P_+(ZT,\eta)$, the dashed ones to $P_-(ZT,\eta)$. The dotted line indicates the relation between maximum efficiency (2.10) and power at maximum efficiency (2.18) for $0 \leq ZT < \infty$. Analogously, the dashdotted line corresponds to maximum power (2.16) and efficiency at maximum power (2.11).

which must be non-negative as a consequence of the inequalities (2.4) following from the second law.

We will now first discuss bounds on efficiency. Optimizing (2.7) and (2.6) respectively with respect to $\mathcal{F}_\rho$ under the condition $P > 0$ yields the expressions

$$\eta_{\max}(ZT) = \eta_C \frac{\sqrt{ZT+1}-1}{\sqrt{ZT+1}+1} \tag{2.10}$$

for maximum efficiency and

$$\eta^*(ZT) = \eta_C \frac{ZT}{4+2ZT} \tag{2.11}$$

for efficiency at maximum power. Both of these quantities are monotonically increasing functions of ZT. In the limit $ZT \to \infty$, they reach their respective upper bounds, which are η_C for $\eta_{\max}$ and $\eta_{CA} = \eta_C/2$ for η^*.

For a complete assessment of the performance of a heat engine, its power output must be taken into account. Here, we introduce a joint benchmark parameter covering both, power and efficiency. To this end, we solve (2.7) for $\mathcal{F}_\rho$ thus fixing the normalized efficiency

$$\bar{\eta} \equiv \frac{\eta}{\eta_C}. \tag{2.12}$$

Inserting the resulting relation

$$\mathcal{F}_\rho = -\mathcal{F}_q \frac{L_{qq}}{L_{\rho q}} \left(\frac{ZT(\bar{\eta}+1)}{(1+ZT)} - \sqrt{\frac{ZT^2(\bar{\eta}+1)^2}{4(1+ZT)^2} - \frac{ZT\bar{\eta}}{1+ZT}} \right) \tag{2.13}$$

into (2.6) yields the power at given efficiency $0 \le \eta \le \eta_C$,

$$P_\pm(ZT,\eta) = 4P_0\bar{\eta}\left(\frac{2+ZT(1-\bar{\eta})}{2(1+ZT)} \pm \sqrt{\frac{ZT^2(1+\bar{\eta})^2}{4(1+ZT)^2} - \frac{ZT\bar{\eta}}{1+ZT}}\right), \tag{2.14}$$

where the constraint

$$\frac{4\bar{\eta}}{(\bar{\eta}-1)^2} \le ZT < \infty, \tag{2.15}$$

which is equivalent to $\eta \le \eta_{\max}(ZT)$ must be obeyed. The two branches of the function $P_\pm(ZT,\eta)$, which are plotted in Fig. 2.2, correspond to two admissible values of P for fixed η and ZT. For $\eta = \eta^*$, the upper branch $P_+(ZT,\eta) \ge P_-(ZT,\eta)$ reaches its maximum

$$P_{\max}(ZT) = P_0\frac{ZT}{1+ZT}. \tag{2.16}$$

Here, we defined the standard power

$$P_0 \equiv \frac{T_c\mathcal{F}_q^2 L_{qq}}{4}. \tag{2.17}$$

The maximum efficiency $\eta_{\max}$ is attained at the power output

$$P^*(ZT) = \frac{4P_0}{\sqrt{1+ZT}}\frac{\sqrt{1+ZT}-1}{\sqrt{1+ZT}+1}. \tag{2.18}$$

As shown by the dotted line in Fig. 2.2, $P^*(ZT)$ decays linearly to zero as η approaches η_C. This result confirms the general expectation that a high efficiency inevitably comes at the price of small power. Moreover, in the limit $ZT \to \infty$, (2.14) reduces to

$$P_+(\eta) = 4P_0\bar{\eta}(1-\bar{\eta}) \quad \text{and} \quad P_-(\eta) = 0. \tag{2.19}$$

Since, for any η, $P_+(\eta)$ increases monotonically with ZT, it follows that the quadratic function of efficiency (2.19) is a universal bound on power in the sense that it applies to any time-reversal-symmetric thermoelectric heat engine in linear response.

2.3 Broken Time-Reversal Symmetry: Profound Changes

In the presence of a fixed magnetic field $\mathbf{B}$, the reciprocal relation (2.5) does not lead to any restrictions on the kinetic coefficients such that the second law (2.4), effectively, is the only constraint. Therefore, in contrast to the symmetric case, where one dimensionless parameter is sufficient, two such parameters are necessary to quantify the performance of thermoelectric heat engines with broken time-reversal symmetry. Following Benenti *et al.*, we introduce

$$x \equiv \frac{L_{\rho q}}{L_{q\rho}} \quad \text{and} \quad y \equiv \frac{L_{\rho q}L_{q\rho}}{L_{\rho\rho}L_{qq} - L_{\rho q}L_{q\rho}}, \tag{2.20}$$

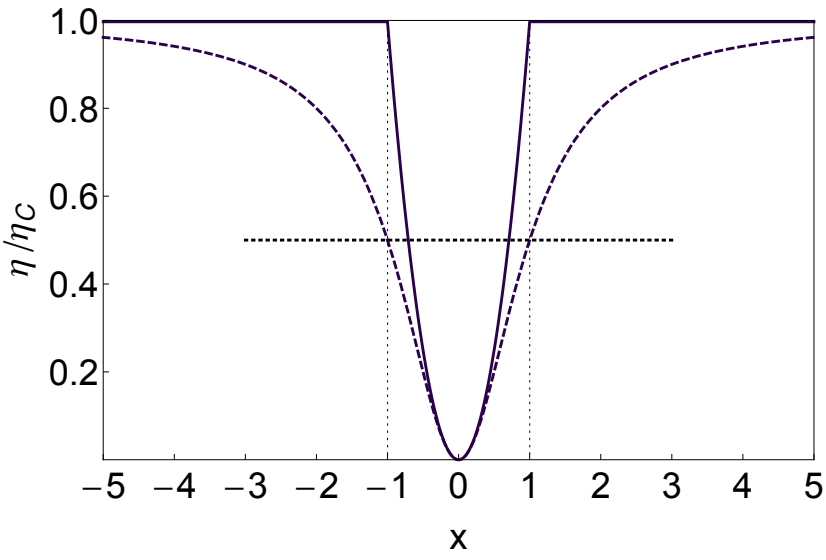

Figure 2.3: Bounds on efficiency for thermoelectric heat engines with broken time-reversal symmetry in units of η_C as functions of the asymmetry parameter x. The solid line shows the bound on maximum efficiency (2.25), the dashed line corresponds to the bound on efficiency at maximum power (2.26). The dotted line indicates the Curzon-Ahlborn value $\eta_C/2$.

where x quantifies the asymmetry between the kinetic coefficients $L_{\rho q}$ and $L_{q\rho}$ and y is a generalization of the figure of merit (2.9), to which it reduces for $\mathbf{B} = 0$. These parameters are related via the inequalities

$$h(x) \leq y \leq 0 \quad \text{for} \quad x < 0 \quad \text{and} \quad 0 \leq y \leq h(x) \quad \text{for} \quad x \geq 0 \tag{2.21}$$

with

$$h(x) \equiv \frac{4x}{(x-1)^2}, \tag{2.22}$$

which follow from (2.4) and thus express the second law.

In terms x and y, the maximum efficiency and the efficiency at maximum power, which are obtained in the same way as in the time-reversal symmetric case, read

$$\eta_{\max}(x,y) = \eta_C x \frac{\sqrt{y+1}-1}{\sqrt{y+1}+1} \tag{2.23}$$

and

$$\eta^*(x,y) = \eta_C \frac{xy}{4+2y}, \tag{2.24}$$

respectively. For any $x \in \mathbb{R}$, these functions increase monotonically with $|y|$. Consequently, setting $y = h(x)$ leads to the upper bounds

$$\eta_{\max}(x) \equiv \eta_{\max}(x, h(x)) = \eta_C \begin{cases} 1 & \text{for} \quad |x| \geq 1 \\ x^2 & \text{for} \quad |x| < 1 \end{cases} \tag{2.25}$$

and

$$\eta^*(x) \equiv \eta^*(x, h(x)) = \eta_C \frac{x^2}{1+x^2}, \tag{2.26}$$

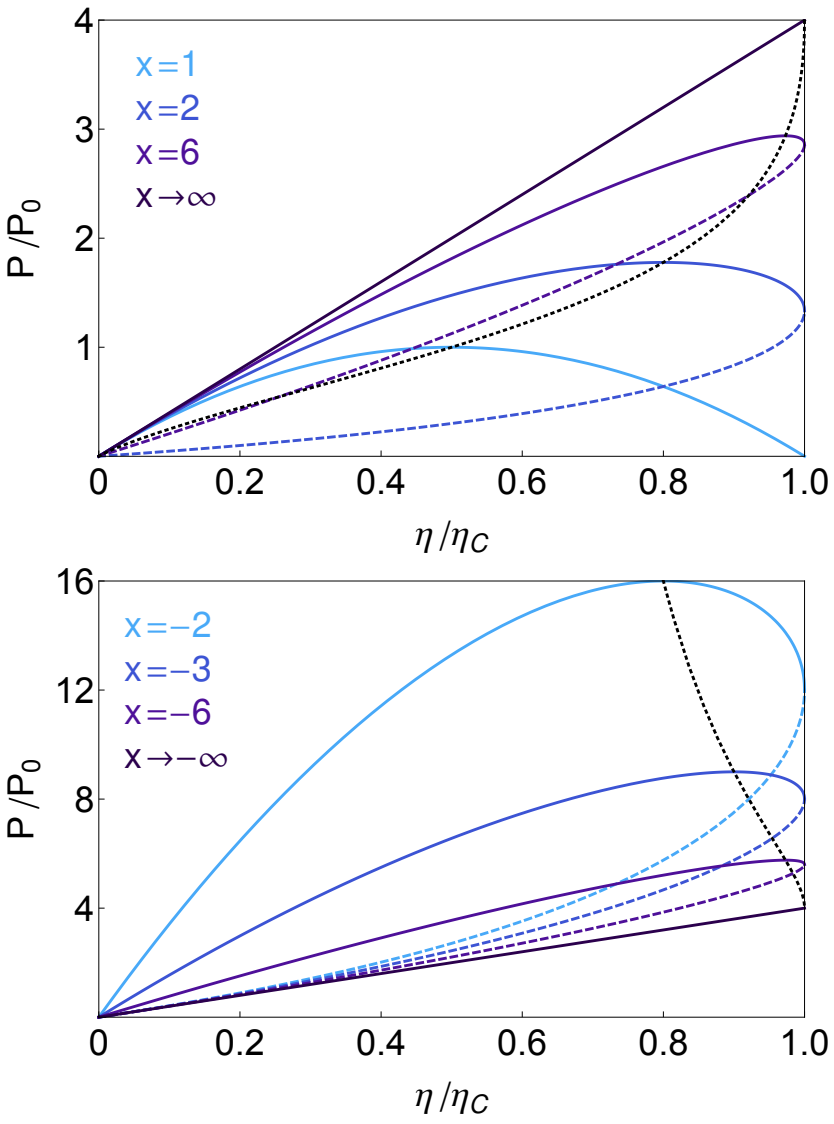

Figure 2.4: Bounds on the power output of a thermoelectric heat engine with broken time-reversal symmetry in unites of P_0 as functions of the efficiency in units of η_C for various positive (upper panel) and negative (lower panel) values of the asymmetry parameter x. The solid lines correspond to the upper bound (2.30), the dashed ones to the lower bound (2.31). In the limit $x \to \pm\infty$, both of these bounds converge to $P = 4P_0\eta/\eta_C$. The dotted line, in both panels, indicates the relation between the upper bound on maximum power (2.34) and the bound (2.26) on efficiency at maximum power.

which are plotted in Fig. 2.3. We find that, in principle, the maximum efficiency can reach η_C for any $|x| \geq 1$. Moreover, as $|x|$ becomes larger than 1, the efficiency at maximum power can surpass its symmetric bound $\eta_C/2$, which holds only for $|x| = 1$. In the limit $x \to \pm\infty$, it might even approach the Carnot value. This result suggests that thermoelectric heat engines with broken time-reversal symmetry can outperform their symmetric counterparts.

We will now explore how the bound on power (2.19) is affected by a magnetic field. Following the lines of the previous section, we fix the efficiency (2.7) by putting

$$\mathcal{F}_\rho = -\mathcal{F}_q \frac{L_{qq}}{L_{\rho q}} \left(\frac{y(x+\bar{\eta})}{2(1+y)} - \sqrt{\frac{y^2(x+\bar{\eta})}{4(1+y)^2} - \frac{xy\bar{\eta}}{1+y}} \right). \tag{2.27}$$

Evaluating (2.6) then yields the power output

$$P_\pm(x,y,\eta) = 4P_0\bar{\eta} \left(\frac{x(2+y) - y\bar{\eta}}{2x(1+y)} \pm \sqrt{\frac{y^2(x+\bar{\eta})^2}{4x^2(1+y)^2} - \frac{y\bar{\eta}}{x(1+y)}} \right) \tag{2.28}$$

as a function of x, y and η, where $x \in \mathbb{R}$, $0 \le \eta \le \eta_{\max}(x)$,

$$\frac{4x\bar{\eta}}{(x-\bar{\eta})^2} \le y \le h(x) \quad \text{if} \quad x \ge 0 \quad \text{and} \quad h(x) \le y \le \frac{4x\bar{\eta}}{(x-\bar{\eta})^2} \quad \text{if} \quad x < 0. \tag{2.29}$$

For any x and η within this range, the two branches $P_+(x,y,\eta)$ and $P_-(x,y,\eta) \le P_-(x,y,\eta)$ of (2.28) are, respectively, monotonically increasing and decreasing with respect to $|y|$. Hence, by setting $y = h(x)$, we obtain the upper bound

$$P_+(x,\eta) \equiv P_+(x,h(x),\eta) = 4P_0\bar{\eta}\frac{x^2 - 1 + 2(1-\bar{\eta}) + 2\sqrt{(x^2-\bar{\eta})(1-\bar{\eta})}}{(1+x)^2} \tag{2.30}$$

and the lower bound

$$P_-(x,\eta) \equiv P_-(x,h(x),\eta) = 4P_0\bar{\eta}\frac{x^2 - 1 + 2(1-\bar{\eta}) - 2\sqrt{(x^2-\bar{\eta})(1-\bar{\eta})}}{(1+x)^2}. \tag{2.31}$$

on power. These bounds are plotted in Fig. 2.4. Strikingly, we observe that for $x > 1$ and $x \le -1$, Carnot efficiency might be reached at the finite power

$$P_+(x,\eta_{\mathrm{C}}) = P_-(x,\eta_{\mathrm{C}}) = 4P_0\frac{x-1}{x+1}. \tag{2.32}$$

This result is *a priori* surprising, since the elementary analysis presented here has fully incorporated the constraints imposed by the second law. It can be explained as follows. In the light of the reciprocal relation (2.5), the expression (2.3) for the total rate of entropy production suggests a natural splitting of the currents J_ρ and J_q into a reversible and irreversible part defined by

$$J_i^{\mathrm{rev}} \equiv \frac{L_{ij} - L_{ji}}{2}\mathcal{F}_j \quad \text{and} \quad J_i^{\mathrm{irr}} \equiv L_{ii}\mathcal{F}_i + \frac{L_{ij} + L_{ji}}{2}\mathcal{F}_j \quad \text{with} \quad i,j = \rho,q. \tag{2.33}$$

Obviously, J_i^{rev} vanishes for $\mathbf{B} = 0$, i.e., unbroken time-reversal symmetry. However, once the latter is broken, although not contributing to $\dot{S}$, the reversible currents can, in principle, become arbitrarily large, since besides (2.4), no further general relations between $L_{ij}(\mathbf{B})$ and $L_{ji}(\mathbf{B})$ are known. Such unconstrained reversible currents ultimately give rise to the possibility of dissipationless transport and thus permit Carnot efficiency at finite power as first noticed by Benenti *et al.* [27].

For $\eta = \eta^*(x)$, the upper bound on power (2.30) attains its global maximum

$$P_+(x) \equiv P_+(x,\eta^*(x)) = P_0\frac{4x^2}{(1+x)^2} \tag{2.34}$$

with respect to η. Like the expression (2.32) for the upper bound on power at Carnot efficiency, this result suggests that the power output might diverge as x approaches -1 from below. These singularities are, however, only apparent as the following argument shows. We recall that, in order to obtain (2.28), the affinity $\mathcal{F}_\rho$ was chosen according to (2.27). For $y = h(x)$, $x < -1$ and $\eta = \eta_{\mathrm{C}}$, this relation becomes

$$\mathcal{F}_\rho = \mathcal{F}_q\frac{L_{qq}}{L_{\rho q}}\frac{2x}{x+1}. \tag{2.35}$$

Consequently, since the analysis leading to (2.32) and (2.34) relies on the linear response assumption $|\mathcal{F}_\rho| \ll \mu_\mathrm{c}/T_\mathrm{c}$, these expressions are justified only for

$$\mathcal{F}_q \ll \frac{\mu_\mathrm{c}}{T_\mathrm{c} L_{qq}} |L_{\rho q}| \frac{x+1}{2x}. \tag{2.36}$$

Inserting the definition of P_0, (2.17), and (2.36) into (2.32) and (2.34) shows that, for $x \leq -1$, we must have

$$P_+(x, \eta_\mathrm{C}) = P_-(x, \eta_\mathrm{C}) \ll \frac{\mu_\mathrm{c}^2 L_{\rho q}^2}{T_\mathrm{c} L_{qq}} \frac{x^2-1}{4x^2} \tag{2.37}$$

and

$$P_+(x) \ll \frac{\mu_\mathrm{c}^2}{T_\mathrm{c}} \frac{L_{\rho q}^2}{4 L_{qq}} \tag{2.38}$$

whenever the linear response regime applies.

Finally, as a special system, we consider a fully antisymmetric engine, which is characterized by vanishing diagonal kinetic coefficients $L_{\rho\rho} = L_{qq} = 0$ and asymmetry parameter $x = -1$, i.e., $L_{\rho q} = -L_{q\rho} \neq 0$. Since, under these conditions, the rate of entropy production (2.3) vanishes irrespective of the values of the affinities $\mathcal{F}_\rho$ and $\mathcal{F}_q$, such a device automatically operates reversibly, i.e., at Carnot efficiency. Moreover, it delivers the finite power output

$$P = -T_\mathrm{c} \mathcal{F}_q \mathcal{F}_\rho L_{\rho q}, \tag{2.39}$$

which follows directly from (2.6). We note that (2.39) is linear in both affinities. such that optimization with respect to $\mathcal{F}_\rho$ would be meaningless. Therefore, the concept of maximum power, as we use it here, is ill-defined for a fully antisymmetric thermoelectric heat engine.

2.4 Conclusion

In summary, we have introduced the basic notions of linear irreversible thermodynamics and applied them to study the performance of thermoelectric heat engines in terms of various benchmark parameters. For time-reversal symmetric devices, we found that these parameters depend only on the thermoelectric figure of merit $ZT \geq 0$, where best performance is achieved for $ZT \to \infty$. This limit is often referred to as strong coupling, since it requires a particle current J_ρ that is proportional to the heat current J_q [6,10]. It has been shown that this condition can indeed be realized if the device acts as a perfect energy filter, whose energy dependent transmission function consists of a single delta-peak [19–21].

In the second part of this chapter, we investigated the influence of an external magnetic field on the performance of thermoelectric heat engines. By following the lines of Benenti *et al.*, we demonstrated that broken time-reversal symmetry might allow engines, which produce finite power while operating reversibly. We have shown that this intriguing phenomenon can be traced back to reversible currents, which do not contribute to the total rate of entropy production. The search for putative bounds on the kinetic coefficients that constrain these currents will be the central subject of the next chapter.

Chapter 3

Multi-Terminal Systems

For progress investigating possible constraints on the kinetic coefficients beyond the second law and Onsager's reciprocal relations, the phenomenological setup discussed in the previous chapter must be made more specific. Here, we focus on thermoelectric nano-devices, which can be described within the Landauer-Büttiker approach. After introducing the general multi-terminal setup, we briefly summarize the essentials of this formalism, which provides explicit expressions for the kinetic coefficients in terms of quantum mechanical transmission probabilities encoding the microscopic properties of the system. Inelastic scattering events, which are crucial to break the symmetry between the off-diagonal kinetic coefficients, are incorporated phenomenologically in terms of probe-terminals.

The arguably most simple model of this type, for which a non-symmetric matrix of kinetic coefficients can be obtained, thus involves one probe terminal besides the two real terminals. For this minimal setup, we show that current-conservation indeed leads to an additional constraint on the kinetic coefficients, which is stronger than the second law. Moreover, this constraint implies that, once the timer-reversal symmetry is broken, the efficiency of the three-terminal model as a thermoelectric heat engine must be substantially smaller than the Carnot value. By generalizing the concepts introduced for the three-terminal case, we prove that analogous results hold for models with an arbitrary number of terminals. The corresponding bounds become, however, successively weaker as this number increases. In the limit of infinitely many probes, we end up with the situation described by Benenti *et al.* [27], in which the second law is effectively the only constraint.

This result prompts the question, whether not only efficiency but also power can be bounded. Here, we show that, at least within the multi-terminal setup, such bounds indeed exist. Specifically, we derive a universal constraint on the kinetic coefficients that is independent of the number of terminals and allows to recover the quadratic relation between power and efficiency known from time-reversal symmetric engines. Furthermore, for systems involving only a few terminals, we provide strong numerical evidence for the existence of an even stronger constraint, which leads to a significantly sharper bound on power than the one discussed before.

In order to illustrate our general results, in the last part of this chapter, we discuss a simple mechanical model for a thermoelectric heat engine based on the Nernst effect. In particular we show that this model saturates the corresponding bounds on maximum efficiency and efficiency at maximum power in the limit of large magnetic fields and low particle densities in the reservoirs.

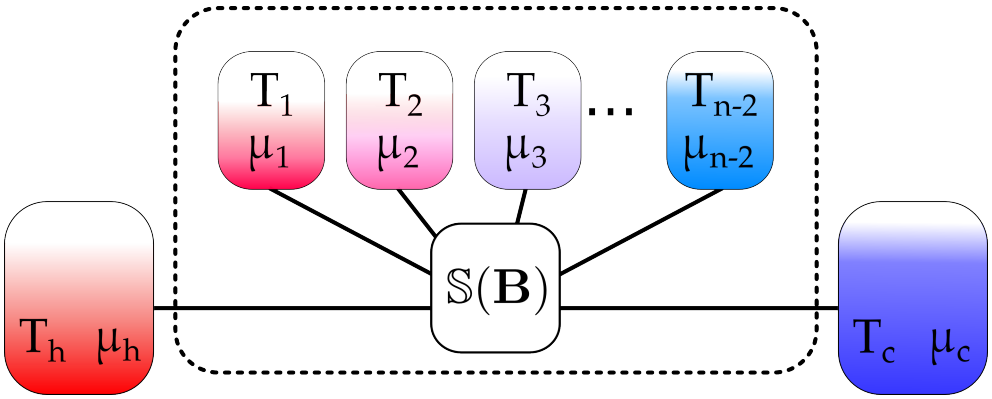

Figure 3.1: Sketch of the multi-terminal model for thermoelectric transport. On the effective level, where the terminals $1, \ldots, n-2$ are considered as probes, the entire dashed box represents a conductor, which is connected to two real terminals. The symbols are explained in the main text of Sec. 3.1.

3.1 Setup

We consider the model schematically shown in Fig. 3.1. A central region equipped with a constant magnetic field $\mathbf{B}$ is connected to n independent electronic reservoirs (terminals) of respective chemical potential μ_α and temperature T_α, where $\alpha = \mathrm{h}, 1, \ldots, n-2, \mathrm{c}$.

3.1.1 Thermodynamic Description

Currents and Affinities

In order to describe the thermoelectric transport process in a multi-terminal geometry within the framework of linear irreversible thermodynamics, we fix the reference chemical potential μ_c and temperature T_c and define the affinities

$$\mathcal{F}_\rho^\alpha \equiv \frac{\mu_\alpha - \mu_\mathrm{c}}{T_\mathrm{c}} \equiv \frac{\Delta\mu_\alpha}{T_\mathrm{c}} \quad \text{and} \quad \mathcal{F}_q^\alpha \equiv \frac{T_\alpha - T_\mathrm{c}}{T_\mathrm{c}^2} \equiv \frac{\Delta T_\alpha}{T_\mathrm{c}^2} \quad \text{for} \quad \alpha = \mathrm{h}, 1, \ldots, n-2 \tag{3.1}$$

By J_ρ^α and J_q^α we denote the particle and the heat current leaving the reservoir α, respectively. Within the linear response regime, which is valid as long as the chemical potential and temperature differences $\Delta\mu_\alpha$ and ΔT_α are small compared to the respective references values, currents and affinities are related via the phenomenological equations [5]

$$\mathbf{J} = \mathbb{L}^n \boldsymbol{\mathcal{F}}. \tag{3.2}$$

Here, we introduced the current vector

$$\mathbf{J} \equiv \begin{pmatrix} \mathbf{J}_\mathrm{h} \\ \vdots \\ \mathbf{J}_{n-2} \end{pmatrix} \quad \text{and the affinity vector} \quad \boldsymbol{\mathcal{F}} \equiv \begin{pmatrix} \boldsymbol{\mathcal{F}}_\mathrm{h} \\ \vdots \\ \boldsymbol{\mathcal{F}}_{n-2} \end{pmatrix} \tag{3.3}$$

with the respective subunits

$$\mathbf{J}_\alpha \equiv \begin{pmatrix} J_\rho^\alpha \\ J_q^\alpha \end{pmatrix} \quad \text{and} \quad \boldsymbol{\mathcal{F}}_\alpha \equiv \begin{pmatrix} \mathcal{F}_\rho^\alpha \\ \mathcal{F}_q^\alpha \end{pmatrix}. \tag{3.4}$$

Analogously, we divide the matrix of kinetic coefficients

$$\mathbb{L}^n \equiv \begin{pmatrix} \mathbb{L}^n_{\mathrm{hh}} & \cdots & \mathbb{L}^n_{\mathrm{h}\,n-2} \\ \vdots & \ddots & \vdots \\ \mathbb{L}^n_{n-2\mathrm{h}} & \cdots & \mathbb{L}^n_{n-2\,n-2} \end{pmatrix} \in \mathbb{R}^{2(n-1)\times 2(n-1)} \tag{3.5}$$

into 2×2 blocks $\mathbb{L}^n_{\alpha\beta} \in \mathbb{R}^{2\times 2}$, where $\alpha,\beta = \mathrm{h},\ldots,n-2$.

Heat Engine

A thermoelectric heat engine can be realized within the multi-terminal model by considering the terminals $1,\ldots,n-2$ as probes mimicking inelastic scattering. To this end, the temperature and chemical potential of the corresponding reservoirs have to be adjusted in such a way that they do not exchange any net quantities with the real terminals. This constraint reads

$$\begin{pmatrix} 0 \\ \vdots \\ 0 \end{pmatrix} = \begin{pmatrix} \mathbf{J}_1 \\ \vdots \\ \mathbf{J}_{n-2} \end{pmatrix} = \begin{pmatrix} \mathbb{L}^n_{1\mathrm{h}} & \cdots & \mathbb{L}^n_{1\,n-2} \\ \vdots & \ddots & \vdots \\ \mathbb{L}^n_{n-2\mathrm{h}} & \cdots & \mathbb{L}^n_{n-2\,n-2} \end{pmatrix} \begin{pmatrix} \boldsymbol{\mathcal{F}}_1 \\ \vdots \\ \boldsymbol{\mathcal{F}}_{n-2} \end{pmatrix}. \tag{3.6}$$

By assuming the matrix

$$\mathbb{L}^n_{[[1]]} \equiv \begin{pmatrix} \mathbb{L}^n_{11} & \cdots & \mathbb{L}^n_{1\,n-2} \\ \vdots & \ddots & \vdots \\ \mathbb{L}^n_{n-2\,1} & \cdots & \mathbb{L}^n_{n-2\,n-2} \end{pmatrix} \in \mathbb{R}^{2(n-2)\times 2(n-2)} \tag{3.7}$$

to be invertible, we can solve the self-consistency relations (3.6) for $\boldsymbol{\mathcal{F}}_1,\ldots,\boldsymbol{\mathcal{F}}_{n-2}$ obtaining

$$\begin{pmatrix} \boldsymbol{\mathcal{F}}_1 \\ \vdots \\ \boldsymbol{\mathcal{F}}_{n-2} \end{pmatrix} = -\left(\mathbb{L}^n_{[[1]]}\right)^{-1} \begin{pmatrix} \mathbb{L}^n_{1\mathrm{h}} \\ \vdots \\ \mathbb{L}^n_{n-2\,\mathrm{h}} \end{pmatrix}. \tag{3.8}$$

After inserting this solution into (3.2) and identifying the heat current $J_q \equiv J^{\mathrm{h}}_q$ and the particle current $J_\rho \equiv J^{\mathrm{h}}_\rho$ leaving the hot reservoir, we end up with the reduced system

$$\begin{pmatrix} J_\rho \\ J_q \end{pmatrix} = \mathbb{L} \begin{pmatrix} \mathcal{F}_\rho \\ \mathcal{F}_q \end{pmatrix} \tag{3.9}$$

of phenomenological equations. Here, the effective matrix of kinetic coefficients is given by

$$\mathbb{L} \equiv \mathbb{L}^n_{\mathrm{hh}} - \left(\mathbb{L}^n_{\mathrm{h}1},\ldots,\mathbb{L}^n_{\mathrm{h}\,n-2}\right)\left(\mathbb{L}^n_{[[1]]}\right)^{-1} \begin{pmatrix} \mathbb{L}^n_{1\mathrm{h}} \\ \vdots \\ \mathbb{L}^n_{n-2\,\mathrm{h}} \end{pmatrix} \equiv \begin{pmatrix} L_{\rho\rho} & L_{\rho q} \\ L_{q\rho} & L_{qq} \end{pmatrix} \tag{3.10}$$

and the affinities $\mathcal{F}_\rho \equiv \mathcal{F}^{\mathrm{h}}_\rho = \Delta\mu_{\mathrm{h}}/T_{\mathrm{c}} < 0$ and $\mathcal{F}_q \equiv \mathcal{F}^{\mathrm{h}}_q = \Delta T_{\mathrm{h}}/T^2_{\mathrm{c}} > 0$ have to be chosen such that $J_\rho > 0$ for the model to work as a proper heat engine.

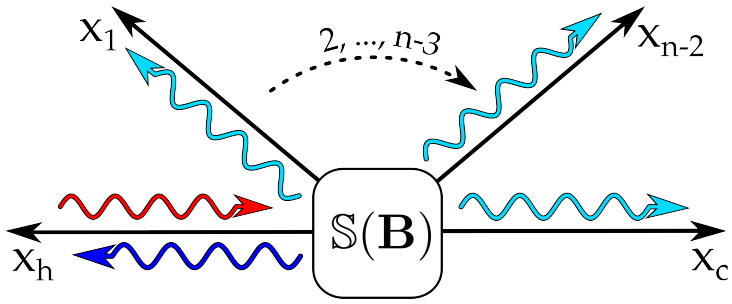

Figure 3.2: Illustration of a single-particle scattering process on a star-shaped network consisting of n leads attached to a central region, which is subject to a magnetic field $\mathbf{B}$. An incoming wave on the lead h (red) is partly reflected back (dark blue) and partly transmitted to the other leads (light blue). The amplitudes of incoming and outgoing waves are related via the scattering matrix $\mathbb{S}(\mathbf{B})$. The position along the lead α is parameterized by the distance $x_\alpha \in (0, \infty]$ to the scattering region, where $\alpha = \mathrm{h}, 1, \ldots, n-2, \mathrm{c}$.

3.1.2 Scattering Formalism

Within the scattering approach to quantum transport, the conductor is modeled as a central region equipped with an arbitrary potential landscape, where a constant magnetic field $\mathbf{B}$ can be applied externally. Particles can enter and leave this region via n one-dimensional and semi-infinite perfect leads. A single particle with mass m and sharp energy $E > 0$ reaching the central region in the lead α is scattered into the lead β with amplitude $S_{\beta\alpha}(E)$, where $\alpha, \beta = \mathrm{h}, 1, \ldots, n-2, \mathrm{c}$. This process, which is illustrated in Fig. 3.2, is described by the scattering state $|\Psi_E^\alpha\rangle$ satisfying the asymptotic boundary conditions

$$\Psi_E^\alpha(x_\beta) = \sqrt{\frac{m}{2\pi k\hbar^2}}\left(\delta_{\alpha\beta}e^{ikx_\beta} + S_{\beta\alpha}(E)e^{-ikx_\beta}\right) \quad \text{with} \quad k \equiv \frac{\sqrt{2mE}}{\hbar}. \tag{3.11}$$

Here, $\hbar$ denotes Planck's constant, $\Psi_E^\alpha(x)$ is the wave function corresponding to $|\Psi_E^\alpha\rangle$ and x parameterizes the position on the network formed by the central region and the semi-infinite leads. The normalization factor has been chosen such that the orthogonality relation

$$\langle\Psi_{E_1}^\alpha|\Psi_{E_2}^\beta\rangle = \delta_{\alpha\beta}\delta(E_1 - E_2) \tag{3.12}$$

is fulfilled.

The specific properties of the central region are encoded in the scattering amplitudes $S_{\beta\alpha}(E)$, which are conveniently collected in a matrix

$$\mathbb{S}(E) \equiv \begin{pmatrix} S_{\mathrm{hh}}(E) & \cdots & S_{\mathrm{hc}}(E) \\ \vdots & \ddots & \vdots \\ S_{\mathrm{ch}}(E) & \cdots & S_{\mathrm{cc}}(E) \end{pmatrix} \in \mathbb{C}^{n\times n} \tag{3.13}$$

This scattering matrix is subject to two important constraints. First, the time-reversal invariance of unitary dynamics implies the symmetry

$$\mathbb{S}(E, \mathbf{B}) = \mathbb{S}^t(E, -\mathbf{B}), \tag{3.14}$$

where we have reintroduced the magnetic field $\mathbf{B}$, which is notationally suppressed whenever it is not needed explicitly. Second, current conservation requires that $\mathbb{S}(E)$ is unitary. We note that the latter property crucially relies on a proper normalization of the scattering states, see [46, 47] for a detailed discussion of this issue.

Since the scattering states (3.11) are unbound, their physical interpretation requires some additional care. Two particular intricacies have to be overcome. First, the wave function $\Psi_E^\alpha(x)$ is not square-integrable and thus $|\Psi_E^\alpha(x)|^2$ can not be interpreted as a probability density. Second, the flux

$$j_E^\alpha(x) \equiv \frac{i\hbar}{2m}\Big(\Psi_E^a(x)\partial_x\Psi_E^{\alpha*}(x) - \Psi_E^{\alpha*}(x)\partial_x\Psi_E^\alpha(x)\Big) \tag{3.15}$$

of the wave function $\Psi_E^\alpha(x)$ does not vanish at infinity. Specifically, evaluating (3.15) at an arbitrary position x_β in the lead β using the asymptotic wave function (3.11) yields the spatially constant value

$$j_E^\alpha(x_\beta) = \frac{1}{4\pi\hbar}\left(\delta_{\alpha\beta} - |S_{\beta\alpha}(E)|^2\right). \tag{3.16}$$

These conceptual difficulties can be overcome by imagining distant sources and sinks of particles, which are not covered by Schrödinger's equation but rather must be modeled separately [55]. In such a setup, the scattering states can be interpreted as describing a flux of particles between these sources and sinks within a finite region of space.

Understanding this physical picture, we will now establish the relation between the scattering matrix $\mathbb{S}(E)$ and the matrix of kinetic coefficients $\mathbb{L}^n$ introduced in (3.2). To this end, we assume that, in the far distance from the central region, each lead is connected to a reservoir, which continuously injects non-interacting, fermionic particles into the system. Particles coming from the central region are absorbed reflectionless as soon as they reach one of the reservoirs. The scattering states $|\Psi_E^\alpha\rangle$ are then populated according to the respective Fermi-distribution

$$F_\alpha(E) \equiv \frac{1}{1+\exp\left((E-\mu_\alpha)/(k_\mathrm{B}T_\alpha)\right)}, \tag{3.17}$$

where k_B denotes Boltzmann's constant. Consequently, the net particle current flowing from the reservoir α into the system reads

$$J_\rho^\alpha = \sum_{\beta=\mathrm{h},\ldots,\mathrm{c}} \int_0^\infty dE\; j_E^\beta(x_\alpha)F_\beta(E). \tag{3.18}$$

In order to obtain this result, we first combine the expression (3.16) for the current generated in the lead β by a particle injected into the scattering state $|\psi_E^\alpha\rangle$ with the Fermi-distribution (3.17) of the corresponding reservoir α. Second, we sum up the contributions from all independent reservoirs. Analogously, we find the energy current

$$J_E^\alpha \equiv \sum_{\beta=\mathrm{h},\ldots,\mathrm{c}} \int_0^\infty dE\; j_E^\beta(x_\alpha)F_\beta(E)E. \tag{3.19}$$

leaving the reservoir α and the corresponding heat current [43]

$$J_q^\alpha = J_E^\alpha - \mu_\alpha J_\rho^\alpha = \sum_{\beta=\mathrm{h},\ldots,\mathrm{c}} \int_0^\infty dE\; j_E^\beta(x_\alpha)F_\beta(E)(E-\mu_\alpha). \tag{3.20}$$

Finally, inserting (3.16) and (3.17) into (3.18) and (3.20) and expanding the resulting expressions in the gradients $\Delta\mu_\alpha$ and ΔT_α yields the expression

$$\mathbb{L}^n_{\alpha\beta} = \int_0^\infty dE\, f(E) \begin{pmatrix} 1 & E-\mu_\mathrm{c} \\ E-\mu_\mathrm{c} & (E-\mu_\mathrm{c})^2 \end{pmatrix} \left(\delta_{\alpha\beta} - |S_{\alpha\beta}(E)|^2\right) \tag{3.21}$$

for the subunits of the matrix of kinetic coefficients (3.5), where

$$f(E) \equiv \frac{1}{4k_\mathrm{B}h\cosh^2\left[(E-\mu_\mathrm{c})/(2k_\mathrm{B}T_\mathrm{c})\right]}. \tag{3.22}$$

We note that, irrespective of the specific values of the scattering amplitudes $S_{\alpha\beta}(E)$, the 2×2-blocks (3.21) are still symmetric. Consequently, in a two-terminal setup, where the effective matrix of kinetic coefficient (3.10) equals the block $\mathbb{L}^n_{\mathrm{hh}}$, the off-diagonal kinetic coefficients $L_{\rho q}$ and $L_{q\rho}$ have to be identical. However, since, according to (3.14), the presence of a magnetic field permits the scattering matrix $\mathbb{S}(E,\mathbf{B})$ to be non-symmetric, for $n>2$, we can have $\mathbb{L}^n_{\alpha\beta} \neq \mathbb{L}^n_{\beta\alpha}$. Therefore, if at least one probe terminal is incorporated, the reduced matrix (3.10) can acquire a non-vanishing antisymmetric part as desired.

For later purposes, we define the transmission matrix

$$\mathbb{T}(E) \equiv \begin{pmatrix} T_{\mathrm{hh}}(E) & \cdots & T_{\mathrm{hc}}(E) \\ \vdots & \ddots & \vdots \\ T_{\mathrm{ch}}(E) & \cdots & T_{\mathrm{cc}}(E) \end{pmatrix} \equiv \begin{pmatrix} |S_{\mathrm{hh}}(E)|^2 & \cdots & |S_{\mathrm{hc}}(E)|^2 \\ \vdots & \ddots & \vdots \\ |S_{\mathrm{ch}}(E)|^2 & \cdots & |S_{\mathrm{cc}}(E)|^2 \end{pmatrix} \in \mathbb{R}^{n\times n}. \tag{3.23}$$

Obviously, $\mathbb{T}(E)$ inherits the symmetry (3.14) from the scattering matrix, i.e.,

$$\mathbb{T}(E,\mathbf{B}) = \mathbb{T}^t(E,-\mathbf{B}). \tag{3.24}$$

Furthermore, since $\mathbb{S}(E)$ is unitary, the transmission coefficients $0 \leq T_{\alpha\beta}(E) \leq 1$ have to obey the sum rules

$$\sum_{\alpha=\mathrm{h},\ldots,\mathrm{c}} T_{\alpha\beta}(E) = \sum_{\beta=\mathrm{h},\ldots,\mathrm{c}} T_{\alpha\beta}(E) = 1. \tag{3.25}$$

By combining (3.5) and (3.21), the matrix of kinetic coefficients $\mathbb{L}^n$ can now be expressed as an integral over tensor products given by

$$\mathbb{L}^n = \int_0^\infty dE\, f(E) \left(\mathbb{1} - \mathbb{T}_{[n]}(E)\right) \otimes \begin{pmatrix} 1 & E-\mu_\mathrm{c} \\ E-\mu_\mathrm{c} & (E-\mu_\mathrm{c})^2 \end{pmatrix}. \tag{3.26}$$

Here, $\mathbb{1}$ denotes the identity matrix and $\mathbb{T}_{[n]}(E)$ arises from $\mathbb{T}(E)$ by deleting the last row and column. Consequently, the matrix $\mathbb{T}_{[n]}(E)$ must be doubly substochastic, which means that all entries of $\mathbb{T}_{[n]}(E)$ are non-negative and any row and column sums up to a value not greater than one. This property will play a crucial role for our subsequent investigations.

3.2 The Minimal Model: Three Terminals

On the primary level, a three-terminal system is characterized by a 4×4 matrix of kinetic coefficients

$$\mathbb{L}^3 = \begin{pmatrix} \mathbb{L}_{\mathrm{hh}} & \mathbb{L}_{\mathrm{h1}} \\ \mathbb{L}_{\mathrm{1h}} & \mathbb{L}_{11} \end{pmatrix}. \tag{3.27}$$

After implementing the self-consistency conditions (3.6), an effective model is obtained, which is described by a 2×2 matrix of kinetic coefficients $\mathbb{L}$ and can be operated as a thermoelectric heat engine. We now proceed in two steps. First, we prove a constraint on the asymmetry of the reduced matrix $\mathbb{L}$ that leads to a stronger bound on the effective kinetic coefficients than the second law. Second, we show how this new bound can be used to restrict the efficiency of the three-terminal model as a thermoelectric heat engine.

3.2.1 Bound on the Effective Kinetic Coefficients

The key idea of our analysis is to consider the Hermitian matrices

$$\mathbb{K}^3 \equiv \mathbb{L}^3 + \mathbb{L}^{3t} + i\sqrt{3}\left(\mathbb{L}^3 - \mathbb{L}^{3t}\right) \in \mathbb{C}^{4\times 4}. \tag{3.28}$$

and

$$\mathbb{K} \equiv (\mathbb{L} + \mathbb{L}^t) + i\sqrt{3}(\mathbb{L} - \mathbb{L}^t) \equiv \begin{pmatrix} K_{\rho\rho} & K_{\rho q} \\ K_{q\rho} & K_{qq} \end{pmatrix} \in \mathbb{C}^{2\times 2}, \tag{3.29}$$

where $\mathbb{L}^3$ is the full 4×4 matrix of kinetic coefficients, while $\mathbb{L}$ is the reduced matrix. As we show in App. 3A, the matrix (3.29) is positive semidefinite. Moreover, since for any $\mathbf{z} \in \mathbb{C}^2$

$$\mathbf{z}^\dagger \mathbb{K} \mathbf{z} = \mathbf{z}'^\dagger \mathbb{K}^3 \mathbf{z}' \quad \text{with} \quad \mathbf{z}' \equiv \begin{pmatrix} \mathbf{z} \\ -(\mathbb{L}^3_{11})^{-1}\mathbb{L}^3_{1\mathrm{h}}\mathbf{z} \end{pmatrix}, \tag{3.30}$$

it follows that the matrix $\mathbb{K}$ must have the same property. Consequently, the matrix elements of $\mathbb{K}$ have to obey the inequalities

$$K_{\rho\rho}, K_{qq} \geq 0 \quad \text{and} \quad K_{\rho\rho}K_{qq} - K_{\rho q}K^*_{\rho q} \geq 0. \tag{3.31}$$

We note that the K_{ij} $(i, j = \rho, q)$ are rather complicated functions of the primary kinetic coefficients, which would make it a quite challenging task to obtain (3.31) directly from (3.10) and (3.21). If we insert the definition (3.29) of the K_{ij} in terms of the effective kinetic coefficients L_{ij} into (3.31), we immediately get the relation

$$L_{\rho\rho}L_{qq} + L_{\rho q}L_{q\rho} - L^2_{\rho q} - L^2_{q\rho} \geq 0. \tag{3.32}$$

We emphasize that (3.32) provides a much stronger constraint than the second law (2.4), since the former can be rewritten as

$$L_{\rho\rho}L_{qq} - (L_{\rho q} + L_{q\rho})^2/4 \geq 3(L_{\rho q} - L_{q\rho})^2/4. \tag{3.33}$$

Indeed, we recover (2.4) only if $L_{\rho q}$ is equal to $L_{q\rho}$. As soon as the kinetic coefficients contain finite antisymmetric parts, the left hand side of (3.33) must be strictly larger than zero. In other words, the reversible currents associated with the antisymmetric part of $\mathbb{L}$ come at the price of a stronger lower bound on the kinetic coefficients and hence on the rate of entropy production (2.3) than the bare second law requires.

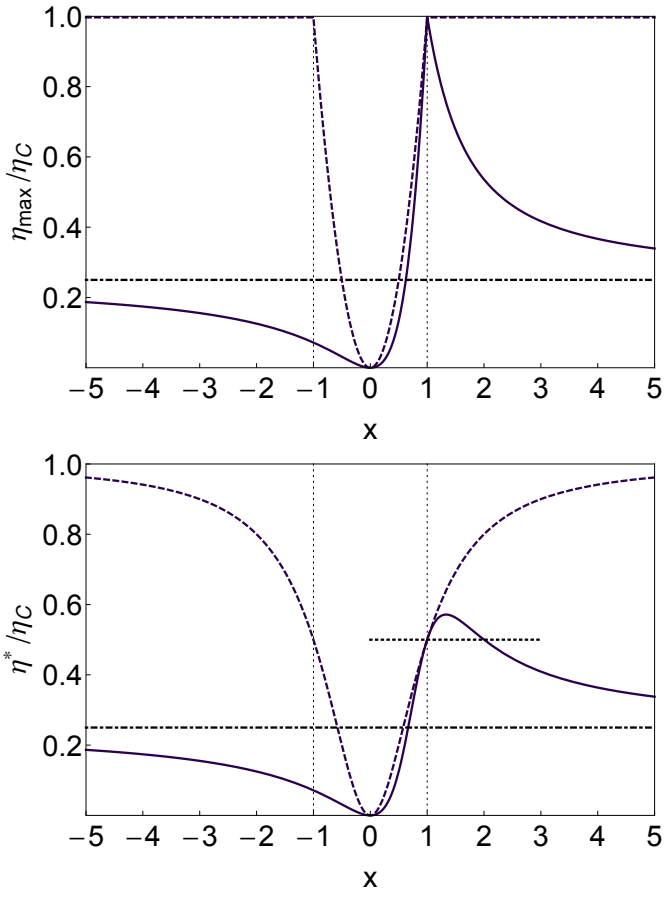

Figure 3.3: Bounds on the efficiency of the three-terminal model as a thermoelectric heat engine in units of η_C as a function of the asymmetry parameter x. The upper diagram shows the maximum efficiency $\eta_{\max}$, the lower one the efficiency at maximum power η^*. The solid curves represent the bounds following from relation (3.32). In the limit $x \to \pm\infty$ both functions asymptotically approach the value 1/4, which is shown by the dash-dotted lines. For comparison, the bounds obtained by Benentie *et al.* [27] solely from the second law (2.4) have been included as dashed curves. The dotted line in the lower panel indicates the Curzon-Ahlborn limit $\eta_{CA} = \eta_C/2$.

3.2.2 Bounds on Efficiency

The new bound (3.32) has profound consequences for the performance of the model as a thermoelectric heat engine. Expressed in terms of the dimensionless parameters x and y, the inequality (3.32) reads

$$h_3(x) \le y \le 0 \quad \text{if} \quad x < 0, \qquad 0 \le y \le h_3(x) \quad \text{if} \quad x \ge 0, \tag{3.34}$$

where

$$h_3(x) \equiv \frac{x}{(x-1)^2}. \tag{3.35}$$

We now recall the respective expressions (2.23) and (2.24) for the maximum efficiency $\eta_{\max}(x,y)$ and the efficiency at maximum power $\eta^*(x,y)$ as functions of x and y. Since, for any x, these benchmarks monotonically increase with $|y|$ they both become maximal for $y = h_3(x)$. The resulting bounds

$$\eta_{\max}(x) \equiv \eta_{\max}(x, h_3(x)) = \eta_C x \frac{\sqrt{(x-1)x+1} - |x-1|}{\sqrt{(x-1)x+1} + |x-1|} \tag{3.36}$$

and

$$\eta^*(x) \equiv \eta^*(x, h_3(x)) = \eta_C \frac{x^2}{4x^2 - 6x + 4} \tag{3.37}$$

are plotted in Fig. 3.3. It shows how the maximum efficiency decays rapidly as the asymmetry parameter x deviates from its symmetric value 1. In the limit $x \to \pm\infty$, maximum efficiency and efficiency at maximum power both approach $\eta_C/4$. This result implies essentially that, from the perspective of maximally attainable efficiency, the thermodynamic cost of the reversible currents is larger than the benefit they bring.

For efficiency at maximum power, the situation is somewhat different. If x is only slightly larger than 1, the Curzon-Ahlborn limit $\eta_{CA} = \eta_C/2$, reached for $x = 1$, can be overcome in a small range of x values with a maximum of $4\eta_C/7$ at $x = 4/3$. This result shows that, despite the strong bounds on η_{max}, it may, in principle, be possible to improve the performance of the machine by breaking the time-reversal symmetry slightly.

3.3 Multiple Terminals

The results of the preceding section naturally raise the question whether bounds similar to (3.32) exist in models with more than three terminals. Here, we first derive a set of non-trivial relations beyond the second law, which follow from current conservation and universally constrain the kinetic coefficients describing the multi-terminal setup. We then show that these constraints imply bounds on the efficiency of the multi-terminal model as a thermoelectric heat engine.

3.3.1 Bounds on Kinetic Coefficients

These bounds can be derived by first quantifying the asymmetry of the primary matrix of kinetic coefficients $\mathbb{L}^n$. For an arbitrary positive semidefinite matrix $\mathbb{A} \in \mathbb{R}^{m\times m}$, we define an asymmetry index by

$$\mathcal{S}(\mathbb{A}) \equiv \min\left\{ s \in \mathbb{R} |\, \forall \mathbf{z} \in \mathbb{C}^m \quad \mathbf{z}^\dagger \left(s\left(\mathbb{A} + \mathbb{A}^t\right) + i\left(\mathbb{A} - \mathbb{A}^t\right)\right)\mathbf{z} \geq 0 \right\}. \tag{3.38}$$

Some of the basic properties of properties of this asymmetry index are outlined in Sec. 5.1. We note that a quite similar quantity was introduced by Crouzeix and Gutan [56] in another context.

We will proceed in two steps. First, we show that the asymmetry index of the primary matrix of kinetic coefficients $\mathbb{L}^n$ and all its principal submatrices is bounded from above for any finite number of terminals n. Second, we will derive therefrom a set of new bounds on the elements of $\mathbb{L}^n$, which go beyond the second law.

For the first step, we define the quadratic form

$$Q(\mathbf{z}, s) \equiv \mathbf{z}^\dagger \Big(s\left(\mathbb{L}^n_{\{\{A\}\}} + \mathbb{L}^{nt}_{\{\{A\}\}}\right) + i\left(\mathbb{L}^n_{\{\{A\}\}} - \mathbb{L}^{nt}_{\{\{A\}\}}\right)\Big)\mathbf{z} \tag{3.39}$$

for any $\mathbf{z} \in \mathbb{C}^m$ and any $s \in \mathbb{R}$. Here, $A \subseteq \{1, \ldots, n-1\}$ denotes a set of $m \leq n-1$ indices. The matrix $\mathbb{L}^n_{\{\{A\}\}}$ arises from $\mathbb{L}^n$ by taking all blocks $\mathbb{L}^n_{\alpha\beta}$ with column and row index in A, i.e., $\mathbb{L}^n_{\{\{A\}\}}$ is a principal submatrix of $\mathbb{L}^n$, which preserves the 2×2 block structure shown in (3.5). Comparing (3.39) with the definition (3.38) reveals that the minimum s for which $Q(\mathbf{z}, s)$ is positive semidefinite equals the asymmetry index of $\mathbb{L}^n_{\{\{A\}\}}$. Next, by recalling (3.26) we rewrite the matrix $\mathbb{L}^n_{\{\{A\}\}}$ in the rather compact form

$$\int_0^\infty dE\, f(E)\left(\mathbb{1} - \mathbb{T}_{\{A\}}(E)\right) \otimes \begin{pmatrix} 1 & E-\mu_c \\ E-\mu_c & (E-\mu_c)^2 \end{pmatrix}, \tag{3.40}$$

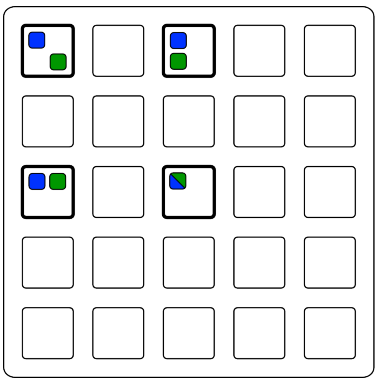

$$\begin{array}{ll} \mathbb{L}^n \in \mathbb{R}^{2(n-1)\times 2(n-1)} & \mathcal{S}\big(\mathbb{L}^n\big) \le \cot\left(\frac{\pi}{n}\right) \\ \downarrow & \downarrow \\ \mathbb{L}^n_{\{\{\alpha,\beta\}\}} \in \mathbb{R}^{4\times 4} & \mathcal{S}\big(\mathbb{L}^n_{\{\{\alpha,\beta\}\}}\big) \le \cot\left(\frac{\pi}{3}\right) \\ \downarrow & \downarrow \\ \mathbb{L}^n_{\{\alpha i,\beta j\}} \in \mathbb{R}^{2\times 2} & \mathcal{S}\big(\mathbb{L}^n_{\{\alpha i,\beta j\}}\big) \le \cot\left(\frac{\pi}{3}\right) \end{array}$$

Figure 3.4: Schematic illustration of the reduction from $\mathbb{L}^n$ to $\mathbb{L}^n_{\{\alpha i,\beta j\}}$. The big square represents $\mathbb{L}^n$ for the case $n = 6$, the smaller ones correspond to the 2×2 blocks introduced in (3.5). By taking the bold framed squares, the 4×4 matrix $\mathbb{L}^n_{\{\{\alpha,\beta\}\}}$ is obtained for the case $\alpha = 1$ and $\beta = 3$. The filled squares represent the elements of the 2×2 matrix $\mathbb{L}^n_{\{\alpha i,\beta j\}}$ introduced in for $(i,j) = (1,1)$ (blue) and $(i,j) = (2,1)$ (green).

where $\mathbb{T}_{\{A\}}(E) \in \mathbb{R}^{m\times m}$ is obtained from $\mathbb{T}(E)$ defined in (3.23) by taking the rows and columns indexed by A. Decomposing $\mathbf{z}$ as

$$\mathbf{z} \equiv \mathbf{z}_1 \otimes \begin{pmatrix} 1 \\ 0 \end{pmatrix} + \mathbf{z}_2 \otimes \begin{pmatrix} 0 \\ 1 \end{pmatrix} \quad \text{with} \quad \mathbf{z}_1, \mathbf{z}_2 \in \mathbb{C}^m \tag{3.41}$$

and inserting (3.40) and (3.41) into (3.39) yields

$$Q(\mathbf{z}, s) = \int_0^\infty dE\, f(E)\mathbf{y}^\dagger(E)\mathbb{V}^n_{\{A\}}(E,s)\mathbf{y}(E). \tag{3.42}$$

Here, we introduced the vector

$$\mathbf{y}(E) \equiv \mathbf{z}_1 + (E - \mu_c)\mathbf{z}_2 \tag{3.43}$$

and the Hermitian matrix

$$\mathbb{V}^n_{\{A\}} \equiv s\Big(2\mathbb{1} - \mathbb{T}_{\{A\}}(E) - \mathbb{T}^t_{\{A\}}(E)\Big) - i\Big(\mathbb{T}_{\{A\}}(E) - \mathbb{T}^t_{\{A\}}(E)\Big) \in \mathbb{C}^{m\times m}, \tag{3.44}$$

which is positive semidefinite for any

$$s \ge \mathcal{S}\left(\mathbb{1} - \mathbb{T}_{\{A\}}(E)\right). \tag{3.45}$$

However, since $\mathbb{T}(E)$ is doubly stochastic by virtue of the sum rules (3.25), the matrix $\mathbb{T}_{\{A\}}(E)$ must be doubly substochastic and it follows from Corollary 2 proven in Ch. 5:

$$\mathcal{S}\left(\mathbb{1} - \mathbb{T}_{\{A\}}(E)\right) \le \cot\left(\frac{\pi}{m+1}\right). \tag{3.46}$$

Hence, independently of E, the matrix $\mathbb{K}_{\{A\}}(E,s)$ is positive semidefinite for any

$$s \ge \cot\left(\frac{\pi}{m}\right). \tag{3.47}$$

Finally, we can infer from (3.42) that $Q(\mathbf{z}, s)$ is positive semidefinite for any s, which obeys (3.47). Consequently, with (3.39), we have the desired bound on the asymmetry index of $\mathbb{L}^n_{\{\{A\}\}}$ as

$$\mathcal{S}\left(\mathbb{L}^n_{\{\{A\}\}}\right) \leq \cot\left(\frac{\pi}{m+1}\right). \tag{3.48}$$

We emphasize that this bound ultimately follows from current conservation.

We will now demonstrate that (3.48) puts indeed strong bounds on the kinetic coefficients. To this end, we extract a 2×2 principal submatrix from $\mathbb{L}^n$ by a two-step procedure, which is schematically summarized in Fig. 3.4. In the first step, we consider the 4×4 principal submatrix of $\mathbb{L}^n$ given by

$$\mathbb{L}^n_{\{\{\alpha,\beta\}\}} \equiv \begin{pmatrix} \mathbb{L}^n_{\alpha\alpha} & \mathbb{L}^n_{\alpha\beta} \\ \mathbb{L}^n_{\beta\alpha} & \mathbb{L}^n_{\beta\beta} \end{pmatrix}, \tag{3.49}$$

which arises from $\mathbb{L}^n$ by taking only the blocks with row and column index equal to α or β. From (3.48), we immediately get with $m = 2$

$$\mathcal{S}\left(\mathbb{L}^n_{\{\{\alpha,\beta\}\}}\right) \leq \cot\left(\frac{\pi}{3}\right) = \frac{1}{\sqrt{3}}. \tag{3.50}$$

Next, from (3.49), we take a 2×2 principal submatrix

$$\mathbb{L}^n_{\{\alpha i,\beta j\}} \equiv \begin{pmatrix} (\mathbb{L}^n_{\alpha\alpha})_{ii} & (\mathbb{L}^n_{\alpha\beta})_{ij} \\ (\mathbb{L}^n_{\beta\alpha})_{ji} & (\mathbb{L}^n_{\beta\beta})_{jj} \end{pmatrix} \equiv \begin{pmatrix} L^n_{11} & L^n_{12} \\ L^n_{21} & L^n_{22} \end{pmatrix}, \tag{3.51}$$

where $\left(\mathbb{L}^n_{\alpha\beta}\right)_{ij}$ with $i, j = 1, 2$ denotes the (i, j)-entry of the block matrix $\mathbb{L}^n_{\alpha\beta}$. By virtue of Proposition 3 proven in Ch. 5, the inequality (3.50) implies

$$\mathcal{S}\left(\mathbb{L}^n_{\{\alpha i,\beta j\}}\right) \leq \frac{1}{\sqrt{3}}, \tag{3.52}$$

which is equivalent to requiring the Hermitian matrix

$$\mathbb{K}^n_{\{\alpha i,\beta j\}} \equiv \frac{1}{\sqrt{3}}\left(\mathbb{L}^n_{\{\alpha i,\beta j\}} + \mathbb{L}^{nt}_{\{\alpha i,\beta j\}}\right) + i\left(\mathbb{L}^n_{\{\alpha i,\beta j\}} - \mathbb{L}^{nt}_{\{\alpha i,\beta j\}}\right) \equiv \begin{pmatrix} K^n_{11} & K^n_{12} \\ K^{n*}_{12} & K^n_{22} \end{pmatrix} \tag{3.53}$$

to be positive semidefinite. Since the diagonal entries of $\mathbb{K}^n_{\{\alpha i,\beta j\}}$ are obviously non-negative, this condition reduces to

$$\operatorname{Det} \mathbb{K}^n_{\{\alpha i,\beta j\}} = K^n_{11} K^n_{22} - \left|K^n_{12}\right|^2 \geq 0. \tag{3.54}$$

Finally, expressing the K^n_{ij} again in terms of the L^n_{ij} yields the new constraint

$$L^n_{11} L^n_{22} - \left(L^n_{12} + L^n_{21}\right)^2/4 \geq 3\left(L^n_{12} - L^n_{21}\right)^2/4. \tag{3.55}$$

This bound holds for the elements of any 2×2 principal submatrix of the full matrix of kinetic coefficients $\mathbb{L}^n$, irrespective of the number n of terminals. Compared to relation

(3.55), the second law requires $\mathbb{L}^n_{\{\alpha i,\beta j\}}$ to be positive semidefinite, which is equivalent to $L^n_{11}, L^n_{22} \geq 0$ and the weaker constraint

$$L^n_{12}L^n_{22} - \left(L^n_{12} + L^n_{21}\right)^2/4 \geq 0. \tag{3.56}$$

At this point, we emphasize that the procedure shown here for 2×2 principal submatrices of $\mathbb{L}^n$ could be easily extended to larger principal submatrices. The result would be a whole hierachy of constraints involving more and more kinetic coefficients. However, (3.55) is the strongest bound following from (3.48), which can be expressed in terms of only four of these coefficients.

3.3.2 Bounds on Efficiency

We will now explore the consequences of the bound (3.48) on the performance of the multi-terminal model as a thermoelectric heat engine with broken time-reversal symmetry. To this end, we recall the expression (3.10) for the effective matrix of kinetic coefficients $\mathbb{L}$, which arises by considering the terminals $1,\dots,n-2$ as probe terminals not contributing to the actual transport process. Since $\mathbb{L}$ is not a principal submatrix of $\mathbb{L}^n$, the bound (3.48) does not apply directly. However, $\mathbb{L}$ can be written as the Schur complement (see Sec. 5.3 for the definition)

$$\mathbb{L} = \mathbb{L}^n/\mathbb{L}^n_{[[1]]}, \tag{3.57}$$

the asymmetry index of which is dominated by the asymmetry index of $\mathbb{L}^n$ as proven in Proposition 4 of Ch. 5. Consequently, we have

$$\mathcal{S}(\mathbb{L}) = \mathcal{S}\left(\mathbb{L}^n/\mathbb{L}^n_{[[1]]}\right) \leq \mathcal{S}(\mathbb{L}^n) \leq \cot\left(\frac{\pi}{n}\right) \tag{3.58}$$

or, equivalently,

$$L_{\rho\rho}L_{qq} - \left(L_{\rho q} + L_{q\rho}\right)^2/4 \geq \tan^2\left(\frac{\pi}{n}\right)\left(L_{\rho q} - L_{q\rho}\right)^2. \tag{3.59}$$

This constraint shows that whenever $L_{\rho q} \neq L_{q\rho}$, the rate of entropy production (2.3) must be strictly larger than zero, thus ruling out the option of dissipationless transport generated solely by reversible currents for any model with a finite number n of terminals. For any $n > 3$ the constraint (3.59) is weaker than (3.55). The reason is that the kinetic coefficients showing up in (3.59) are not elements of the full matrix $\mathbb{L}^n$ but rather involve the inversion of $\mathbb{L}^n_{[1,2]}$ defined in (3.7). Still, this constraint is stronger than the bare second law, which requires only

$$L_{\rho\rho}L_{qq} - \left(L_{\rho q} + L_{q\rho}\right)^2/4 \geq 0, \tag{3.60}$$

irrespective of whether or not $\mathbb{L}$ is symmetric.

Restating the new bound (3.59) in terms of the dimensionless parameters x and y yields

$$h_n(x) \leq y \leq 0 \quad \text{if} \quad x < 0, \qquad 0 \leq y \leq h_n(x) \quad \text{if} \quad x \geq 0 \tag{3.61}$$

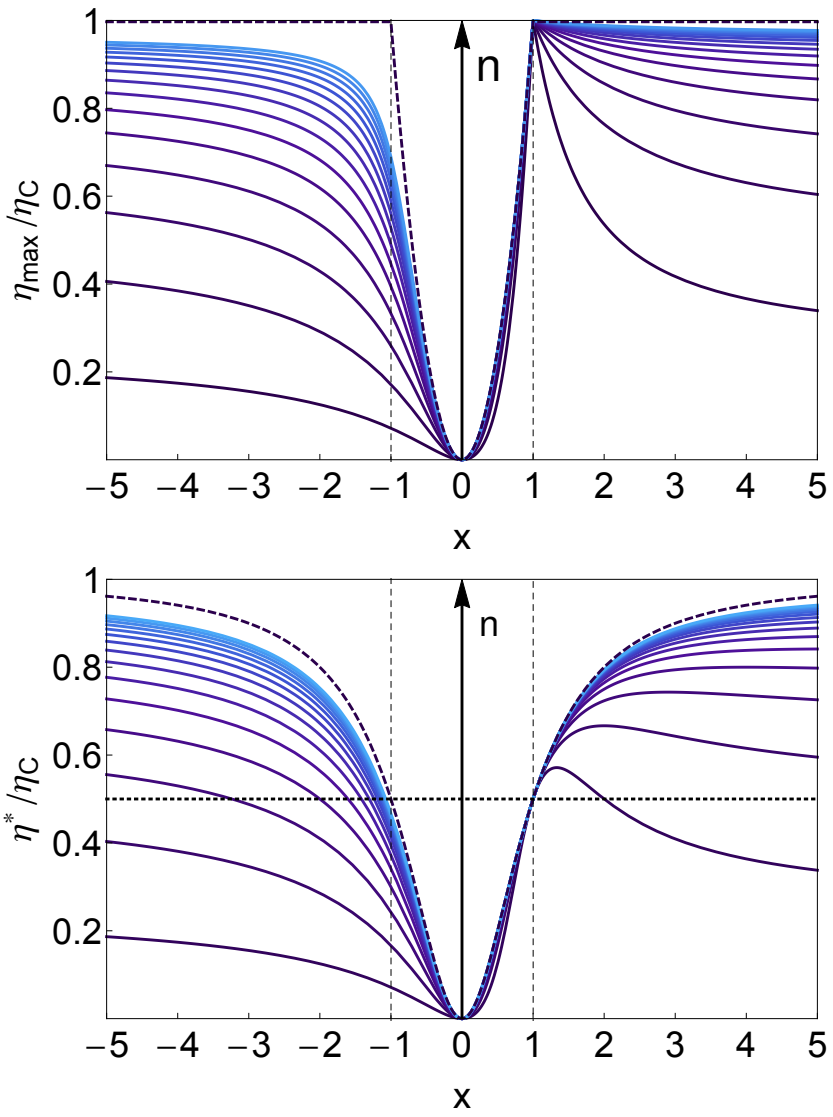

Figure 3.5: Bounds on the efficiency of the multi-terminal model as a thermoelectric heat engine as functions of the asymmetry parameter x and in units of η_C. The upper panel shows the bound (3.63) on maximum efficiency, the lower one corresponds to the bound (3.64) on efficiency at maximum power. In both panels, the solid blue lines, from bottom to top, belong to models with $n = 3, \ldots, 17$ terminals and the dashed line corresponds to the bound following from the bare second law as obtained by Benenti *et al.*. The dotted line in the lower panel marks th Curzon-Ahlborn limit $\eta_{CA} = \eta_C/2$.

with

$$h_n(x) \equiv \frac{4x}{(x-1)^2}\cos^2\left(\frac{\pi}{n}\right). \tag{3.62}$$

Consequently, the maximum efficiency $\eta_{\max}(x,y)$ and the efficiency at maximum power $\eta^*(x,y)$, which were defined in (2.23) and (2.24), respectively, and both are monotonically increasing functions of $|y|$, are subject to the bounds

$$\eta_{\max}(x) \equiv \eta_{\max}(x, h_n(x)) = \eta_C x \frac{\sqrt{4x\cos^2(\pi/n) + (x-1)^2} - |x-1|}{\sqrt{4x\cos^2(\pi/n) + (x-1)^2} + |x-1|} \tag{3.63}$$

and

$$\eta^*(x) \equiv \eta^*(x, h_n(x))\eta_C \frac{x^2\cos^2(\pi/n)}{(x-1)^2 + 2x\cos^2(\pi/n)}. \tag{3.64}$$

These bounds are plotted in Fig. 3.5 as functions of x for an increasing number n of terminals. For $n = 3$, we recover the results (3.36) and (3.37) obtained previously for

the three-terminal model. In the limit $n \to \infty$, $\eta_{\max}(x)$ and $\eta^*(x)$ both converge to the respective bound derived by Benenti *et al.* [27] within an analysis relying only on the second law. However, for finite n, $\eta_{\max}(x)$ is constrained to be strictly smaller than η_{C}, as soon as x deviates from 1. Thus, from the perspective of maximum efficiency, breaking the time-reversal symmetry is not beneficial, at least within the multi-terminal setup.

The bound (3.64) on efficiency at maximum power acquires the Curzon-Ahlborn value $\eta_{\mathrm{CA}} = \eta_{\mathrm{C}}/2$ for $x = 1$. For $|x| > 1$, however, it becomes significantly higher even for a small number$n$ of terminals. Specifically, we observe that $\eta^*(x)$ exceeds η_{CA} for any $n \geq 3$ in a certain range of x values. For $n \geq 4$, this range includes all $x > 1$. Furthermore, $\eta^*(x)$ attains its global maximum

$$\eta^{**} \equiv \frac{\eta_{\mathrm{C}}}{1 + \sin^2(\pi/n)} \tag{3.65}$$

at the finite value $x = 1/\sin^2(\pi/n)$. Remarkably, both $\eta_{\max}(x)$ and $\eta^*(x)$ approach the same asymptotic value $\eta^{\infty} = \eta_{\mathrm{C}} \cos^2(\pi/n)$ for $x \to \pm\infty$.

3.4 Bounds on Power

In the previous section, we have shown that current conservation leads to stronger bounds on the efficiency of multi-terminal thermoelectric generators than the bare second law. We will now demonstrate in two steps that the same fundamental principle also restricts the power of such devices in a non-trivial way. First, we prove a universal relation between power and efficiency, which holds for any multi-terminal model and rules out the option of Carnot efficiency at finite power. Second, we provide strong numerical evidence that this bound can be strengthened if the number of terminals is fixed.

3.4.1 A Universal Bound on Power

The fundamental bound on power that shall be discussed here can be derived in four steps. First, we prove that, for any

$$\mathbf{x}^1_\alpha \equiv \left(x'^1_\alpha, x''^1_\alpha\right)^t,\ \mathbf{x}^2_\alpha \equiv \left(x'^2_\alpha, x''^2_\alpha\right)^t \in \mathbb{R}^2 \quad \text{with} \quad \alpha = \mathrm{h}, 1, \ldots, n-2, \mathrm{c}, \tag{3.66}$$

the quadratic form

$$Q_{\mathrm{W}}\left(\{\mathbf{x}^1_\alpha\}, \{\mathbf{x}^2_\alpha\}\right) \equiv \sum_{\alpha,\beta=\mathrm{h},\ldots,\mathrm{c}} \left(\delta_{\alpha\beta}\mathbf{x}^{1t}_\alpha \mathbb{N} \mathbf{x}^1_\beta + 2\mathbf{x}^{1t}_\alpha \mathbb{L}^n_{\alpha\beta}\mathbf{x}^2_\beta + \mathbf{x}^{2t}_\alpha \left(\mathbb{L}^n_{\alpha\beta} + \mathbb{L}^n_{\beta\alpha}\right)\mathbf{x}^2_\beta\right) \tag{3.67}$$

with

$$\mathbb{N} \equiv \int_0^\infty dE\, f(E) \begin{pmatrix} 1 & E-\mu_{\mathrm{c}} \\ E-\mu_{\mathrm{c}} & (E-\mu_{\mathrm{c}})^2 \end{pmatrix} \equiv \begin{pmatrix} N_{\rho\rho} & N_{\rho q} \\ N_{\rho q} & N_{qq} \end{pmatrix} \in \mathbb{R}^{2\times 2} \tag{3.68}$$

(3.22) is positive semidefinite. To this end, we note that, after inserting the Landauer-Büttiker formula (3.21), (3.66) and (3.68), (3.67) can be rewritten as

$$Q_{\mathrm{W}}\left(\{\mathbf{x}^1_\alpha\}, \{\mathbf{x}^2_\alpha\}\right) = \int_0^\infty dE\, f(E)\mathbf{w}^t(E)\mathbb{W}(E)\mathbf{w}(E), \tag{3.69}$$

where

$$\mathbb{W}(E) \equiv \begin{pmatrix} \mathbb{1} & \mathbb{1} - \mathbb{T}(E) \\ \mathbb{1} - \mathbb{T}^t(E) & 2\mathbb{1} - \mathbb{T}(E) - \mathbb{T}^t(E) \end{pmatrix} \in \mathbb{R}^{2n \times 2n} \tag{3.70}$$

and

$$\mathbf{w}(E) \equiv \left(x'^1_{\mathrm{h}}, \ldots, x'^1_{\mathrm{c}}, x'^2_{\mathrm{h}}, \ldots, x'^2_{\mathrm{c}}\right)^t + (E - \mu_{\mathrm{c}}) \left(x''^1_{\mathrm{h}}, \ldots, x''^1_{\mathrm{c}}, x''^2_{\mathrm{h}}, \ldots, x''^2_{\mathrm{c}}\right)^t \in \mathbb{R}^{2n}. \tag{3.71}$$

Since, the sum rules (3.25) imply that, for any $E \geq 0$, the transmission matrix $\mathbb{T}(E)$ is bistochastic, the matrix $\mathbb{W}(E)$ is positive semidefinite as we prove in App. 3B. Consequently, it follows from (3.69) that $Q_{\mathrm{W}}(\{\mathbf{x}^1_\alpha\}, \{\mathbf{x}^2_\alpha\}) \geq 0$ and our proof is completed.

Second, evaluating (3.67) for

$$\mathbf{x}^1_1 = \cdots = \mathbf{x}^1_{n-2} = \mathbf{x}^2_{\mathrm{c}} = \mathbf{0} \quad \text{and} \quad \begin{pmatrix} \mathbf{x}^2_1 \\ \vdots \\ \mathbf{x}^2_{n-2} \end{pmatrix} = -\left(\mathbb{L}^n_{[[1]]}\right)^{-1} \begin{pmatrix} \mathbb{L}^n_{1\mathrm{h}} \\ \vdots \\ \mathbb{L}^n_{n-2\,n} \end{pmatrix}, \tag{3.72}$$

yields

$$\mathbf{x}^{1t}_{\mathrm{h}} \mathbb{N} \mathbf{x}^1_{\mathrm{h}} + \mathbf{x}^{1t}_{\mathrm{c}} \mathbb{N} \mathbf{x}^1_{c} + 2\mathbf{x}^{1t}_{\mathrm{h}} \mathbb{L} \mathbf{x}^2_{\mathrm{h}} + 2\mathbf{x}^{1t}_{\mathrm{c}} \mathbb{L}' \mathbf{x}^2_{\mathrm{h}} + 2\mathbf{x}^{2t}_{\mathrm{h}} \mathbb{L} \mathbf{x}^2_{\mathrm{h}} \geq 0, \tag{3.73}$$

where $\mathbb{L}$ is the effective matrix of kinetic coefficients (3.10) and

$$\mathbb{L}' \equiv \mathbb{L}^n_{\mathrm{ch}} - \left(\mathbb{L}^n_{\mathrm{c}1}, \ldots, \mathbb{L}^n_{\mathrm{c}n-2}\right) \left(\mathbb{L}^n_{[[1]]}\right)^{-1} \begin{pmatrix} \mathbb{L}^n_{1\mathrm{h}} \\ \vdots \\ \mathbb{L}_{n-2\mathrm{h}} \end{pmatrix}. \tag{3.74}$$

The sum of these two matrices vanishes, since

$$\begin{aligned} \mathbb{L} + \mathbb{L}' &= \mathbb{L}^n_{\mathrm{hh}} + \mathbb{L}^n_{\mathrm{ch}} - \left(\mathbb{L}^n_{\mathrm{h}1} + \mathbb{L}^n_{\mathrm{c}1}, \ldots, \mathbb{L}_{\mathrm{h}n-2} + \mathbb{L}_{\mathrm{c}n-2}\right) \left(\mathbb{L}^n_{[[1]]}\right)^{-1} \begin{pmatrix} \mathbb{L}^n_{1\mathrm{h}} \\ \vdots \\ \mathbb{L}^n_{n-2\mathrm{h}} \end{pmatrix} \\ &= \mathbb{L}^n_{\mathrm{hh}} + \mathbb{L}^n_{\mathrm{ch}} + \sum_{\alpha=1,\ldots,n-2} \left(\mathbb{L}^n_{\alpha 1}, \ldots, \mathbb{L}_{\alpha n-2}\right) \left(\mathbb{L}^n_{[[1]]}\right)^{-1} \begin{pmatrix} \mathbb{L}^n_{1\mathrm{h}} \\ \vdots \\ \mathbb{L}^n_{n-2\mathrm{h}} \end{pmatrix} \\ &= \mathbb{L}^n_{\mathrm{hh}} + \mathbb{L}^n_{\mathrm{ch}} + \left((\mathbb{1}, \ldots, \mathbb{1})\, \mathbb{L}^n_{[[1]]}\right) \left(\mathbb{L}^n_{[[1]]}\right)^{-1} \begin{pmatrix} \mathbb{L}^n_{1\mathrm{h}} \\ \vdots \\ \mathbb{L}^n_{n-2\mathrm{h}} \end{pmatrix} = \mathbb{O}, \end{aligned} \tag{3.75}$$

where $\mathbb{O}$ denotes the zero matrix. In the second line, we used the identity

$$\sum_{\alpha=\mathrm{h},\ldots,\mathrm{c}} \mathbb{L}_{\alpha\beta} = \mathbb{O}, \tag{3.76}$$

which is easily verified by combining the Landauer-Büttiker expression (3.21) for the matrix blocks $\mathbb{L}^n_{\alpha\beta}$ with the sum rules (3.25) for the transmission coefficients. Inserting $\mathbb{L}' = -\mathbb{L}$ into (3.73) and setting

$$\mathbf{x}^1_{\mathrm{h}} = -\mathbb{N}^{-1}\mathbb{L}\mathbf{x}^2_{\mathrm{h}} \quad \text{and} \quad \mathbf{x}^1_{\mathrm{c}} = \mathbb{N}^{-1}\mathbb{L}\mathbf{x}^2_{\mathrm{h}} \tag{3.77}$$

yields

$$\mathbf{x}_{\mathrm{h}}^{2t}\left(\mathbb{L}-\mathbb{L}^{t}\mathbb{N}^{-1}\mathbb{L}\right)\mathbf{x}_{\mathrm{h}}^{2}\geq 0. \tag{3.78}$$

Thus, since the vector $\mathbf{x}_{\mathrm{h}}^{2}\in\mathbb{R}^{2}$ is arbitrary, the matrix

$$\mathbb{M}\equiv\frac{1}{2}(\mathbb{L}+\mathbb{L}^{t})-\mathbb{L}^{t}\mathbb{N}^{-1}\mathbb{L} \tag{3.79}$$

must be positive semidefinite.

For the third step, we notice that the matrix

$$\mathbb{A}\equiv\begin{pmatrix}\frac{1}{2}\left(\mathbb{L}^{t}+\mathbb{L}\right) & \mathbb{L}^{t}\\ \mathbb{L} & \mathbb{N}\end{pmatrix}\in\mathbb{R}^{4\times 4}, \tag{3.80}$$

must be positive semidefinite, since, first, $\mathbb{N}$ is obviously positive definite and, second, the Schur complement $\mathbb{A}/\mathbb{N}=\mathbb{M}$ is positive semidefinite as we have proven in the second step. These two conditions are both, sufficient and necessary, for $\mathbb{A}$ to be positive semidefinite [57]. Consequently, all principal minors of $\mathbb{A}$ must be non-negative [57]. In particular, we have

$$\begin{aligned}\mathrm{Det}\,\mathbb{A}_{[3]}&=\mathrm{Det}\begin{pmatrix}L_{\rho\rho} & (L_{\rho q}+L_{q\rho})/2 & L_{q\rho}\\ (L_{\rho q}+L_{q\rho})/2 & L_{qq} & L_{qq}\\ L_{q\rho} & L_{qq} & N_{qq}\end{pmatrix}\\ &=N_{qq}\left(L_{\rho\rho}L_{qq}-(L_{\rho q}+L_{q\rho})^{2}/4\right)-L_{qq}\left(L_{\rho\rho}L_{qq}-L_{\rho q}L_{q\rho}\right)\geq 0.\end{aligned} \tag{3.81}$$

Thus, we obtain the upper bound

$$L_{qq}\leq N_{qq}\frac{L_{\rho\rho}L_{qq}-(L_{\rho q}+L_{q\rho})^{2}/4}{L_{\rho\rho}L_{qq}-L_{\rho q}L_{q\rho}}=N_{qq}\left(1-\frac{y}{h(x)}\right) \tag{3.82}$$

on the diagonal kinetic coefficient L_{qq}. We emphasize that, like the bounds discussed in the previous section, (3.82) ultimately follows from the sum rules (3.25) and thus should be regarded as a consequence of the fundamental law of current conservation.

Finally, in the fourth step of this analysis, we show that (3.82) implies a universal bound on the power output of the multi-terminal model as a thermoelectric heat engine. To this end, we recall the expression (2.28)

$$P_{+}(x,y,\eta)=T_{\mathrm{c}}\mathcal{F}_{q}^{2}L_{qq}\left(\frac{x(2+y)-y\bar{\eta}}{2x(1+y)}+\sqrt{\frac{y^{2}(x+\bar{\eta})^{2}}{4x^{2}(1+y)^{2}}-\frac{y\bar{\eta}}{x(1+y)}}\right), \tag{3.83}$$

for the maximum power output at fixed efficiency η. Replacing herein L_{qq} by its upper bound (3.82) yields

$$\begin{aligned}P_{+}(x,y,\eta)&\leq\hat{P}(x,y,\eta)\\ &\equiv 4\bar{P}_{0}\left(1-\frac{y}{h(x)}\right)\left(\frac{x(2+y)-y\bar{\eta}}{2x(1+y)}+\sqrt{\frac{y^{2}(x+\bar{\eta})^{2}}{4x^{2}(1+y)^{2}}-\frac{y\bar{\eta}}{x(1+y)}}\right),\end{aligned} \tag{3.84}$$

where

$$\bar{P}_0 \equiv \frac{T_c \mathcal{F}_q^2 N_{qq}}{4} = \frac{k_B^2 T_c^4 \mathcal{F}_q^2}{16h} q \tag{3.85}$$

and the dimensionless factor q is given in (3.92). For any fixed x and η, the bound (3.84) becomes the weakest with respect to y for

$$y^*(x,\eta) = \frac{4x\bar{\eta}}{(x-1)(1+x-2\bar{\eta})} \quad \text{if} \quad |x| \geq 1 \tag{3.86}$$

and

$$y^*(x,\eta) = \frac{4\bar{\eta}}{x - x^3 - 2\bar{\eta} + 2x\bar{\eta}} \quad \text{if} \quad |x| < 1. \tag{3.87}$$

Plugging (3.86) into (3.84) yields the remarkably simple expression

$$\hat{P}_{\max}(x,\eta) \equiv \hat{P}(x, y^*(x,\eta), \eta) = 4\bar{P}_0 \begin{cases} \bar{\eta}(1-\bar{\eta}) & \text{for} \quad |x| \geq 1 \\ \bar{\eta}(1-\bar{\eta}/x^2) & \text{for} \quad |x| < 1 \end{cases}. \tag{3.88}$$

This result shows that, irrespective of the total number n of terminals, the power output must vanish at least as $(4\bar{P}_0/\eta_C)(\eta_C - \eta)$ whenever η approaches the Carnot value. We therefore can conclude that the new constraint (3.88) rules out the option of Carnot efficiency at finite power for any system that can be described by a multi-terminal model with an arbitrary number of probe terminals. Moreover, (3.88) reveals that, within this class of models, $\bar{P}_0$ is a universal upper bound on power, which is attainable only at the Curzon-Ahlborn efficiency $\eta_{CA} = \eta_C/2$.

3.4.2 Detailed Bounds

The expression of the bound (3.82) in terms of the dimensionless parameters x and y suggests that, for any finite n, the function $h(x)$ might be replaced by $h_n(x)$. In this subsection, we confirm the resulting bound

$$L_{qq} \leq N_{qq}\left(1 - \frac{y}{h_n(x)}\right), \tag{3.89}$$

which is stronger than (3.82) for $n < \infty$, by randomly generating transmission coefficients obeying the sum rules (3.25) and exploiting the matrix structure (3.26).

Numerical Procedure and Results

Since it is convenient to work with dimensionless quantities, we first introduce the new integration variable $\varepsilon \equiv (E - \mu_c)/(k_B T_c)$ in (3.21) and, second, define the rescaled matrix blocks

$$\bar{\mathbb{L}}_{\alpha\beta} \equiv \int_{-\nu}^{\infty} d\varepsilon \; \bar{f}(\varepsilon) \begin{pmatrix} 1/p & \varepsilon/\sqrt{pq} \\ \varepsilon/\sqrt{pq} & \varepsilon^2/q \end{pmatrix} \left(\delta_{ij} - \bar{T}_{\alpha\beta}(\varepsilon)\right) \equiv \mathbb{D}\mathbb{L}_{\alpha\beta}\mathbb{D}, \tag{3.90}$$

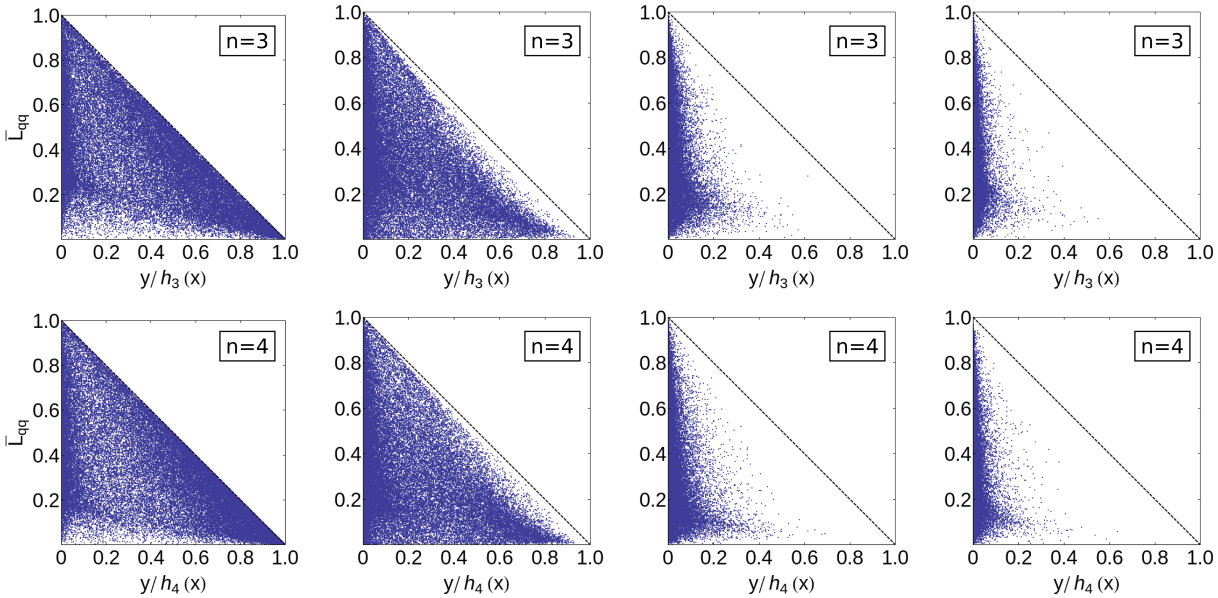

Figure 3.6: Scatter plots of the rescaled kinetic coefficient $\bar{L}_{qq}$ as a function of the ratio $y/h_n(x)$ for respectively 50000 randomly chosen n-terminal models. The dashed line is given by $\bar{L}_{qq} = 1 - y/h_n(x)$. To generate these data, we used the set of permutations A_3 (upper row) and the set A_4 for $n = 4$ (lower row)[1]. While for all plots the sign of the w_k is chosen randomly, $|w_k|$ is sampled from an increasingly large interval $\Delta \subseteq [0, 1]$. Specifically, we have from left to right $\Delta = [1, 1]$, $\Delta = [0.99, 1]$, $\Delta = [0.5, 1]$, $\Delta = [0, 1]$.

where

$$\mathbb{D} \equiv \sqrt{\frac{4h}{T_\mathrm{c}}} \begin{pmatrix} 1/\sqrt{p} & 0 \\ 0 & 1/(k_\mathrm{B} T_\mathrm{c} \sqrt{q}) \end{pmatrix}, \tag{3.91}$$

$\bar{f}(\varepsilon) \equiv \cosh^{-2}(\varepsilon/2)$ and $\bar{T}_{\alpha\beta}(\varepsilon) \equiv T_{\alpha\beta}(\varepsilon k_\mathrm{B} T_\mathrm{c} + \mu_\mathrm{c})$. The scaling parameters p and q are defined by

$$\begin{aligned} \begin{pmatrix} p \\ q \end{pmatrix} &\equiv \int_{-\nu}^{\infty} d\varepsilon \, \bar{f}(\varepsilon) \begin{pmatrix} 1 \\ \varepsilon^2 \end{pmatrix} = \begin{pmatrix} 2\{1 + \tanh(\nu/2)\} \\ 2\nu\{\nu - 4\ln(1 + e^\nu) + \nu \tanh(\nu/2)\} - 8\mathrm{Li}_2(-e^\nu) \end{pmatrix} \\ &\xrightarrow{\nu \to \infty} \begin{pmatrix} 4 \\ 4\pi^2/3 \end{pmatrix}, \end{aligned} \tag{3.92}$$

where $\nu \equiv \mu_\mathrm{c}/k_\mathrm{B} T_\mathrm{c}$ and Li_2 denotes the dilogarithm.

Next, to obtain a tractable parameterization of the matrix blocks (3.90), we exploit the fact that the rescaled transmission matrix $\bar{\mathbb{T}}(\varepsilon)$ with elements $(\bar{\mathbb{T}}(\varepsilon))_{\alpha\beta} \equiv \bar{T}_{\alpha\beta}(\varepsilon)$ is bistochastic, i.e., for any fixed ε, its elements fulfill the same sum rules (3.25) as the $T_{\alpha\beta}(E)$. Consequently, by virtue of the Birkhoff-von Neumann theorem [57], there is a set of N permutation matrices $\mathbb{P}_k$ and positive numbers $\lambda_k(\varepsilon) \in \mathbb{R}$ such that

$$\bar{\mathbb{T}}(\varepsilon) = \sum_{k=1}^{N} \lambda_k(\varepsilon) \mathbb{P}_k \quad \text{and} \quad \sum_{k=1}^{N} \lambda_k(\varepsilon) = 1. \tag{3.93}$$

[1] $A_3 \equiv \{(1)(2,3), (1,3)(2), (1,3,2)\}$
$A_4 \equiv \{(1)(2)(3,4), (1,4)(2,3), (1,4,2,3)\}$

Inserting this decomposition into (3.90) and formally carrying out the integration yields

$$\bar{\mathbb{L}}_{\alpha\beta} = \sum_{k=1}^{N} \left(\delta_{\alpha\beta} - (\mathbb{P}_k)_{\alpha\beta}\right) \mathbb{F}_k, \tag{3.94}$$

where

$$\mathbb{F}_k \equiv \int_{-\nu}^{\infty} d\varepsilon\, \bar{f}(\varepsilon)\lambda_k(\varepsilon) \begin{pmatrix} 1/p & \varepsilon/\sqrt{pq} \\ \varepsilon/\sqrt{pq} & \varepsilon^2/q \end{pmatrix} \tag{3.95}$$

is a positive semidefinite, symmetric matrix of dimension 2. Due to these properties of the $\mathbb{F}_k$, there exist some numbers $\sigma_k, a_k \in (0,\infty)$, $w_k \in [-1,1]$, such that

$$\mathbb{F}_k = \sigma_k \begin{pmatrix} 1 & w_k a_k \\ w_k a_k & a_k^2 \end{pmatrix}. \tag{3.96}$$

Combining this expression for $\mathbb{F}_k$ with the decomposition (3.94) gives a parameterization of the dimensionless matrix blocks $\bar{\mathbb{L}}_{\alpha\beta}$ in terms of N permutation matrices $\mathbb{P}_k$ of dimension n and $3N$ real parameters σ_k, a_k, w_k. The latter are constrained by the two important sum rules

$$\sum_{k=1}^{N} \sigma_k = \sum_{k=1}^{N} \sigma_k a_k^2 = 1, \tag{3.97}$$

which follow directly by comparing (3.96) with (3.95) and using the sum rule (3.93) for the $\lambda_k(\varepsilon)$. We note that, in principle, there is a third sum rule

$$\sqrt{pq} \sum_{k=1}^{N} \sigma_k w_k a_k = \int_{-\nu}^{\infty} d\varepsilon\, \bar{f}(\varepsilon)\varepsilon = \ln(16) + 4\ln\left(\cosh(\nu/2)\right) - 2\nu\tanh\left(\nu/2\right). \tag{3.98}$$

However, for simplicity, this constraint will not be used within our analysis.

We now proceed as follows. First, we chose a fixed set of N distinct, n-dimensional permutation matrices $A_{\mathrm{P}} \equiv \{\mathbb{P}_k\}_{k=1}^{N}$ and randomly pick a large number of parameter sets $A_{\mathrm{F}} \equiv \{\sigma_k, a_k, w_k\}_{k=1}^{N}$ such that for any of these sets the sum rules (3.97) are fulfilled. Second, for any of the sets A_{F}, we evaluate the matrix blocks $\bar{\mathbb{L}}_{\alpha\beta}$ according to (3.94) and (3.96) and subsequently calculate the rescaled effective matrix of kinetic coefficients $\bar{\mathbb{L}}$ using (3.10) with the $\mathbb{L}_{\alpha\beta}$ replaced by $\bar{\mathbb{L}}_{\alpha\beta}$. Third, for any individual of the thus obtained matrices $\bar{\mathbb{L}}$, we determine the values of the parameters x and y by inserting the elements of $\bar{\mathbb{L}}$ into the definitions (2.20). This step is justified, since it is readily seen that the effective matrix of kinetic coefficients $\mathbb{L}$ is connected to its rescaled counterpart via the transformation $\mathbb{L} = \mathbb{D}^{-1}\bar{\mathbb{L}}\mathbb{D}^{-1}$ and therefore the scaling factors contained in $\mathbb{D}$ cancel if the elements of $\mathbb{L}$ are plugged into (2.20). Finally, we plot the rescaled kinetic coefficient $\bar{\mathbb{L}}_{qq}$, i.e., the lower right entry of the matrix $\bar{\mathbb{L}}$, against the ratio $y/h_n(x)$.

We begin with the minimal cases $n = 3$ and $n = 4$. Fig. 3.6 shows the results of the procedure outlined above for two representative sets A_{P} of respectively three permutation

[2] $A_5 \equiv \{(1,3)(2)(4,5), (1)(2,4)(3,5), (1,4,3,2,5)\}$
$A_6 \equiv \{(1)(2)(3,6)(4,5), (1,6,4,2,5,3), (1,6,4)(2,3,5)\}$
$A_7 \equiv \{(1,3)(2,4)(5)(6,7), (1,5,7)(2,6)(3,4), (1,7,4,5,2,6,3)\}$
$A_8 \equiv \{(1,6)(2,8)(3,4,7,5), (1,5,4)(2,3)(6,8)(7), (1,7,6,3,2,8,5)(4)\}$

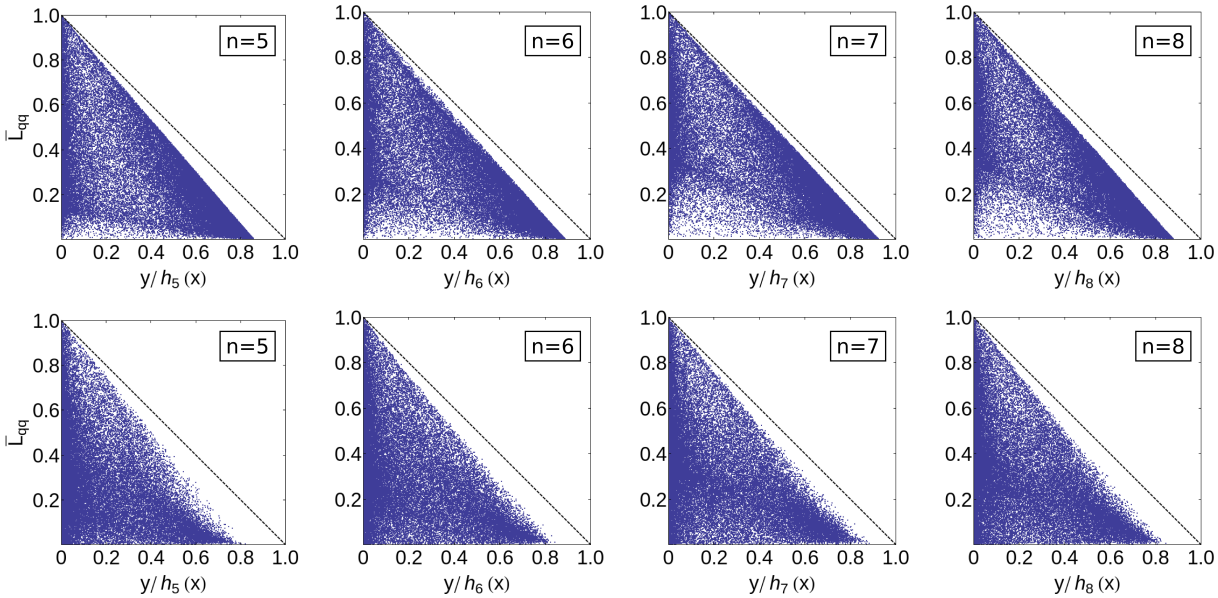

Figure 3.7: Scatter plots of the rescaled kinetic coefficient $\bar{L}_{qq}$ as a function of the ratio $y/h_n(x)$ for respectively 50000 randomly chosen n-terminal models. The upper row corresponds to $\Delta = [1, 1]$, the lower one to $\Delta = [0.99, 1]$. From left to the right, the number of terminals is $n = 5, \ldots, 9$. The sets of permutations used to generate the shown data are $A_5, \ldots, A_8$[2].

matrices and all w_k randomly chosen from an increasingly large interval. We observe that for any of these models the inequality (3.89) is respected and, for some of them, even saturated. Our numerical data further suggests that this bound is independent of the choice and number N of distinct permutation matrices $\mathbb{P}_k$ in the set A_P, where N must be larger than two and at least one of the $\mathbb{P}_k$ has to be non-symmetric to obtain a non-symmetric matrix of effective kinetic coefficients. However, if N is increased, it becomes more and more improbable to find models, for which $\bar{L}_{qq}$ attains the bound (3.89) or comes even close to it. Likewise, we find that as the interval Δ, from which the w_k are drawn, is enlarged, the sharp boundary visible in the plots shown in Fig. 3.6 deteriorates rapidly. Therefore, we are convinced that the data presented in the first row of Fig. 3.6 cover a representative subset of the extreme points in the given parameter space with respect to the inequality (3.89).

For $n > 4$, in Fig. 3.7, we show representative data, which have been obtained for $N = 3$ permutation matrices $\mathbb{P}_k$. The bound (3.89) holds for any of the randomly chosen models. However, in contrast to the cases $n = 3$ and $n = 4$, we were not able to achieve saturation. Even by increasing the number N beyond 3, this finding persists. Sampling the absolute values of the w_k from a finite interval Δ, like for 3 and 4 terminals, leads to a decay of the sharp boundary lines appearing in the upper row of Fig. 3.7. It therefore remains an open question at this stage, whether or not, for $n > 4$, there are models that saturate the bound (3.89).

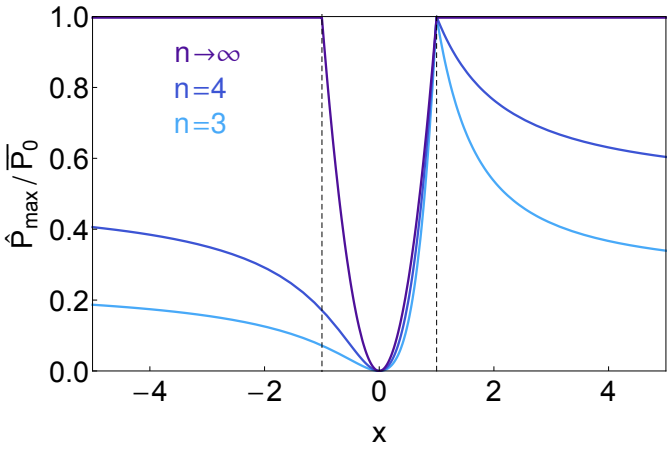

Figure 3.8: Bound (3.100) on the rescaled maximum power output $P_{\max}(x,y)/\bar{P}_0$ of the multi-terminal model as a thermoelectric generator as a function of the asymmetry parameter x for $n = 3$, $n = 4$ and the limiting case $n \to \infty$.

Maximum Power

We will now demonstrate in two steps that the constraint (3.89) leads to a more restrictive bound on power than (3.82). First, we maximize (2.6) with respect to $\mathcal{F}_\rho$, thus obtaining the maximum power

$$P_{\max}(x,y) = T_c \mathcal{F}_q^2 L_{qq} \frac{xy}{4(1+y)}. \tag{3.99}$$

Second, replacing L_{qq} by its upper bound (3.89) and optimizing the resulting expression with respect to y gives the upper bound on maximum power

$$\begin{aligned} \hat{P}_{\max}(x) \equiv \hat{P}_{\max}(x, y^*(x)) &\equiv \bar{P}_0 \frac{\sqrt{h_n(x)+1}-1}{\sqrt{h_n(x)+1}+1} \\ &= P_0 x \frac{\sqrt{4x\cos^2(\pi/n)+(x-1)^2}-|x-1|}{\sqrt{4x\cos^2(\pi/n)+(x-1)^2}+|x-1|}, \end{aligned} \tag{3.100}$$

where

$$y^*(x) \equiv \sqrt{h_n(x)+1}-1. \tag{3.101}$$

Remarkably, our new bound (3.100) on maximum power shows the same functional dependence on x as the bound (3.63) on the maximum efficiency.

The bound (3.100) is plotted in Fig. 3.8. In the limit $x \to \pm\infty$, $\hat{P}_{\max}(x)$ asymptotically approaches the value $\bar{P}_0 \cos^2(\pi/n)$. Furthermore, irrespectively of n, $\hat{P}_{\max}(x)$ attains the global maximum $\bar{P}_0$ for $x = 1$. Moreover, Fig. 3.8 reveals that the bound (3.100) becomes successively weaker as the number of terminals increases. In particular, for $n \to \infty$, $\hat{P}_{\max}(x)$ is equal to $\bar{P}_0$ whenever $|x| \geq 1$.

Bounding Power by Efficiency

We will now show that, for any finite number of terminals n, the constraint (3.89) allows to strengthen the bound (3.88) on power as a function of efficiency. To this end, first, we replace L_{qq} with its upper bound (3.89) in the expression (3.83) for the maximum power

output at fixed efficiency η. Second, we maximize the resulting expression

$$\hat{P}(x,y,\eta) = 4\bar{P}_0\left(1-\frac{y}{h_n(x)}\right)\left(\frac{x(2+y)-y\bar{\eta}}{2x(1+y)}+\sqrt{\frac{y^2(x+\bar{\eta})^2}{4x^2(1+y)^2}-\frac{y\bar{\eta}}{x(1+y)}}\right) \tag{3.102}$$

with respect to y. This procedure yields the upper bound

$$\hat{P}_{\max}(x,\eta) \equiv \hat{P}(x,y^*(x,\eta),\eta) \tag{3.103}$$

with

$$y^*(x,\eta) \equiv \bar{\eta}\frac{2x+(2x-\bar{\eta})h_n(x)+\sqrt{1+h_n(x)}\,(2x+(x-\bar{\eta})h_n(x))}{x^2-2x\bar{\eta}+(\bar{\eta}-x)^2h_n(x)}, \tag{3.104}$$

which is plotted in Fig. 3.9. We find that $\hat{P}_{\max}(x,\eta)$ vanishes linearly whenever η approaches its previously identified upper bound (3.63). In the limit $n\to\infty$, for which the bound $\hat{P}_{\max}(x,\eta)$ becomes the weakest, we end up with the simple expression (3.84), which we have proven exactly in the previous subsection.

Power at Maximum Efficiency

After having determined the maximum power of the multi-terminal model as a heat engine for given efficiency η, as another quantity of interest, we will now investigate power at maximum efficiency. To this end, we recall that, generally, the maximum efficiency (2.23) of a thermoelectric generator in the linear response regime is found by optimizing the efficiency (2.7) with respect to $\mathcal{F}_\rho$ under the condition $P\geq 0$. Inserting the thus-determined $\mathcal{F}_\rho$ into the expression (2.6) for the power output gives the power at maximum efficiency

$$P^*(x,y) \equiv T_{\mathrm{c}}\mathcal{F}_q^2 L_{qq}\frac{x}{\sqrt{1+y}}\frac{\sqrt{1+y}-1}{\sqrt{1+y}+1}. \tag{3.105}$$

By estimating L_{qq} in terms of its upper bound (3.89) and eliminating y in favor of $\eta_{\max}$ using (2.23), we obtain the bound

$$\hat{P}^*(x,\eta_{\max}) \equiv 4\bar{P}_0\bar{\eta}_{\max}\left(\frac{h_n(x)(x-\bar{\eta}_{\max})^2-4x\bar{\eta}_{\max}}{h_n(x)(x^2-\bar{\eta}_{\max}^2)}\right) \tag{3.106}$$

on the power output at maximum efficiency, where $\bar{\eta}_{\max}\equiv\eta_{\max}/\eta_{\mathrm{C}}$.

Fig. 3.9 shows plots of the function $\hat{P}^*(x,\eta_{\max})$ for $n=3$, $n=4$ and the limiting case $n\to\infty$. For any finite n, this function shows a non-trivial global maximum. Specifically, we find the maximum $\simeq 0.726\bar{P}_0$ at $(x,\bar{\eta}_{\max})\simeq(1.132,0.422)$ for $n=3$ and the maximum $\simeq 0.779P_0$ at $(x,\bar{\eta}_{\max})\simeq(1.373,0.432)$ for $n=4$. For $n\to\infty$, the global maximum converges to $\bar{P}_0$. However, this value can be reached only asymptotically for $\bar{\eta}_{\max}=1/2$ and $x\to\pm\infty$. Moreover, we find that, independent of the number of terminals n and the value of the asymmetry parameter x, the power at maximum efficiency vanishes like $(4\bar{P}_0/\eta_{\mathrm{C}})(\eta_{\max}(x)-\eta_{\max})$ when $\eta_{\max}$ saturates its upper bound (3.63).

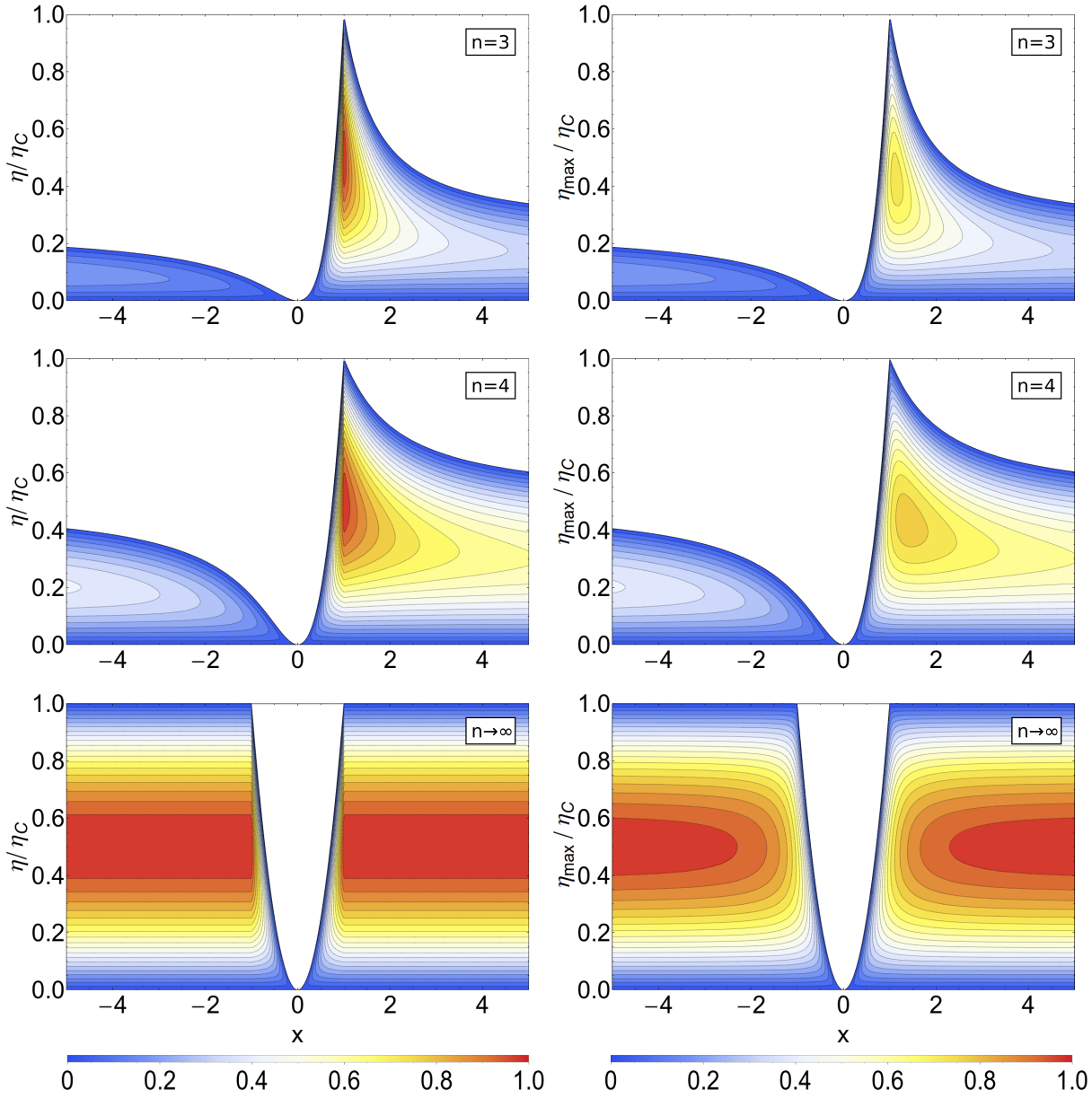

Figure 3.9: Bounds on the power of the n-terminal model as a thermoelectric heat engine in units of $\bar{P}_0$ and as functions of the asymmetry parameter x and the normalized efficiency $\bar{\eta} = \eta/\eta_C$ for $n = 3$, $n = 4$ and $n \to \infty$. The white regions in the plots are forbidden by the bound on efficiency (3.63). The left column corresponds to the bound on power for given efficiency $\hat{P}_{\max}(x, \eta)$, the right column to the bound (3.106) on power at maximum efficiency.

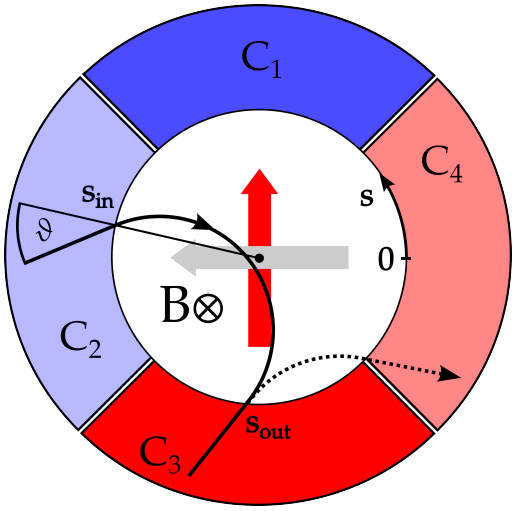

Figure 3.10: Scheme of the classical Nernst engine. The vertical heat current (red arrow) between the reservoirs C_h and C_c with temperatures $T_\mathrm{h} > T_\mathrm{c}$ drives a horizontal particle current (gray arrow) from reservoir C_2 to C_1 with respective chemical potentials μ_1 and $\mu_2 < \mu_1$. The bold black line denotes a classical trajectory leaving the reservoir C_1 at s_in and entering C_h at s_out, where $0 \le s \le 2\pi R$ parameterizes the circumference. The dotted line shows the corresponding reversed trajectory for an entry at s_out, which does not coincide with the original one, since the magnetic field $\mathbf{B}$ breaks the time-reversal symmetry. For further symbols, see main text.

3.5 A Classical Nernst Engine

The Nernst effect describes the emergence of an electrical voltage perpendicular to a heat current traversing an isotropic conductor in the presence of a constant magnetic field [25]. While Seebeck-based devices, for which the heat and the particle current are coupled without a magnetic field, have been the subject of intensive research efforts during the last decades [14–17], only a few attempts were made to utilize the Nernst effect for power generation more than 50 years ago [58–61]. This lack of interest may have been caused by the uncompetitive net efficiency of such devices, which is inevitably suppressed by the energetic cost of the strong magnetic fields they require. Due to their working principle, Nernst-based generators are, however, ideal systems to investigate the influence of a magnetic field on the performance of thermoelectric heat engines.

Here, discuss a simple mechanical model for a thermoelectric engine based on the Nernst effect, which has been studied by J. Stark within his master thesis [62]. To this end, we first introduce a classical counterpart of the quantum mechanical multi-terminal setup discussed so far. We then show that Liouville's theorem implies bounds the maximum efficiency and the efficiency at maximum power of this model as a Nernst engine, which are analogous to (3.63) and (3.64), respectively. Specializing on a particularly simple setup, for which the kinetic coefficients have been calculated explicitly [62], we demonstrate that these bounds can be saturated in the limit of large magnetic fields and small fugacities in the thermochemical baths.

3.5.1 System

Currents

As shown in Fig. 3.10, we consider a two-dimensional, potential-free, circular central region of radius R perpendicularly penetrated by a magnetic field $\mathbf{B}$ and surrounded by four thermoechemical reservoirs C_α. Each of these reservoirs covers a segment of length $l = \pi R/2$ of the boundary and injects non-interacting particles into the central area. The fluxes entering and leaving the system through the reservoirs can be determined as follows. Any particle that reaches the circular boundary from one of the reservoirs is assumed

to enter the central region. Such a minimalistic assumption of perfectly transparent boundaries has been shown to be thermodynamically consistent [63] and allows us to calculate the fluxes explicitly. Maxwell-Boltzmann statistics in the reservoirs modeled as ideal gases maintained at equilibrium with temperature T_α and chemical potential μ_α implies a total particle current [62],

$$J_\rho^{\alpha+} \equiv \int_l ds \int_0^\infty dE \int_{-\pi/2}^{\pi/2} d\vartheta \; u_\alpha(E) \cos\vartheta = \frac{\sqrt{2\pi m (k_\mathrm{B} T_\alpha)^3}}{h^2} l \exp\left(\mu_\alpha/(k_\mathrm{B} T_\alpha)\right) \tag{3.107}$$

flowing from the reservoir C_α into the system, where

$$u_\alpha(E) \equiv \sqrt{2mE} \exp\left(-(E-\mu_\alpha)/(k_\mathrm{B} T_\alpha)\right)/h^2, \tag{3.108}$$

m denotes the mass of the particles, E their kinetic energy and h Planck's constant. For the definition of the coordinates s and ϑ, see Fig. 3.10. Likewise, assuming that each particle hitting the boundary from inside the central region is absorbed in the adjacent reservoir, the steady-state current flowing into C_α reads

$$J_\rho^{\alpha-} \equiv \sum_{\beta=\mathrm{h},\ldots,\mathrm{c}} \int_l ds \int_0^\infty dE \int_{-\pi/2}^{\pi/2} d\vartheta \; u_\beta(E) \cos\vartheta \tau_\alpha(E,s,\vartheta). \tag{3.109}$$

In (3.109), we have introduced the conditional probability $\tau_\alpha(E,s,\vartheta)$ for a particle of energy E entering at position s with angle ϑ to reach the boundary of the reservoir C_α after passing through the central region. Since we assume purely Hamiltonian dynamics inside the central region, this probability can either be 1 or 0.

By combining (3.107) and (3.109), we arrive at the expression

$$J_\rho^\alpha \equiv J_\rho^{\alpha+} - J_\rho^{\alpha-} = \sum_{\beta=\mathrm{h},\ldots,\mathrm{c}} \int_0^\infty dE \; \left(2l\delta_{\alpha\beta} - \tilde{T}_{\alpha\beta}(E)\right) u_\beta(E) \tag{3.110}$$

for the net particle current leaving the reservoir C_α. An analogous calculation yields the corresponding heat current

$$J_q^\alpha \equiv \sum_{\beta=\mathrm{h},\ldots,\mathrm{c}} \int_0^\infty dE \; (E-\mu_\alpha) \left(2l_\alpha\delta_{\alpha\beta} - \tilde{T}_{\alpha\beta}(E)\right) u_\beta(E). \tag{3.111}$$

Here, we have introduced the classical transmission coefficients

$$\tilde{T}_{\alpha\beta}(E) \equiv \int_l ds \int_{-\pi/2}^{\pi/2} d\vartheta \; \tau_\alpha(E,s,\vartheta) \cos\vartheta \geq 0. \tag{3.112}$$

In analogy with their quantum mechanical counterparts, these coefficients fulfill the sum rules

$$\sum_{\beta=\mathrm{h},\ldots,\mathrm{c}} \tilde{T}_{\alpha\beta}(E) = 2l \quad \text{and} \quad \sum_{\alpha=\mathrm{h},\ldots,\mathrm{c}} \tilde{T}_{\alpha\beta}(E) = 2l, \tag{3.113}$$

which are a consequence of Liouville's theorem as we prove in App. 3C.

Kinetic Coefficients

We now focus on the linear response regime. To this end, we chose the reference values T_c and μ_1 for temperature and chemical potential, respectively, and define the gradients $\Delta T_\alpha = T_\alpha - T_\mathrm{c}$ and $\Delta\mu_\alpha = \mu_\alpha - \mu_1$ for $\alpha = \mathrm{h}, 1, 2, \mathrm{c}$. Linearizing the currents (3.110) and (3.111) yields six phenomenological relations

$$\mathbf{J}^{\mathrm{NE}} = \mathbb{L}^{\mathrm{NE4}} \boldsymbol{\mathcal{F}}^{\mathrm{NE}}, \tag{3.114}$$

where the current and the affinity vector are defined as

$$\mathbf{J}^{\mathrm{NE}} \equiv \left(J_\rho^{\mathrm{h}}, J_q^{\mathrm{h}}, J_q^1, J_\rho^2, J_q^2, J_\rho^{\mathrm{c}}\right)^t \tag{3.115}$$

and

$$\begin{aligned} \boldsymbol{\mathcal{F}}^{\mathrm{NE}} &\equiv \left(\mathcal{F}_\rho^{\mathrm{h}}, \mathcal{F}_q^{\mathrm{h}}, \mathcal{F}_q^1, \mathcal{F}_\rho^2, \mathcal{F}_q^2, \mathcal{F}_\rho^{\mathrm{c}}\right)^t \\ &\equiv \frac{1}{T_\mathrm{c}} \left(\Delta\mu_\mathrm{h}, \Delta T_\mathrm{h}/T_\mathrm{c}, \Delta T_1/T_\mathrm{c}, \Delta\mu_2, \Delta T_2/T_\mathrm{c}, \Delta\mu_\mathrm{c}\right)^t. \end{aligned} \tag{3.116}$$

The matrix of kinetic coefficients $\mathbb{L}^{\mathrm{NE4}}$ is obtained from the extended matrix

$$\mathbb{M}^{\mathrm{NE4}} \equiv \int_0^\infty dE\, u(E) \left(\mathbb{D} - \tilde{\mathbb{T}}(E)\right) \otimes \begin{pmatrix} 1 & E-\mu_\mathrm{c} \\ E-\mu_\mathrm{c} & (E-\mu_\mathrm{c})^2 \end{pmatrix}. \tag{3.117}$$

by deleting the rows and columns 3 and 8, i.e.,

$$\mathbb{L}^{\mathrm{NE4}} = \mathbb{M}^{\mathrm{NE4}}_{[3,8]}. \tag{3.118}$$

Here, we defined the function

$$u(E) \equiv \sqrt{2mE} \exp\left(-(E-\mu_1)/(k_\mathrm{B}T_\mathrm{c})\right)/h^2 \tag{3.119}$$

and the matrices

$$\mathbb{D} \equiv \mathrm{diag}(l, l, l, l) \tag{3.120}$$

and

$$\tilde{\mathbb{T}}(E) \equiv \begin{pmatrix} \tilde{T}_{\mathrm{hh}}(E) & \cdots & \tilde{T}_{\mathrm{hc}}(E) \\ \vdots & \ddots & \vdots \\ \tilde{T}_{\mathrm{ch}}(E) & \cdots & \tilde{T}_{\mathrm{cc}}(E) \end{pmatrix}. \tag{3.121}$$

The asymmetry of the matrix $\mathbb{L}^{\mathrm{NE4}}$ can be bounded in two steps. First, we consider the matrix $\mathbb{M}^{\mathrm{NE4}}$. Obviously, the expression (3.117) is structurally identical with the Landauer-Büttiker formula (3.40) for the kinetic coefficients of the quantum mechanical multi-terminal model. Furthermore, since, due to the sum rules (3.113), the matrix $\tilde{\mathbb{T}}(E)$ is sum-symmetric, repeating the lines (3.39) to (3.48) with $\mathbb{M}^{\mathrm{NE4}}$ in place of $\mathbb{L}^n_{[[A]]}$ and using Corollary 3 instead of Corollary 2 yields the bound[1]

$$\mathcal{S}\left(\mathbb{M}^{\mathrm{NE4}}\right) \leq \cot\left(\frac{\pi}{4}\right) \tag{3.122}$$

[1] In the special setup considered here, each reservoir covers an equal part of the boundary of the central region. Consequently, up to an irrelevant scaling factor, the matrix $\tilde{\mathbb{T}}(E)$ is bistochastic and Corollary 1 would be sufficient to prove (3.122). Due to Corollary 3, this bound, however also holds in more general geometries with reservoirs of unequal width.

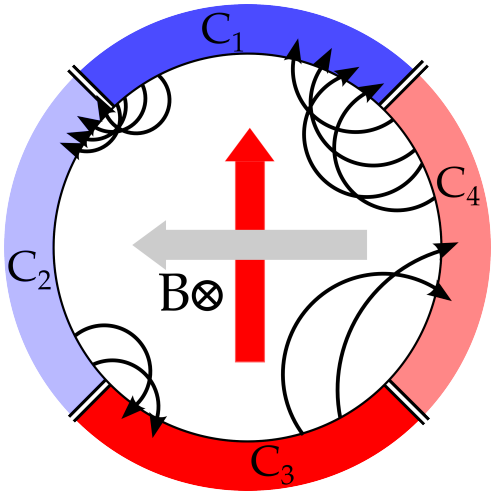

Figure 3.11: Operation principle of the classical Nernst engine. The circular arrows show characteristic trajectories of non-interacting particles for a strong magnetic field **B**. Since the typical Larmor-radii are small compared to the radius of the central region, particles can be exchanged only between next-neighboring reservoirs. The radius and number of the trajectories reflect the temperature and chemical potential, i.e., density, of the respective reservoir they originate from. Due to the boundary conditions (3.124), a heat current from the bottom to the top arises, which drives a particle current from right to left.

on the asymmetry index of $\mathbb{M}^{\mathrm{NE4}}$. Second, since $\mathbb{L}^{\mathrm{NE4}}$ is a principal submatrix of $\mathbb{M}^{\mathrm{NE4}}$, Proposition 3 implies

$$\mathcal{S}\left(\mathbb{L}^{\mathrm{NE4}}\right) \leq \mathcal{S}\left(\mathbb{M}^{\mathrm{NE4}}\right) \leq \cot\left(\frac{\pi}{4}\right) = 1. \tag{3.123}$$

3.5.2 Nernst Engine

Operation Principle

For a Nernst engine, we put $\Delta\mu_2 < 0$ and $\Delta T_{\mathrm{h}} > 0$ and impose the boundary conditions

$$J_\rho^{\mathrm{c}} = J_\rho^{\mathrm{h}} = 0 \quad \text{and} \quad J_q^1 = J_q^2 = 0, \tag{3.124}$$

which allow us to eliminate the affinities $\mathcal{F}_\rho^{\mathrm{c}}, \mathcal{F}_\rho^{\mathrm{h}}, \mathcal{F}_q^1$ and $\mathcal{F}_q^2$ in (3.114). These conditions ensure that the particle current occurs only horizontally and heat flows only vertically in the setup of Fig. 3.10 and Fig. 3.11. As indicated in Fig. 3.11, the operation principle of the Nernst engine can then be understood in terms of typical trajectories as follows. The lower reservoir C_{h} is at high temperature but relatively low chemical potential. Therefore, it transmits few but fast particles to the right reservoir C_2. Since this reservoir has lower temperature but higher chemical potential, it injects slower but more particles in order to compensate for the inflowing heat current. Thus, heat is dissipated into the upper, cold reservoir C_{c}. Now, the number of particles in C_{c} has to be conserved on average. Consequently, its chemical potential must be relatively high to ensure that many but slow particles are transferred to the left reservoir C_1. Finally, due to $T_1 > T_{\mathrm{c}}$, a small particle current from C_1 to C_{h} is sufficient to compensate for the net heat current C_1 has received from C_{c}. Summing up, the heat current from C_{h} to C_{c} drives a particle current uphill from C_2 to C_1.

Bounds on Kinetic Coefficients and Efficiency

Due to the boundary conditions (3.124), the net transport process in the Nernst engine is captured by two phenomenological equations

$$\begin{pmatrix} J_\rho \\ J_q \end{pmatrix} = \mathbb{L}^{\mathrm{NE}} \begin{pmatrix} \mathcal{F}_\rho \\ \mathcal{F}_q \end{pmatrix}, \tag{3.125}$$

where $J_\rho \equiv J_\rho^2$, $J_q \equiv J_q^{\mathrm{h}}$, $\mathcal{F}_\rho \equiv \mathcal{F}_\rho^2$, $\mathcal{F}_q \equiv \mathcal{F}_q^{\mathrm{h}}$ and

$$\mathbb{L}^{\mathrm{NE}} \equiv \begin{pmatrix} L_{\rho\rho}^{\mathrm{NE}} & L_{\rho q}^{\mathrm{NE}} \\ L_{q\rho}^{\mathrm{NE}} & L_{qq}^{\mathrm{NE}} \end{pmatrix} \tag{3.126}$$

is the matrix of effective kinetic coefficients. This matrix can be obtained from the full matrix of kinetic coefficients $\mathbb{L}^{\mathrm{NE4}}$ by, first, reordering rows and columns according to

$$\mathbb{L}^{\mathrm{NE4}} \to \mathbb{L}'^{\mathrm{NE4}} \equiv \mathbb{P}\mathbb{L}^{\mathrm{NE4}}\mathbb{P}, \tag{3.127}$$

and, second, taking the Schur complement

$$\mathbb{L}^{\mathrm{NE}} = \mathbb{L}'^{\mathrm{NE4}}/\mathbb{L}'^{\mathrm{NE4}}_{[1,2]}, \tag{3.128}$$

where

$$\mathbb{P} \equiv \begin{pmatrix} 0 & 0 & 0 & 1 & 0 & 0 \\ 0 & 1 & 0 & 0 & 0 & 0 \\ 0 & 0 & 1 & 0 & 0 & 0 \\ 1 & 0 & 0 & 0 & 0 & 0 \\ 0 & 0 & 0 & 0 & 1 & 0 \\ 0 & 0 & 0 & 0 & 0 & 1 \end{pmatrix} \tag{3.129}$$

denotes a symmetric permutation matrix and $\mathbb{L}'^{\mathrm{NE4}}_{[1,2]}$ arises from $\mathbb{L}'^{\mathrm{NE4}}$ by deleting the first two rows and columns.

Besides the second law requiring

$$L_{\rho\rho}^{\mathrm{NE}}, L_{qq}^{\mathrm{NE}} \geq 0 \quad \text{and} \quad L_{\rho\rho}^{\mathrm{NE}} L_{qq}^{\mathrm{NE}} - (L_{\rho q}^{\mathrm{NE}} + L_{q\rho}^{\mathrm{NE}})^2/4 \geq 0, \tag{3.130}$$

the effective kinetic coefficients (3.128) are subject to two additional constraints. First, the two mirror symmetries of the model imply that the off-diagonal coefficients are connected via the relation [62]

$$L_{\rho q}^{\mathrm{NE}} = -L_{q\rho}^{\mathrm{NE}}. \tag{3.131}$$

Second, by virtue of Proposition 1 and Proposition 4 provided in Ch. 5, we have

$$\mathcal{S}\left(\mathbb{L}^{\mathrm{NE}}\right) = \mathcal{S}\left(\mathbb{L}'^{\mathrm{NE4}}/\mathbb{L}'^{\mathrm{NE4}}_{[1,2]}\right) \leq \mathcal{S}\left(\mathbb{L}'^{\mathrm{NE4}}\right) = \mathcal{S}\left(\mathbb{P}\mathbb{L}^{\mathrm{NE4}}\mathbb{P}\right) = \mathcal{S}\left(\mathbb{L}^{\mathrm{NE4}}\right) \leq 1. \tag{3.132}$$

This bound on the asymmetry index of $\mathbb{L}^{\mathrm{NE}}$ implies the relation

$$L_{\rho\rho}^{\mathrm{NE}} L_{qq}^{\mathrm{NE}} - \left(L_{\rho q}^{\mathrm{NE}}\right)^2 \geq 0. \tag{3.133}$$

The power output and efficiency of the Nernst engine are given by

$$P = -\Delta\mu_2 J_\rho = -T_{\mathrm{c}} \mathcal{F}_\rho J_\rho \tag{3.134}$$

and

$$\eta = P/J_q, \tag{3.135}$$

respectively. Maximizing these quantities with respect to $\mathcal{F}_\rho$ under the condition $P > 0$ yields the maximum efficiency

$$\eta_{\max}(\mathcal{Z}T) = \eta_C \frac{1-\sqrt{1-\mathcal{Z}T}}{1+\sqrt{1-\mathcal{Z}T}} \tag{3.136}$$

and the efficiency at maximum power

$$\eta^*(\mathcal{Z}T) = \eta_C \frac{\mathcal{Z}T}{2-\mathcal{Z}T}. \tag{3.137}$$

Obviously, like for conventional, time-reversal symmetric thermoelectric devices, the benchmark parameters $\eta_{\max}$ and η^* depend only on a single dimensionless quantity, the thermomagnetic figure of merit

$$\mathcal{Z}T \equiv \frac{\left(L_{\rho q}^{\mathrm{NE}}\right)^2}{L_{\rho\rho}^{\mathrm{NE}} L_{qq}^{\mathrm{NE}} - \left(L_{\rho q}^{\mathrm{NE}}\right)^2}. \tag{3.138}$$

This parameter is usually given in the form $\mathcal{Z}T = (NB)^2\sigma T/\kappa$, where NB is the thermomagnetic power, T the reference temperature, σ the electrical and κ the thermal conductivity [25]. However, this definition coincides with the one given in (3.138), if the transport coefficients NB, σ and κ are identified correctly with the effective kinetic coefficients [62].

Two bounds successively constrain the parameter $\mathcal{Z}T$. First, the condition (3.130), which, due to the symmetry (3.131), reduces to $L_{\rho\rho}^{\mathrm{NE}}, L_{qq}^{\mathrm{NE}} \geq 0$, leads to [61]

$$0 \leq \mathcal{Z}T \leq 1. \tag{3.139}$$

Second, the constraint (3.133) implies

$$0 \leq \mathcal{Z}T \leq 1/2. \tag{3.140}$$

Obviously, the constraint (3.140), which ultimately relies on Liouville's theorem, is stronger than (3.139). In particular, while the second law, in principle, allows both, the maximum efficiency and the efficiency at maximum power to approach η_C in the limit $\mathcal{Z}T \to 1$, the bound (3.140) implies the significantly lower limits

$$\eta_{\max} \leq (3-2\sqrt{2})\eta_C \simeq 0.172\eta_C \tag{3.141}$$

and

$$\eta^* \leq \eta_C/6 \simeq 0.167\eta_C. \tag{3.142}$$

These universal bounds on the efficiency of a classical Nernst engine arise from the four-terminal setup and the symmetry (3.131) but are independent of further details of the geometry and the strength of the magnetic field. Moreover, (3.141) and (3.142) would hold for any potential landscape inside the central region preserving the two mirror symmetries of the system. In particular, one may include potential barriers separating the central area from the reservoirs. We note that any additional potential arising from differently biased reservoirs can be safely neglected within the linear response regime, since, quite generally, the linear transport coefficients, i.e., here the effective kinetic coefficients (3.128), do not depend on the applied external fields.

Strong Field Limit

The simple circular shape of the single particle trajectories inside the central region permits to compute the classical transmission coefficients (3.112) and thus the kinetic coefficients (3.128) explicitly for any strength of the magnetic field [62]. For convenience, we will, however, focus on the strong field limit $\mathcal{B} \gg 1$ here, where the matrix of kinetic coefficient assumes the particularly simple form

$$\mathbb{L}^{\mathrm{NE}} = \frac{J_0}{2\sqrt{\pi}\mathcal{B}} \begin{pmatrix} 1 & k_{\mathrm{B}}T_{\mathrm{c}}\sqrt{v-1} \\ -k_{\mathrm{B}}T_{\mathrm{c}}\sqrt{v-1} & k_{\mathrm{B}}^2T_{\mathrm{c}}^2(1+v) \end{pmatrix} + \mathcal{O}\left(\frac{1}{\mathcal{B}^2}\right). \tag{3.143}$$

In (3.143), we defined the dimensionless parameter

$$v \equiv 1 + \left(2 - \mu_1/(k_{\mathrm{B}}T_{\mathrm{c}})\right)^2 \tag{3.144}$$

and the rescaled magnetic field

$$\mathcal{B} \equiv \frac{|q|\,|\mathbf{B}|\,R}{\sqrt{2k_{\mathrm{B}}T_{\mathrm{c}}mc}}, \tag{3.145}$$

where q denotes the charge of one particle and c the speed of light. The quantity

$$J_0 \equiv \sqrt{m\left(2\pi k_{\mathrm{B}}T_{\mathrm{c}}\right)^3}R\exp\left(\mu_1/(k_{\mathrm{B}}T_{\mathrm{c}})\right)/h^2 \tag{3.146}$$

corresponds to the total particle current flowing into the central region at thermal equilibrium, i.e., for $\Delta T_\alpha = \Delta\mu_\alpha = 0$, as one can easily infer from (3.107).

The maximum efficiency and the efficiency at maximum power in the strong field regime are found as

$$\eta_{\max} = \eta_{\mathrm{C}}\frac{\sqrt{2v} - \sqrt{1+v}}{\sqrt{2v} + \sqrt{2+v}} \tag{3.147}$$

and

$$\eta^* = \eta_{\mathrm{C}}\frac{v-1}{6v+2} \tag{3.148}$$

by inserting (3.143) into (3.138), (3.136) and (3.137), respectively. Hence, the bounds (3.141) and (3.142) are asymptotically tight, since they can be reached for $v \to \infty$, i.e., for $\mu_1/(k_{\mathrm{B}}T_{\mathrm{c}}) \to -\infty$. However, in this limit, the equilibrium current $J_0 \sim \exp\left(\mu_1/(k_{\mathrm{B}}T_{\mathrm{c}})\right)$, and likewise the matrix of kinetic coefficients (3.143), decay exponentially. Thus, the saturation of the bounds (3.141) and (3.142) comes at the price of vanishing power. Finally, we note that the limit $\mu_1/(k_{\mathrm{B}}T_{\mathrm{c}}) \to \infty$, is incompatible with the classical approach used here, since it would lead to an exponentially high equilibrium fugacity $\exp\left(\mu_1/k_{\mathrm{B}}T_{\mathrm{c}}\right)$ in the reservoirs. Under these conditions, quantum effects can, however, not be neglected anymore [5].

3.6 Conclusion

In this chapter, we have derived various non-trivial bounds on the performance figures of the multi-terminal model as a thermoelectric heat engine with broken time-reversal symmetry. Starting with the minimal case of three terminals, we proved that current conservation implies substantially stronger bounds on maximum efficiency and efficiency at maximum power than the bare second law. Generalizing to systems with an arbitrary number n of terminals, we found that these bounds become successively weaker as n increases. In particular, for large n, they reduce effectively to the constraints imposed by the second law.

In the next step, we focused on power rather than efficiency. After introducing suitable normalization factors, we demonstrated that current conservation leads to yet another constraint on the effective kinetic coefficients, which is independent of n. This constraint allows to recover the efficiency-dependent bound on power known from time-reversal symmetric engines up to a scaling factor. Hence, we have shown that the power of any thermoelectric heat engine that can be described by a multi-terminal model vanishes at least linearly when its efficiency approaches the Carnot value. Moreover, we found strong numerical evidence for the existence of an even stronger constraint in systems with a small number of terminals. This detailed constraint implies a bound on power that is a rather involved function of efficiency and decays linearly to zero as η approaches its upper bound for a fixed number n of terminals and a fixed value of the asymmetry parameter x. For large n, this function converges to the simple quadratic relation proven before.

Our new efficiency-dependent bound on power assumes its maximum $\bar{P}_0$ at the Curzon-Ahlborn value $\eta_{\mathrm{CA}} = \eta_{\mathrm{C}}/2$. Interestingly, by setting $\mu_{\mathrm{c}} = 0$, we get $\bar{P}_0 = (1/24)\pi^2 k_{\mathrm{B}}^2 \Delta T_{\mathrm{h}}^2/h$. This value is only about a factor 1.3 larger than the bound $P_{\mathrm{gen}}^{\mathrm{qb2}} \simeq 0.0321\pi^2 k_{\mathrm{B}}^2 \Delta T_{\mathrm{h}}^2/h$ for $N = 1$ conduction channels, i.e., one-dimensional leads, which was recently derived by Whitney [64,65]. The bound $P_{\mathrm{gen}}^{\mathrm{qb2}}$ was obtained for a quantum coherent conductor in the non-linear regime and for vanishing magnetic field. The deviation from our result might be explained by the fact that Whitney's analysis does not include probe terminals or any other sources of dephasing.

Finally, we discussed a classical model for a thermoelectric heat engine based on the Nernst effect. Since, for a potential-free central region, the single-particle trajectories are circles in this model, the kinetic coefficients could be calculated exactly under the assumption of non-interacting particles. It turned out that the maximum efficiency and the efficiency at maximum power of the classical Nernst engine is subject to upper bounds following from Liouville's theorem, which are substantially smaller than η_{C} and η_{CA}, respectively. These bounds can, however, be saturated in the limit of a strong magnetic field and small fugacities in the thermochemical baths.

Appendix

3.A Proof that the Matrix (3.29) is positive semidefinite

Here, we prove that the Hermitian matrix

$$\mathbb{K}^3 = \mathbb{L}^3 + \mathbb{L}^{3t} + i\sqrt{3}\left(\mathbb{L}^3 - \mathbb{L}^{3t}\right) \in \mathbb{C}^{4\times 4}. \tag{3.149}$$

as introduced in (3.28) is positive semidefinite. To this end, we notice that any complex vector $\mathbf{z} \in \mathbb{C}^4$ can be written as

$$\mathbf{z} = \mathbf{z}_1 \otimes \begin{pmatrix} 1 \\ 0 \end{pmatrix} + \mathbf{z}_2 \otimes \begin{pmatrix} 0 \\ 1 \end{pmatrix} \quad \text{with} \quad \mathbf{z}_1, \mathbf{z}_2 \in \mathbb{C}^2. \tag{3.150}$$

Using this decomposition and the representation (3.26) of the matrix $\mathbb{L}^3$, we obtain

$$\mathbf{z}^\dagger \mathbb{K}^3 \mathbf{z} = \int_0^\infty dE\, f(E) \mathbf{y}^\dagger(E) \mathbb{V}^3(E) \mathbf{y}(E), \tag{3.151}$$

where we defined the vector

$$\mathbf{y}(E) \equiv \mathbf{z}_1 + (E - \mu_c)\mathbf{z}_2 \in \mathbb{C}^2 \tag{3.152}$$

and the matrix

$$\mathbb{V}^3 \equiv \begin{pmatrix} 2(1 - T_{hh}) & -T_{h1} - T_{1h} - i\sqrt{3}(T_{h1} - T_{1h}) \\ -T_{h1} - T_{1h} + i\sqrt{3}(T_{h1} - T_{1h}) & 2(1 - T_{11}) \end{pmatrix}. \tag{3.153}$$

Since the function $f(E)$ is positive for any E, the identity (3.151) reveals that if $\mathbb{V}^3(E)$ is positive semidefinite, the same holds for $\mathbb{K}^3$. Note that, from (3.152) onwards, we notationally suppress the dependence of the transmission coefficients $T_{\alpha\beta}$ and the matrix $\mathbb{V}^3$ on energy E, which is considered as fixed for the rest of the proof.

In order to show that $\mathbb{V}^3$ is positive semi-definite, we first observe that both diagonal entries of $\mathbb{V}^3$ are obviously non-negative. It therefore suffice to show that the determinant of $\mathbb{V}$ is non-negative. The direct calculation of the determinant yields

$$\frac{\text{Det } \mathbb{V}^3}{4} = (1 - T_{hh})(1 - T_{11}) - T_{h1}^2 - T_{1h}^2 + T_{1h}T_{h1}. \tag{3.154}$$

Now, we distinguish two cases. First, we assume $T_{h1} \geq T_{1h}$ and rewrite (3.154) as

$$\begin{aligned} \frac{\text{Det } \mathbb{V}^3}{4} &= (T_{h1} + T_{hc})(T_{h1} + T_{c1}) - T_{h1}^2 - T_{1h}^2 + T_{1h}T_{h1} \\ &= T_{h1}T_{c1} + T_{hc}T_{h1} + T_{hc}T_{c1} + T_{1h}(T_{h1} - T_{1h}) \geq 0. \end{aligned} \tag{3.155}$$

Here, we used the sum rules (3.25), which are a direct consequence of the unitarity of the scattering matrix. On the other hand, if $T_{\mathrm{h1}} < T_{\mathrm{1h}}$, we can use (3.25) to write

$$\begin{aligned}\frac{\operatorname{Det}\mathbb{V}^3}{4} &= (T_{\mathrm{1h}}+T_{\mathrm{ch}})(T_{\mathrm{1h}}+T_{\mathrm{1c}}) - T_{\mathrm{h1}}^2 - T_{\mathrm{1h}}^2 + T_{\mathrm{1h}}T_{h1} \\ &= T_{\mathrm{1h}}T_{\mathrm{1c}} + T_{\mathrm{ch}}T_{\mathrm{1h}} + T_{\mathrm{ch}}T_{\mathrm{1c}} + T_{\mathrm{h1}}(T_{\mathrm{1h}} - T_{\mathrm{h1}}) \geq 0.\end{aligned} \tag{3.156}$$

In conclusion, we have shown that $\operatorname{Det}\mathbb{V}^3 \geq 0$ and therefore the proof that $\mathbb{K}^3$ is positive semidefinite is complete.

3.B Proof that the matrix (3.71) is positive semidefinite

We proceed in two steps. First, we observe that, for any bistochastic matrix $\mathbb{T} \in \mathbb{R}^{n\times n}$, the matrix $\mathbb{T}^t\mathbb{T}$ is again bistochastic. Consequently, the matrix

$$2\mathbb{1} - \mathbb{T} - \mathbb{T}^t - (\mathbb{1}-\mathbb{T}^t)(\mathbb{1}-\mathbb{T}) = \mathbb{1} - \mathbb{T}^t\mathbb{T} \tag{3.157}$$

is positive semidefinite by virtue of Corollary 1. Second, using this result, for any $\mathbf{x}_1, \mathbf{x}_2 \in \mathbb{R}^n$, we obtain

$$\begin{aligned}&(\mathbf{x}_1^t, \mathbf{x}_2^t)\begin{pmatrix}\mathbb{1} & \mathbb{1}-\mathbb{T}\\ \mathbb{1}-\mathbb{T}^t & 2\mathbb{1}-\mathbb{T}-\mathbb{T}^t\end{pmatrix}\begin{pmatrix}\mathbf{x}_1\\ \mathbf{x}_2\end{pmatrix} \\ &\quad= \mathbf{x}_1^t\mathbf{x}_1 + \mathbf{x}_1^t(\mathbb{1}-\mathbb{T})\mathbf{x}_2 + \mathbf{x}_2^t(\mathbb{1}-\mathbb{T}^t)\mathbf{x}_1 + \mathbf{x}_2^t(2\mathbb{1}-\mathbb{T}-\mathbb{T}^t)\mathbf{x}_2 \\ &\quad\geq \mathbf{x}_1^t\mathbf{x}_1 + \mathbf{x}_1^t(\mathbb{1}-\mathbb{T})\mathbf{x}_2 + \mathbf{x}_2^t(\mathbb{1}-\mathbb{T}^t)\mathbf{x}_1 + \mathbf{x}_2^t(\mathbb{1}-\mathbb{T}^t)(\mathbb{1}-\mathbb{T})\mathbf{x}_2 \\ &\quad= \left(\mathbf{x}_1^t + \mathbf{x}_2^t(\mathbb{1}-\mathbb{T}^t)\right)\left(\mathbf{x}_1 + (\mathbb{1}-\mathbb{T})\mathbf{x}_2\right) = \left(\mathbf{x}_1 + (\mathbb{1}-\mathbb{T})\mathbf{x}_2\right)^t\left(\mathbf{x}_1 + (\mathbb{1}-\mathbb{T})\mathbf{x}_2\right) \geq 0.\end{aligned} \tag{3.158}$$

Hence, the proof is completed.

3.C Proof of the Sum Rules (3.113)

For an elementary proof of the sum rules (3.113), we consider a particle with fixed energy E injected at the position s_{in} and the angle ϑ_{in}. After traveling through the circular central region, the particle eventually leaves it at the position s_{out} and the angle ϑ_{out} as shown in Fig. 3.10. Since we assume Hamiltonian dynamics inside the central region, there is a one-to-one mapping

$$\mathcal{M}: \begin{pmatrix}s_{\mathrm{in}}\\ \vartheta_{\mathrm{in}}\end{pmatrix} \mapsto \begin{pmatrix}s_{\mathrm{out}}\\ \vartheta_{\mathrm{out}}\end{pmatrix} = \begin{pmatrix}s_{\mathrm{out}}(s_{\mathrm{in}},\vartheta_{\mathrm{in}})\\ \vartheta_{\mathrm{out}}(s_{\mathrm{in}},\vartheta_{\mathrm{in}})\end{pmatrix}. \tag{3.159}$$

The conditional probability $\tau_\alpha(s_{\mathrm{in}},\vartheta_{\mathrm{in}})$ introduced in (3.109), for a particle to reach the reservoir C_α for fixed initial conditions s_{in} and ϑ_{in} reads

$$\tau_\alpha(s_{\mathrm{in}},\vartheta_{\mathrm{in}}) = \int_l ds' \int_{-\pi/2}^{\pi/2} d\vartheta'\, \delta(s'-s_{\mathrm{out}})\delta(\vartheta'-\vartheta_{\mathrm{out}}). \tag{3.160}$$

By recalling the definition (3.112), we get

$$\begin{aligned}\tilde{T}_{\alpha\beta}(E) &= \int_l ds_{\text{in}} \int_{-\pi/2}^{\pi/2} d\vartheta_{\text{in}}\, \tau_\beta(E, s_{\text{in}}, \vartheta_{\text{in}}) \cos\vartheta_{\text{in}} \\ &= \int_l ds_{\text{in}} \int_{-\pi/2}^{\pi/2} d\vartheta_{\text{in}}\, \cos\vartheta_{\text{in}} \int_l ds' \int_{-\pi/2}^{\pi/2} d\vartheta'\, \delta(s' - s_{\text{out}})\delta(\vartheta' - \vartheta_{\text{out}}).\end{aligned} \tag{3.161}$$

Thus, using $4l = 2\pi R$ yields the second of the sum rules (3.113).

To prove the first one, we change integration variables in (3.161) according to

$$\begin{pmatrix} s_{\text{in}} \\ \vartheta_{\text{in}} \end{pmatrix} \mapsto \begin{pmatrix} s_{\text{out}} \\ \vartheta_{\text{out}} \end{pmatrix}, \tag{3.162}$$

thus ending up with

$$\begin{aligned}\sum_{\beta=\text{h},\ldots,\text{c}} \tilde{T}_{\alpha\beta}(E) = \int_l ds' \int_{-\pi/2}^{\pi/2} d\vartheta' \int_0^{2\pi R} ds_{\text{out}} \int_{-\pi/2}^{\pi/2} d\vartheta_{\text{out}}\, \delta(s' - s_{\text{out}})\delta(\vartheta' - \vartheta_{\text{out}}) \\ \times \cos\left(\vartheta_{\text{in}}(s_{\text{out}}, \vartheta_{\text{out}})\right) \mathcal{J}(s_{\text{out}}, \vartheta_{\text{out}}),\end{aligned} \tag{3.163}$$

where

$$\mathcal{J}(s_{\text{out}}, \vartheta_{\text{out}}) \equiv \left| \frac{\partial(s_{\text{in}}, \vartheta_{\text{in}})}{\partial(s_{\text{out}}, \vartheta_{\text{out}})} \right| \tag{3.164}$$

denotes the Jacobian of the change of coordinates (3.162), which can be determined as follows. We introduce the coordinates $\mathbf{Q} \equiv (r, s)$ and $\mathbf{P} \equiv (p_r, p_s)$ in the four-dimensional phase space Γ of a single particle that are connected to the Cartesian coordinates (x, y) and the corresponding momenta (p_x, p_y) via the canonical transformation

$$x = r\cos(s/R), \quad y = r\sin(s/R), \quad p_r = m\dot{r}, \quad p_s = mr^2\dot{s}/R^2. \tag{3.165}$$

Next, within Γ, we define a two-dimensional surface Σ by

$$r = \text{const} \equiv R \quad \text{and} \quad H(\mathbf{Q}, \mathbf{P}) = \text{const} \equiv E, \tag{3.166}$$

where $H(\mathbf{Q}, \mathbf{P})$ denotes the single particle Hamiltonian. This surface, which can be parameterized by the coordinates (s, p_s), is pierced exactly twice by the phase space trajectory. The two intersection points $(s_{\text{in}}, p_{s_{\text{in}}})$ and $(s_{\text{out}}, p_{s_{\text{out}}})$ are connected by the one-to-one mapping

$$\mathcal{M}' : \begin{pmatrix} s_{\text{in}} \\ p_{s_{\text{in}}} \end{pmatrix} \mapsto \begin{pmatrix} s_{\text{out}}(s_{\text{in}}, p_{s_{\text{in}}}) \\ p_{s_{\text{out}}}(s_{\text{in}}, p_{s_{\text{in}}}) \end{pmatrix}. \tag{3.167}$$

From the Poincaré-Cartan theorem [66], it follows that the map $\mathcal{M}'$ is volume conserving on Σ, i.e.,

$$\left| \frac{\partial(s_{\text{in}}, p_{s_{\text{in}}})}{\partial(s_{\text{out}}, p_{s_{\text{out}}})} \right| = 1. \tag{3.168}$$

Rewriting (3.164) as

$$\mathcal{J}(s_{\mathrm{out}},\vartheta_{\mathrm{out}}) = \left|\frac{\partial(s_{\mathrm{in}},\vartheta_{\mathrm{in}})}{\partial(s_{\mathrm{in}},p_{s_{\mathrm{in}}})}\right| \left|\frac{\partial(s_{\mathrm{in}},p_{s_{\mathrm{in}}})}{\partial(s_{\mathrm{out}},p_{s_{\mathrm{out}}})}\right| \left|\frac{\partial(s_{\mathrm{out}},p_{s_{\mathrm{out}}})}{\partial(s_{\mathrm{out}},\vartheta_{\mathrm{out}})}\right| \tag{3.169}$$

leads to

$$\mathcal{J}(s_{\mathrm{out}},\vartheta_{\mathrm{out}}) = \left|\left(\frac{\partial p_{s_{\mathrm{in}}}}{\partial\vartheta_{\mathrm{in}}}\right)_{s_{\mathrm{in}}}\right|^{-1} \left|\left(\frac{\partial p_{s_{\mathrm{out}}}}{\partial\vartheta_{\mathrm{out}}}\right)_{s_{\mathrm{out}}}\right|. \tag{3.170}$$

Given the relations

$$p_{s_{\mathrm{in}}} = \sqrt{2mE}\sin\vartheta_{\mathrm{in}} \quad \text{and} \quad p_{s_{\mathrm{out}}} = \sqrt{2mE}\sin\vartheta_{\mathrm{out}}, \tag{3.171}$$

the partial derivatives showing up in (3.170) are readily evaluated. Thus, we finally arrive at

$$\mathcal{J}(s_{\mathrm{out}},\vartheta_{\mathrm{out}}) = \frac{\cos\vartheta_{\mathrm{out}}}{\cos\left(\vartheta_{\mathrm{in}}(s_{\mathrm{out}},\vartheta_{\mathrm{out}})\right)p}. \tag{3.172}$$

Inserting this result into (3.163) gives the first sum rule (3.113).

We emphasize that the prove of the sum rules (3.113) ultimately relies on the volume-preserving property of Hamiltonian dynamics and, therefore, applies irrespective of a potential inside the central region or the number of reservoirs attached to it. For simplicity, we have focused here on a circular region and reservoirs of equal width. However, generalization to arbitrary geometries is straightforward.

Chapter 4

Periodic Thermodynamics on the Micro- and Nano-Scale

The notion of periodic thermodynamics was originally coined by Kohn in the context of open quantum systems driven by strong laser-fields [67]. Here, we borrow this term to denote a general framework for the thermodynamic description of small systems that are driven by both, a periodic temperature variation and some external parameter modulating their energy. The development of such a theory is the central objective of this chapter. Specifically, in a first step, we show how to express total entropy production by properly identified time-independent affinities and currents without making a linear response assumption. In linear response, time-independent generalized kinetic coefficients akin to the conventional ones known from linear irreversible thermodynamics can be identified. Specializing to a Fokker-Planck dynamics, we show that these coefficients fulfill an Onsager-Casimir type symmetry tracing back to microscopic reversibility. This symmetry allows for non-identical off-diagonal coefficients if the driving protocols are not symmetric under time-reversal. Consequently, in the same manner as in the thermoelectric case, reversible currents arise, which might lead to cyclic heat engines delivering finite power at Carnot efficiency.

Further investigations then lead us to a novel constraint on the kinetic coefficients that is significantly sharper than the second law. By virtue of this constraint, we establish for a large class of cyclic heat engines the same quadratic relation between power and efficiency that has been proven in the previous chapter for multi-terminal thermoelectric heat engines. As one consequence, it follows that the power of periodic micro- and nano-heat engines must vanish at least linearly when their efficiency approaches the Carnot value.

We illustrate our general framework by explicitly working out the paradigmatic case of a Brownian heat engine realized by a colloidal particle in a time-dependent harmonic trap subject to a periodic temperature profile. This case study reveals *inter alia* that our new general bound of power is asymptotically tight.

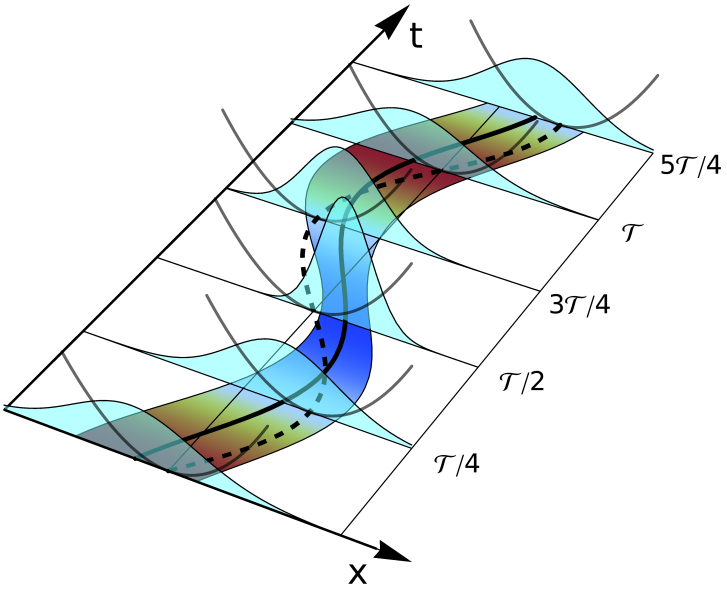

Figure 4.1: Non-equilibrium periodic state of a system with one degree of freedom x in a sinusoidally shifted harmonic potential, represented by gray parabolas, which is embedded in an environment with periodically changing temperature as indicated by the periodic color gradient. The solid line in the x-t plane shows the motion of the center of the Gaussian phase space distribution, which lags behind position of the potential minimum shown as dashed line. At any time t, the width of the colored region equals the width of the phase space distribution, which varies according to the temperature.

4.1 Framework

In this section, we will demonstrate that the notions of irreversible thermodynamics can be transferred to periodically driven systems.

4.1.1 Nonlinear Regime

We begin with a brief review of the energetics of driven systems in thermal contact with a heat bath [10]. Specifically, we consider a classical system with degrees of freedom $\mathbf{x} \equiv (x_1, \ldots, x_n)$ and time-dependent Hamiltonian

$$H(\mathbf{x}, t) \equiv H_0(\mathbf{x}) + \Delta H g_w(\mathbf{x}, t), \tag{4.1}$$

which is immersed in a heat bath, whose temperature $T(t)$ oscillates between the two values T_c and $T_\mathrm{h} > T_\mathrm{c}$. Here, $g_w(\mathbf{x}, t)$ denotes an externally controlled dimensionless function of order 1 and ΔH quantifies the strength of this time-dependent perturbation. The power extracted by the controller thus reads

$$\dot{W}(t) \equiv -\int d^n\mathbf{x}\, \dot{H}(\mathbf{x}, t) p(\mathbf{x}, t), \tag{4.2}$$

where $p(\mathbf{x}, t)$ denotes the normalized probability density to find the system in the state $\mathbf{x}$ at the time t and dots indicate time derivatives throughout the paper. To compensate for this loss in internal energy

$$U(t) = \int d^n\mathbf{x}\, H(\mathbf{x}, t) p(\mathbf{x}, t), \tag{4.3}$$

the system picks up the heat

$$\dot{Q}(t) \equiv \int d^n\mathbf{x}\, H(\mathbf{x}, t) \dot{p}(\mathbf{x}, t). \tag{4.4}$$

from the environment as stipulated by the first law

$$\dot{U}(t) \equiv \dot{Q}(t) - \dot{W}(t). \tag{4.5}$$

We will now pass from time-dependent to constant variables by exploiting the periodic boundary conditions

$$H(\mathbf{x}, t+\mathcal{T}) = H(\mathbf{x}, t) \quad \text{and} \quad T(t+\mathcal{T}) = T(t), \tag{4.6}$$

where $\mathcal{T}$ is the length of one operation cycle. Quite naturally, we invoke the assumption that, given these conditions, the time evolution of the probability density $p(\mathbf{x}, t)$ eventually converges to a periodic limit

$$p^{\mathrm{c}}(\mathbf{x}, t) = p^{\mathrm{c}}(\mathbf{x}, t+\mathcal{T}) \tag{4.7}$$

as illustrated in Fig. 4.1 for a simple system. Once this periodic state is reached, the average entropy production per cycle arises solely due to heat exchange between the system and the environment, since, due to the periodicity of the the distribution $p^{\mathrm{c}}(\mathbf{x}, t)$, no net entropy is generated in the system in a full cycle, i.e., we have

$$\dot{S} = -\frac{1}{\mathcal{T}} \int_0^{\mathcal{T}} dt \, \frac{\dot{Q}(t)}{T(t)}. \tag{4.8}$$

By inserting (4.4) into (4.8) and parameterizing $T(t)$ by a dimensionless function $0 \leq \gamma_q(t) \leq 1$ such that

$$T(t) \equiv \frac{T_{\mathrm{c}} T_{\mathrm{h}}}{T_{\mathrm{h}} + (T_{\mathrm{c}} - T_{\mathrm{h}})\gamma_q(t)}, \tag{4.9}$$

it is straightforward to derive the expression

$$\dot{S} = \frac{\Delta H}{T_{\mathrm{c}}} \frac{1}{\mathcal{T}} \int_0^{\mathcal{T}} dt \int d^n\mathbf{x} \, \dot{g}_w(\mathbf{x}, t) p^{\mathrm{c}}(\mathbf{x}, t) + \left(\frac{1}{T_{\mathrm{c}}} - \frac{1}{T_{\mathrm{h}}} \right) \frac{1}{\mathcal{T}} \int_0^{\mathcal{T}} dt \int d^n\mathbf{x} \, \gamma_q(t) H(\mathbf{x}, t) \dot{p}^{\mathrm{c}}(\mathbf{x}, t) \tag{4.10}$$

using one integration by parts with respect to time. The corresponding boundary terms vanish due to the periodicity of the involved quantities. Obviously (4.10) can be cast in the generic form [5]

$$\dot{S} = \mathcal{F}_w J_w + \mathcal{F}_q J_q, \tag{4.11}$$

by identifying the work flux

$$J_w \equiv \frac{1}{\mathcal{T}} \int_0^{\mathcal{T}} dt \int d^n\mathbf{x} \, \dot{g}_w(\mathbf{x}, t) p^{\mathrm{c}}(\mathbf{x}, t), \tag{4.12}$$

the generalized heat flux

$$J_q \equiv \frac{1}{\mathcal{T}} \int_0^{\mathcal{T}} dt \int d^n\mathbf{x} \, \gamma_q(t) H(\mathbf{x}, t) \dot{p}^{\mathrm{c}}(\mathbf{x}, t) \tag{4.13}$$

and the affinities

$$\mathcal{F}_w \equiv \Delta H/T_\mathrm{c} \quad \text{and} \quad \mathcal{F}_q \equiv 1/T_\mathrm{c} - 1/T_\mathrm{h}. \tag{4.14}$$

Within only a few lines, we have thus obtained our first objective for this chapter, namely, we recovered for periodically time-dependent systems the structure of irreversible thermodynamics. The key point here is the identification of appropriate pairs of affinities and fluxes, whose respective products sum up to the total entropy production.

For later purposes, we note that, after one integration by part with respect to t, the heat flux (4.13) can be rewritten as

$$J_q = \frac{1}{\mathcal{T}} \int_0^{\mathcal{T}} dt \int d^n\mathbf{x}\, \dot{g}_q(\mathbf{x},t) p^\mathrm{c}(\mathbf{x},t) + \frac{\Delta H}{\mathcal{T}} \int_0^{\mathcal{T}} dt \int d^n\mathbf{x}\, \gamma_q(t) g_w(\mathbf{x},t) \dot{p}^\mathrm{c}(\mathbf{x},t) \tag{4.15}$$

where

$$g_q(\mathbf{x},t) \equiv -H_0(\mathbf{x})\gamma_q(t). \tag{4.16}$$

4.1.2 Linear Response Regime

Kinetic Coefficients

We now focus on the linear regime with respect to the temporal gradients ΔH and $\Delta T \equiv T_\mathrm{h} - T_\mathrm{c}$. By expanding the fluxes (4.12) and (4.13), we obtain

$$\begin{aligned} J_w &= L_{ww}\mathcal{F}_w + L_{wq}\mathcal{F}_q + \mathcal{O}(\Delta^2), \\ J_q &= L_{qw}\mathcal{F}_w + L_{qq}\mathcal{F}_q + \mathcal{O}(\Delta^2) \end{aligned} \tag{4.17}$$

with linearized affinities

$$\mathcal{F}_w = \Delta H/T_\mathrm{c} \quad \text{and} \quad \mathcal{F}_q = \Delta T/T_\mathrm{c}^2 + \mathcal{O}\left(\Delta^2\right) \tag{4.18}$$

and kinetic coefficients

$$L_{\alpha\beta} \equiv \left.\frac{\partial J_\alpha}{\partial \mathcal{F}_\beta}\right|_{\mathcal{F}=0} \quad \text{for} \quad \alpha,\beta = w,q. \tag{4.19}$$

The entropy production (4.8) thus reduces to

$$\dot{S} = \sum_{\alpha,\beta=w,g} L_{\alpha\beta}\mathcal{F}_\alpha\mathcal{F}_\beta. \tag{4.20}$$

To guarantee that this expression is nonnegative for any $\mathcal{F}_\alpha$ as stipulated by the second law, the kinetic coefficients must obey the constraints

$$L_{ww}, L_{qq} \geq 0 \quad \text{and} \quad L_{ww}L_{qq} - (L_{wq} + L_{qw})^2/4 \geq 0, \tag{4.21}$$

which we prove explicitly in Sec. 4.2.2 for a large class of systems. It is, however, not evident at this stage whether a reciprocity relation relating $L_{\alpha\beta}$ with $L_{\beta\alpha}$ or any further constraints exist.

Adiabatic Limit

As a first step, we investigate the adiabatic regime, which is characterized by the Hamiltonian $H(\mathbf{x},t)$ and the temperature $T(t)$ changing slowly enough in time such that the system effectively passes through a sequence of equilibrium states, i.e.,

$$p^{\mathrm{c}}(\mathbf{x},t) = \exp\left(-H(\mathbf{x},t)/(k_{\mathrm{B}}T(t))\right)/Z(t) \tag{4.22}$$

with

$$Z(t) \equiv \int d^n\mathbf{x}\, \exp\left(-H(\mathbf{x},t)/(k_{\mathrm{B}}T(t))\right) \tag{4.23}$$

and k_{B} denoting Boltzmann's constant. Expanding (4.22) to linear order in ΔH and ΔT and inserting the result into (4.12), (4.15) and (4.19) gives the universal expression

$$L^{\mathrm{ad}}_{\alpha\beta} \equiv -\frac{1}{k_{\mathrm{B}}} \langle\!\langle \delta\dot{g}_\alpha \delta g_\beta \rangle\!\rangle \tag{4.24}$$

for the adiabatic kinetic coefficients. Here, we introduced the notations

$$\langle\!\langle A \rangle\!\rangle \equiv \frac{1}{\mathcal{T}} \int_0^{\mathcal{T}} dt\ \langle A(t)\rangle \equiv \frac{1}{\mathcal{T}} \int_0^{\mathcal{T}} dt \int d^n\mathbf{x}\, A(\mathbf{x},t) p^{\mathrm{eq}}(\mathbf{x}) \tag{4.25}$$

and

$$\delta A(\mathbf{x},t) \equiv A(\mathbf{x},t) - \langle A(\mathbf{x},t)\rangle \tag{4.26}$$

for any quantity $A(\mathbf{x},t)$ and the equilibrium distribution of the unperturbed system

$$p^{\mathrm{eq}}(\mathbf{x}) \equiv \exp\left(-H_0(\mathbf{x})/(k_{\mathrm{B}}T_{\mathrm{c}})\right)/Z_0 \tag{4.27}$$

with Z_0 denoting the canonical partition function.

Notably, the coefficients (4.24) are fully antisymmetric, i.e.,

$$L^{\mathrm{ad}}_{\alpha\beta} = -L^{\mathrm{ad}}_{\beta\alpha}. \tag{4.28}$$

As might be expected, this property, which can be proven by a simple integration by parts with respect to t, implies vanishing entropy production (4.20) in the adiabatic limit. This avoidance of dissipation can, however, be only achieved for an infinite cycle duration $\mathcal{T}$ and therefore inevitably comes with vanishing fluxes J_α.

Stochastic Dynamics

For further investigations of the kinetic coefficients, we have to specify the dynamics, which governs the time evolution of the probability density $p(\mathbf{x},t)$. Having in mind, in particular, mesoscopic systems surrounded by a fluctuating medium, a suitable choice is given by the Fokker-Planck equation [52]

$$\partial_t p(\mathbf{x},t) = \mathsf{L}(\mathbf{x},t) p(\mathbf{x},t) \tag{4.29}$$

with

$$\mathsf{L}(\mathbf{x},t) \equiv -\partial_{x_i} D_i(\mathbf{x},H,T) + \partial_{x_i}\partial_{x_j} D_{ij}(\mathbf{x},H,T), \tag{4.30}$$

where summation over identical indices is understood and natural boundary conditions are assumed. The Hamiltonian $H(\mathbf{x},t)$ and the temperature $T(t)$ enter via the drift and diffusion coefficients $D_i(\mathbf{x},H,T)$ and $D_{ij}(\mathbf{x},H,T)$, which thus become implicitly time-dependent [1].

We will now formulate a set of conditions on the general Fokker-Planck operator (4.30) to adapt it to the physical situation that we wish to discuss here. Since micro-reversibility plays a crucial role in linear irreversible thermodynamics, we have to ensure that our theory complies with this fundamental principle. To this end, first, at any time t any possible state $\mathbf{x}$ of the system must be associated with the same energy as the time-reversed state $\boldsymbol{\varepsilon}\mathbf{x} \equiv (\varepsilon_1 x_1, \ldots, \varepsilon_n x_n)$ with $\varepsilon_i = 1$ for even and $\varepsilon_i = -1$ for odd variables, i.e.,

$$H(\mathbf{x},t) = H(\boldsymbol{\varepsilon}\mathbf{x},t), \tag{4.31}$$

where, throughout the paper, the transformation $\mathbf{x} \to \boldsymbol{\varepsilon}\mathbf{x}$ is meant to include the reversal of external magnetic fields. Second, the unperturbed Fokker-Planck operator $\mathsf{L}^0(\mathbf{x}) \equiv \mathsf{L}(\mathbf{x},t)|_{\Delta=0}$ must obey the detailed balance condition [52]

$$\mathsf{L}^0(\mathbf{x})p^{\mathrm{eq}}(\mathbf{x}) = p^{\mathrm{eq}}(\mathbf{x})\mathsf{L}^{0\dagger}(\boldsymbol{\varepsilon}\mathbf{x}), \tag{4.32}$$

for the canonical distribution (4.27), which uniquely satisfies

$$\mathsf{L}^0(\mathbf{x})p^{\mathrm{eq}}(\mathbf{x}) = 0. \tag{4.33}$$

The dagger showing up in (4.32), from here onwards, designates the adjoint of the respective operator. Note that, while in (4.33) the operator $\mathsf{L}^0(\mathbf{x})$ acts on the function $p^{\mathrm{eq}}(\mathbf{x})$, (4.32) is to be read as an operator identity becoming meaningful when applied to a specific function of $\mathbf{x}$. Physically, the relation (4.32) means that, once the system has reached its equilibrium state, the rate of transitions from the state $\mathbf{x}$ to the state $\mathbf{x}'$ is balanced by the rate of transitions in the reverse direction.

The equilibrium Fokker-Planck operator $\mathsf{L}^0(\mathbf{x})$ can be naturally decomposed in a reversible and an irreversible contribution

$$\mathsf{L}^0_{\mathrm{rev}}(\mathbf{x}) \equiv (\mathsf{L}^0(\mathbf{x}) - \mathsf{L}^0(\boldsymbol{\varepsilon}\mathbf{x}))/2 \quad \text{and} \quad \mathsf{L}^0_{\mathrm{irr}}(\mathbf{x}) \equiv (\mathsf{L}^0(\mathbf{x}) + \mathsf{L}^0(\boldsymbol{\varepsilon}\mathbf{x}))/2, \tag{4.34}$$

which are characterized by their respective behavior under time reversal. While the irreversible part accounts for dissipative effects induced by the presence of the heat bath, the reversible part describes the intrinsic coupling of the system's degrees of freedom, which is not directly affected by the fluctuating environment. Since this autonomous part of the dynamics should preserve the internal energy of the system, we have to impose the condition

$$\mathsf{L}^{0\dagger}_{\mathrm{rev}}(\mathbf{x})H_0(\mathbf{x}) = 0. \tag{4.35}$$

[1] It is well known that (4.29) leads to a unique, periodic distribution $p^{\mathrm{c}}(\mathbf{x},t)$ in the long time limit if the diffusion matrix is strictly positive definite [54, 68]. However, it is readily seen that this assertion still holds for physically meaningful scenarios with singular diffusion matrix such as the underdamped dynamics described by Kramer's equation [52].

We note that this consideration does not play a role in the overdamped limit, within which the entire time evolution of the system is effectively irreversible due to strongly dominating friction forces.

The notion of detailed balance can not be immediately generalized to situations with external driving and time-dependent temperature. However, in analogy with (4.33), the full Fokker-Planck operator $\mathsf{L}(\mathbf{x},t)$ can still be characterized by the weaker property

$$\mathsf{L}(\mathbf{x},t)\exp\left(-H(\mathbf{x},t)/(k_{\mathrm{B}}T(t))\right)=0, \tag{4.36}$$

which is naturally obeyed in the absence of nonconservative forces and guarantees that the system follows the correct thermal equilibrium state if the Hamiltonian and the temperature are varied quasi-statically.

Finite-Time Kinetic Coefficients

In the linear response regime, the Fokker-Planck operator $\mathsf{L}(t)$ showing up in (4.29) can be replaced by the expansion

$$\mathsf{L}(t)\equiv\mathsf{L}^0+\Delta H\mathsf{L}^H(t)+\Delta T\mathsf{L}^T(t)+\mathcal{O}(\Delta^2), \tag{4.37}$$

where, for simplicity, from (4.37) onwards, we notationally suppress the dependence of any operator on $\mathbf{x}$, whenever there is no need to indicate it explicitly. The Fokker-Planck equation (4.29) can then be solved with due consideration of the boundary condition (4.6) by treating $\mathsf{L}^H(t)$ and $\mathsf{L}^T(t)$ as first order perturbations. The result of this standard procedure [52, 69] reads

$$p^{\mathrm{c}}(\mathbf{x},t)=p^{\mathrm{eq}}(\mathbf{x})+\sum_{X=H,T}\Delta X\int_0^\infty d\tau\; e^{\mathsf{L}^0\tau}\mathsf{L}^X(t-\tau)p^{\mathrm{eq}}(\mathbf{x})+\mathcal{O}(\Delta^2). \tag{4.38}$$

After some algebra involving condition (4.36), which we relegate to appendix 4A for convenience, this solution leads to the compact expression

$$L_{\alpha\beta}=L^{\mathrm{ad}}_{\alpha\beta}+\frac{1}{k_{\mathrm{B}}}\int_0^\infty d\tau\;\langle\!\langle\delta\dot{g}_\alpha(0);\delta\dot{g}_\beta(-\tau)\rangle\!\rangle \tag{4.39}$$

for the kinetic coefficients, where the generalized equilibrium correlation function is defined as

$$\langle\!\langle A(t_1);B(t_2)\rangle\!\rangle\equiv\frac{1}{\mathcal{T}}\int_0^{\mathcal{T}}dt\int d^n\mathbf{x}\begin{cases}A(\mathbf{x},t_1+t)e^{\mathsf{L}^0(t_1-t_2)}B(\mathbf{x},t_2+t)p^{\mathrm{eq}}(\mathbf{x}) & \text{for}\quad (t_1\geq t_2)\\ B(\mathbf{x},t_2+t)e^{\mathsf{L}^0(t_2-t_1)}A(\mathbf{x},t_1+t)p^{\mathrm{eq}}(\mathbf{x}) & \text{for}\quad (t_1<t_2)\end{cases} \tag{4.40}$$

for arbitrary quantities $A(\mathbf{x},t)$ and $B(\mathbf{x},t)$. We recall the definition (4.26) of the δ-notation.

The expression (4.39) admits an illuminating physical interpretation. It shows that the kinetic coefficients of periodically driven can be decomposed into an adiabatic contribution independently identified in (4.24) and a finite-time correction, which has the form of an equilibrium correlation function. This result might therefore be regarded as a generalization of the well established Green-Kubo relations, which relate linear transport

coefficients like electric or thermal conductivity to equilibrium correlation functions of the corresponding currents [69]. In our case, the role of the currents is played by the fluctuation variables $\delta\dot{g}_\alpha(\mathbf{x},t)$ and the ensemble average is augmented by a temporal average over one operation cycle. We note that a similar expression has been obtained for the special case of the effective diffusion constant of a periodically rocked Brownian motor in [70].

Reciprocity Relations

Time-reversal symmetry of microscopic dynamics appears as the detailed balance condition on the level of the Fokker-Planck equation (4.32). By using this relation and the Green-Kubo type formula (4.39), it is straightforward to derive the generalized reciprocity relation

$$L_{\alpha\beta}\left[H(\mathbf{x},t),T(t),\mathbf{B}\right] = L_{\beta\alpha}\left[H(\mathbf{x},-t),T(-t),-\mathbf{B}\right], \tag{4.41}$$

where, the kinetic coefficients are considered as functionals of the time-dependent Hamiltonian and temperature and an external magnetic field $\mathbf{B}$. The technical details of the derivation leading to the relation (4.41) can be found in appendix 4B. Here, we emphasize that, although the setup of this paper differs significantly from the one Onsager dealt with in his pioneering work [71, 72], the symmetry (4.41) and the Onsager's original reciprocal relations share microscopic reversibility as the common physical origin. Since, in the presence of time-dependent driving, full time reversal especially includes reversal of the driving protocols, naturally, these reversed protocols show up in (4.41).

The symmetry (4.41) holds individually for both, the adiabatic kinetic coefficients and the finite-time correction showing up in (4.39). Given the general relation (4.28), it follows that the $\mathsf{L}^{\mathrm{ad}}_{\alpha\beta}$ must vanish if the driving protocols are symmetric under time-reversal.

The additional relation

$$L_{\alpha\beta}\left[\gamma_w(t),\gamma_q(t),\mathbf{B}\right] = L_{\beta\alpha}\left[\gamma_q(t),\gamma_w(t),-\mathbf{B}\right], \tag{4.42}$$

can be proven if the driving $g_w(\mathbf{x},t)$ introduced in (4.1) factorizes according to

$$g_w(\mathbf{x},t) = g_w(\mathbf{x})\gamma_w(t). \tag{4.43}$$

Hence, the off-diagonal kinetic coefficients change place if the magnetic field is reversed and the respective protocols determining the time dependence of the Hamiltonian and the temperature are interchanged. This symmetry does not involve the reversed protocols. It is, however, less universal than (4.41), since it requires the special structure (4.43), see appendix 4B for details.

4.2 Cyclic Stochastic Heat Engines in Linear Response

As a key application of our new approach we will discuss the performance of stochastic heat engines.

4.2.1 Power and Efficiency

The main two benchmark parameters here are, first, the average power output per operation cycle

$$P \equiv -\frac{1}{\mathcal{T}} \int_0^{\mathcal{T}} dt \int d^n\mathbf{x}\, \dot{H}(\mathbf{x},t) p^{\mathrm{c}}(\mathbf{x},t) = -T_{\mathrm{c}} \mathcal{F}_w J_w \tag{4.44}$$

and, second, the efficiency

$$\eta \equiv P/J_q = -T_{\mathrm{c}} \mathcal{F}_w J_w / J_q, \tag{4.45}$$

which is bounded by the Carnot value $\eta_{\mathrm{C}} = 1 - T_{\mathrm{c}}/T_{\mathrm{h}}$ as a direct consequence of the second law $\dot{S} \geq 0$. The latter figure, which is naturally suggested by the representation (4.11) of the entropy production per cycle, should be regarded as a generalization of the conventional thermodynamic efficiency defined for a heat engine operating between two reservoirs of respectively constant temperature. Our formalism includes this scenario as the special case where $\gamma_q(t)$ is chosen as a step function

$$\gamma_q(t) = \begin{cases} 1 & \text{for} \quad 0 \leq t < \mathcal{T}_1 \\ 0 & \text{for} \quad \mathcal{T}_1 \leq t < \mathcal{T} \end{cases} \tag{4.46}$$

with $0 < \mathcal{T}_1 < \mathcal{T}$ such that the system is in contact with the hot temperature T_{h} in the first part of the cycle and the cold temperature T_{c} in the second one.

Under linear response conditions, which we will assume for the rest of this subsection, the fluxes J_α can be eliminated using (4.17) such that the expressions (4.44) and (4.45) reduce to

$$P = -T_{\mathrm{c}} \mathcal{F}_w \left(L_{ww} \mathcal{F}_w + L_{wq} \mathcal{F}_q \right) \tag{4.47}$$

and

$$\eta = -\frac{T_{\mathrm{c}} \mathcal{F}_w \left(L_{ww} \mathcal{F}_w + L_{wq} \mathcal{F}_q \right)}{L_{qw} \mathcal{F}_w + L_{qq} \mathcal{F}_q}, \tag{4.48}$$

respectively. Clearly, these figures are crucially determined by the kinetic coefficients $L_{\alpha\beta}$. In contrast to the thermoelectric case, where the reciprocity relation $L_{\alpha\beta} = L_{\beta\alpha}$ holds without magnetic fields, the analysis of the preceding subsection has revealed that for cyclic heat engines this symmetry is typically broken if the driving protocols are not invariant under time reversal. As pointed out by Benenti *et al.* [27], a non symmetric matrix of kinetic coefficients leads to profound consequences for the performance of thermoelectric devices including the option of Carnot efficiency at finite power.

These results apply likewise to periodically driven systems, since the theoretical framework used here is structurally equivalent to the standard theory of linear irreversible thermodynamics summarized in Ch. 2 and used as a starting point in [27]. Specifically, after redefining the dimensionless parameters (2.20) as

$$x \equiv \frac{L_{wq}}{L_{qw}} \quad \text{and} \quad y \equiv \frac{L_{wq} L_{qw}}{L_{ww} L_{qq} - L_{wq} L_{qw}}, \tag{4.49}$$

the results obtained in Sec. 2.3 for thermoelectric heat engines with broken time-reversal symmetry directly apply to the cyclic engines discussed here. In particular, by using $\mathcal{F}_w$ to fix the efficiency (4.45), one obtains the expression

$$P_{\pm}(x,y,\eta) = T_{\mathrm{c}}\mathcal{F}_q^2 L_{qq}\bar{\eta}\left(\frac{x(2+y)-y\bar{\eta}}{2x(1+y)} \pm \sqrt{\frac{y^2(x+\bar{\eta})^2}{4x^2(1+y)^2} - \frac{y\bar{\eta}}{x(1+y)}}\right) \tag{4.50}$$

with $\bar{\eta} = \eta/\eta_{\mathrm{C}}$ for the power output at given efficiency, which is identical to (2.28). As we have shown in Sec. 2.3, this quantity does not vanish for $\eta = \eta_{\mathrm{C}}$ if $y = h(x) = 4x/(x-1)^2$ and $x > 1$ or $x \leq -1$. Thus, we can conclude that, in precise analogy to thermoelectric engines, neither the second law nor the principle of microscopic reversibility are generally sufficient to bound the power of cyclic heat engines operating at Carnot efficiency to zero.

4.2.2 A New Constraint

We will now prove the existence of an additional constraint on the kinetic coefficients (4.19), which, so far, has been missing in our considerations. To this end, we introduce the symmetric matrix

$$\mathbb{A} \equiv \begin{pmatrix} N_{qq} & L_{qw} & L_{qq} \\ L_{qw} & L_{ww} & \frac{1}{2}(L_{wq}+L_{qw}) \\ L_{qq} & \frac{1}{2}(L_{wq}+L_{qw}) & L_{qq} \end{pmatrix}, \tag{4.51}$$

where

$$N_{qq} \equiv -\frac{1}{k_{\mathrm{B}}}\left\langle\!\left\langle \delta g_q \mathsf{L}^{0\dagger} \delta g_q \right\rangle\!\right\rangle \tag{4.52}$$

will play the role of a normalization constant and $\langle\!\langle \bullet \rangle\!\rangle$ was defined in (4.25). The matrix $\mathbb{A}$ has the nontrivial property of being positive semidefinite such that the determinant of any of its principal submatrices must be nonnegative, as we show in appendix 4C by using only the rather general assumptions of Sec. 4.1.2.

Two important implications follow immediately from this insight. First, by taking the determinant of the lower right 2×2- submatrix, we recover the inequality (4.21), which we inferred from the second law on the phenomenological level and now have proven explicitly. Second, by evaluating the determinant of $\mathbb{A}$, we get the new constraint

$$L_{qq} \leq N_{qq}\frac{L_{ww}L_{qq} - (L_{wq}+L_{qw})^2/4}{L_{ww}L_{qq} - L_{wq}L_{qw}}, \tag{4.53}$$

$$= N_{qq}\left(1 - y/h(x)\right), \tag{4.54}$$

which, in contrast to the bare second law, leads to a bound on power as we have shown Sec. 3.4.1. Specifically, this bound is found by bounding L_{qq} in (4.50) using (4.54) and then maximizing the resulting function with respect to y. This procedure yields the simple result

$$P_{\pm}(x,y,\eta) \leq \hat{P}_{\max}(x,\eta) \equiv 4\bar{P}_0 \begin{cases} \bar{\eta}(1-\bar{\eta}) & \text{for} \quad |x| \geq 1 \\ \bar{\eta}(1-\bar{\eta}/x^2) & \text{for} \quad |x| < 1 \end{cases}, \tag{4.55}$$

with the standard power

$$\bar{P}_0 \equiv T_c \mathcal{F}_q^2 N_{qq}/4. \tag{4.56}$$

For any $|x| \geq 1$ the bound (4.55) restores the quadratic relation between power and efficiency (2.19), which, in the standard analysis not invoking the new bound (4.54) or, equivalently, (3.82), is obtained only for the symmetric case $x = 1$. Consequently, we have shown that, in the linear response regime, the power of any cyclic heat engine comprised by our theoretical framework must vanish at least linearly as its efficiency approaches the Carnot value.

4.3 An Illustrative Example

4.3.1 Model and Kinetic Coefficients

A particularly simple setup for a stochastic heat engine consists of a Brownian particle in one spatial dimension confined in a harmonic potential of variable strength $\kappa(t)$ and immersed in a heat bath of time-dependent temperature $T(t)$ as schematically shown in Fig. 4.1. Originally proposed in [7], this model has recently been realized in a remarkable experiment [30] and can be used to illustrate various aspects of stochastic thermodynamics like the role of feedback [73, 74] and shortcuts to adiabaticity [75].

Here, by applying our general theory developed in the last sections we will calculate the kinetic coefficients for this stochastic heat engine and optimize the protocol $\kappa(t)$ controlling the trap strength to obtain maximum power for given efficiency.

In the overdamped limit, due to the absence of kinetic energy, the Hamiltonian of the system

$$\begin{aligned} &H(x,t) = H_0(x) + \Delta H \gamma_w(x,t) \quad \text{with} \\ &H_0(x) \equiv \frac{\kappa_0}{2} x^2, \quad \Delta H \equiv \kappa x_0^2, \quad g_w(x,t) \equiv \frac{x^2}{2x_0^2} \gamma_w(t) \end{aligned} \tag{4.57}$$

depends only on the position x of the particle. Here, κ_0 is the equilibrium strength of the trap, κ quantifies the strength of the time-dependent driving, $\gamma_w(t)$ denotes the driving protocol and $x_0 \equiv \sqrt{2k_B T_c/\kappa_0}$ is the characteristic length scale of the system. The time evolution of the probability density $p(x,t)$ for finding the particle at the position x is generated by the Fokker-Planck operator

$$\mathsf{L}(t) \equiv \mu \left(\kappa_0 + \kappa g_w(t)\right) \partial_x x + \mu k_B T(t) \partial_x^2, \tag{4.58}$$

which, in equilibrium reduces to

$$\mathsf{L}^0 \equiv \mu \kappa_0 \partial_x x + \mu k_B T_c \partial_x^2. \tag{4.59}$$

Here, μ denotes the mobility and the temperature $T(t) \equiv T_c T_h/(T_h - \Delta T \gamma_q(t))$ oscillates between the cold and the hot levels T_c and $T_h \equiv T_c + \Delta T$. The equilibrium fluctuations showing up in (4.39) read

$$\delta g_\alpha(x,t) = \gamma_\alpha(t) \kappa_0 \xi_\alpha \left(x^2 - k_B T_c/\kappa_0\right) \tag{4.60}$$

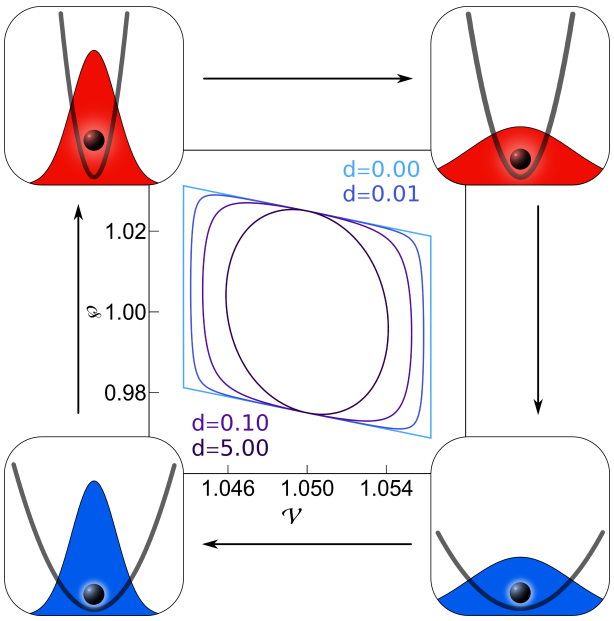

Figure 4.1: Operation cycle of a Brownian heat engine. The vertical axis corresponds to the normalized time-dependent strength of the harmonic trap in units of $\wp \equiv \kappa(t)/\kappa_0$, the horizontal axis to the normalized width $\mathcal{V} \equiv \langle x^2 \rangle/(2x_0^2)$ of the distribution function. This plot is analogous to the pressure volume diagram of a macroscopic heat engine such that the area encircled by the colored lines quantifies the work extracted per operation cycle. Specifically, the plots were obtained using the protocols (4.63) and (4.70) for different values of the shape parameter d, $2\mu\kappa_0\mathcal{T} = 1$, $\eta_C = T_c\mathcal{F}_q = 1/10$ and $\bar{\eta} = 1/2$. The small graphics show sketches of the potential (gray line) and the the phase space distribution, whose color reflects the temperature of the heat bath, at the respective edges of the cycle. For further explanations, see Sec. 4.3.

with

$$\xi_w \equiv 1/(4k_B T_c) \quad \text{and} \quad \xi_q \equiv -1/2. \tag{4.61}$$

Formula (4.39) can be easily evaluated by using the detailed balance relation (4.32) to transform L^0 into $\mathsf{L}^{0\dagger}$, since it is readily seen that the function $x^2 - k_B T_c/\kappa_0$ is a right eigenvector of $\mathsf{L}^{0\dagger}$ with corresponding eigenvalue $-2\mu\kappa_0$. The resulting kinetic coefficients

$$L_{\alpha\beta} = -\frac{2k_B T_c^2 \xi_\alpha \xi_\beta}{\mathcal{T}} \int_0^{\mathcal{T}} dt \left(\dot{\gamma}_\alpha(t)\gamma_\beta(t) - \int_0^\infty d\tau\, \dot{\gamma}_\alpha(t)\dot{\gamma}_\beta(t-\tau) e^{-2\mu\kappa_0\tau} \right) \tag{4.62}$$

are functionals of the protocols $\gamma_\alpha(t)$. Note that, besides the general reciprocity relation (4.41), these coefficients also satisfy the special symmetry relation (4.42), since the factorization condition (4.43) is fulfilled in the example discussed here.

4.3.2 Optimization

The optimal protocol $\gamma_w^*(t,\eta)$ for the strength of the harmonic trap for a given time dependence of temperature $\gamma_q(t)$ maximizes the power output at fixed efficiency η. It is

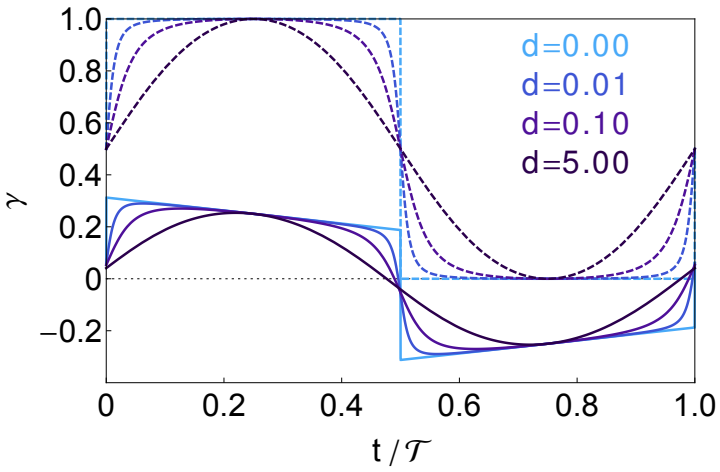

Figure 4.2: Plots of the temperature protocol $\gamma_q(t,d)$ defined in (4.70) (dashed lines) and the corresponding optimal protocol $\gamma_w^*(t,\eta,d)$ for the trap strength (solid lines) obtained from (4.64) for four different values of the parameter d as functions of $t/\mathcal{T}$. For all plots, we have set $2\mu\kappa_0\mathcal{T} = 1$ and $\bar{\eta} = 1/2$. Additionally, the optimal protocol $\gamma_w^*(t)$ has been rescaled by the dimensionless factor $\kappa_0\eta_C/\kappa$.

determined by the variational condition

$$0 \stackrel{!}{=} \frac{\delta}{\delta\gamma_w(t)} P[\gamma_w(t),\gamma_q(t)]\Big|_{P/J_q\stackrel{!}{=}\eta}, \tag{4.63}$$

where the power P and the heat flux J_q are regarded as functionals of $\gamma_w(t)$ and $\gamma_q(t)$. As we show in appendix 4D, this constrained optimization problem has the general solution

$$\gamma_w^*(t,\eta) = \frac{\kappa_0\eta_C}{\kappa}\Big(\bar{\eta}\gamma_q(t) - 2(1-\bar{\eta})\mu\kappa_0\int_0^t d\tau\,(\gamma_q(\tau)-\bar{\gamma}_q)\Big) + \gamma_0 \tag{4.64}$$

for $0 \le t \le \mathcal{T}$, where we used the abbreviations (2.12),

$$\bar{\gamma}_q \equiv \frac{1}{\mathcal{T}}\int_0^{\mathcal{T}} dt\,\gamma_q(t) \tag{4.65}$$

and γ_0 denotes an arbitrary constant. Using this protocol, the maximum power

$$P_{\max}(\eta) = \frac{k_B T_c^3 \mathcal{F}_q^2 \mu\kappa_0}{\mathcal{T}}\bar{\eta}(1-\bar{\eta})\int_0^{\mathcal{T}} dt\,\big(\gamma_q(t)-\bar{\gamma}_q\big)^2, \tag{4.66}$$

can be extracted per operation cycle at efficiency η.

4.3.3 Comparison with General Bound

In order to compare this result with the general bound (4.55), we evaluate the normalization constant

$$N_{qq} = \frac{k_B T_c^2 \mu\kappa_0}{\mathcal{T}}\int_0^{\mathcal{T}} dt\,\gamma_q^2(t) \tag{4.67}$$

defined in (4.52) and rewrite (4.66) as

$$P_{\max}(\eta) = 4\psi\bar{P}_0\bar{\eta}(1-\bar{\eta}), \tag{4.68}$$

where $\bar{P}_0$ is the standard power introduced in (4.55). The dimensionless factor

$$0 \le \psi \equiv \frac{\int_0^{\mathcal{T}} dt\,(\gamma_q(t)-\bar{\gamma}_q)^2}{\int_0^{\mathcal{T}} dt\,\gamma_q^2(t)} \le 1 \tag{4.69}$$

quantifies how close the maximum power found in the optimization comes to the general bound (4.55). Since, $0 \leq \gamma_q(t) \leq 1$, it is reached only for $\bar{\gamma}_q \to 0$. This limit, however, requires $\gamma_q(t) \to 0$ for any t and thus, inevitably, leads to vanishing absolute power.

For an illustration of this issue, we chose $\gamma_q(t)$ as the step function (4.46) such that the system is alternately in contact with a hot and a cold bath, respectively during the time intervals $\mathcal{T}_1$ and $\mathcal{T} - \mathcal{T}_1$. We then find $\psi = 1 - \mathcal{T}_1/\mathcal{T}$ and $P_0 \sim \mathcal{T}_1/\mathcal{T}$. Thus, as $\mathcal{T}_1$ is decreased, ψ comes arbitrarily close to 1 and P_0 decays linearly to zero. This example shows that our bound is asymptotically tight.

A particular advantage of our approach is that it allows to treat situations with a continuously varying temperature of the environment on equal footing with the scenario proposed in [7], which involves instantaneous switchings between a hot and a cold reservoir. In order to illustrate this feature, we consider the specific choice

$$\gamma_q(t,d) \equiv \frac{\sqrt{1+d}\sin(2\pi t/\mathcal{T})}{2\sqrt{\sin^2(2\pi t/\mathcal{T})+d}} + \frac{1}{2} \tag{4.70}$$

for the protocol $\gamma_q(t)$, which, in the linear response regime, is proportional to the temperature $T(t)$. The function (4.70), which interpolates between a step function ($d \to 0$) and a simple sine ($d \to \infty$) [76], is plotted together with the corresponding optimal protocol $\gamma_w^*(t,\eta,d)$ in Fig. 4.2. For these plots, the constant γ_0 showing up in (4.63) has been chosen as

$$\gamma_0 = \frac{\kappa_0\eta_C}{2\kappa}\left(1-\bar{\eta}-\frac{2\mu\kappa_0\mathcal{T}}{\pi}\sqrt{1+d}\cdot\arctan\left(1/\sqrt{d}\right)\right) \tag{4.71}$$

such that

$$\int_0^{\mathcal{T}} dt\, \gamma_w^*(t,\eta,d) = 0,$$

ensuring that the constant part of the potential is included in $H_0(\mathbf{x})$.

We find that, for $d = 0$, this protocol shows two sudden jumps occurring simultaneously with the instantaneous changes of the bath temperature. Such discontinuities were shown to be typical for thermodynamically optimized finite-time protocols connecting two equilibrium states [77]. Since, here, we are concerned with periodic states generated by permanent driving rather than a transient process with equilibrium boundary conditions, it is, however, not surprising that both, the temperature and the trap strength protocol, become continuous as the shape parameter d is increased.

For the protocols (4.63) and (4.70), the parameter ψ becomes

$$\psi = \frac{1+d}{2(1+d)+\sqrt{d(1+d)}}. \tag{4.72}$$

This function decays monotonically from 1/2 for $d = 0$ to 1/3 for $d \to \infty$. Consequently, ψ can not reach its maximum 1 within the class of protocols (4.70). This limitation can be understood from the argument given below (4.69), since, for any d, we have $\bar{\gamma}_q = 1/2$.

The standard power P_0 is proportional to the function $2 + d - \sqrt{d(1+d)}$, which decays monotonically from 2 to 3/2 as d increases from 0 to infinity. Thus, P_0 exhibits the same qualitative dependence on the shape parameter d as the efficiency. We can therefore conclude that, at least within the model considered here, a steeply rising and falling temperature performs better than a smoothly changing one.

4.4 Conclusion

In this chapter, we have demonstrated that non-equilibrium periodic states, which emerge naturally in periodically driven systems, can be endowed with the universal structure of irreversible thermodynamics. Within an elementary analysis starting from the first law, we have naturally identified two time-independent affinities, namely the strength of the time-dependent perturbation of the Hamiltonian and a temporal gradient in the inverse temperature of the heat bath. The corresponding fluxes are time-independent, since they are defined on the level of cycle averages. Nevertheless, our new formalism captures essential finite-time properties of the driven system and permits a discussion of quantities like power, which are out of reach for the laws of classical thermodynamics.

In the linear response regime, our framework permits a consistent definition of kinetic coefficients. By using a quite general stochastic approach, we have proven that these coefficients fulfill a generalized reciprocal relation involving the time-reversed driving protocols. Remarkably, while in thermoelectric systems the off-diagonal kinetic coefficients are identical without external magnetic fields, these coefficients do typically not coincide in periodically driven systems. As we have shown, the reason for this lack of symmetry is that the driving itself breaks the microscopic time-reversal symmetry if the corresponding protocols are considered as fixed. Consequently, ruling out the option of Carnot efficiency at finite power requires an additional constraint on the kinetic coefficients. Here, we have derived such a bound by borrowing from our previous analysis of the multi-terminal model for thermoelectric transport and modeling the micro-dynamics with a general Fokker-Planck equation. To complete our analysis, we have shown that the resulting bound on power is tight within a paradigmatic model of a Brownian heat engine.

Appendix

4.A Derivation of the Expression (4.39) for the Kinetic Coefficients

For an expression of the kinetic coefficients (4.19) depending only on equilibrium quantities the perturbations $\mathsf{L}^X(t)$ showing up in the linear response solution (4.38) have to be eliminated. To this end, we invoke the property (4.36) of the full Fokker-Planck operator. Substituting (4.37) into (4.36), expanding the exponential in ΔH and ΔT and collecting linear order terms provides us with the relations

$$\begin{aligned}\Delta H \mathsf{L}^H(t) p^{\mathrm{eq}}(\mathbf{x}) &= \mathcal{F}_w \mathsf{L}^0 g_w(\mathbf{x},t) p^{\mathrm{eq}}(\mathbf{x})/k_{\mathrm{B}},\\ \Delta T \mathsf{L}^T(t) p^{\mathrm{eq}}(\mathbf{x}) &= \mathcal{F}_q \mathsf{L}^0 g_q(\mathbf{x},t) p^{\mathrm{eq}}(\mathbf{x})/k_{\mathrm{B}},\end{aligned} \tag{4.73}$$

where we used the definition (4.16). Up to corrections of order Δ^2, the periodic distribution $p^{\mathrm{c}}(\mathbf{x},t)$ can thus be rewritten as

$$p^{\mathrm{c}}(\mathbf{x},t) = p^{\mathrm{eq}}(\mathbf{x}) + \sum_{\alpha=w,q} \frac{\mathcal{F}_\alpha}{k_{\mathrm{B}}} \int_0^\infty d\tau\; e^{\mathsf{L}^0\tau} \mathsf{L}^0 g_\alpha(\mathbf{x},t-\tau) p^{\mathrm{eq}}(\mathbf{x}) \tag{4.74}$$

$$= p^{\mathrm{eq}}(\mathbf{x}) + \sum_{\alpha=w,q} \frac{\mathcal{F}_\alpha}{k_{\mathrm{B}}} \int_0^\infty d\tau\; e^{\mathsf{L}^0\tau} \mathsf{L}^0 \delta g_\alpha(\mathbf{x},t-\tau) p^{\mathrm{eq}}(\mathbf{x}) \tag{4.75}$$

$$= p^{\mathrm{eq}}(\mathbf{x}) - \sum_{\alpha=w,q} \frac{\mathcal{F}_\alpha}{k_{\mathrm{B}}} \left(\delta g_\alpha(\mathbf{x},t) p^{\mathrm{eq}}(\mathbf{x}) - \int_0^\infty d\tau\; e^{\mathsf{L}^0\tau} \delta \dot{g}_\alpha(\mathbf{x},t-\tau) p^{\mathrm{eq}}(\mathbf{x}) \right). \tag{4.76}$$

In the second line, we replaced $g_\alpha(\mathbf{x},t)$ with its equilibrium fluctuation defined in (4.26). This modification does not alter the right hand side of (4.74), since $\mathsf{L}^0 p^{\mathrm{eq}}(\mathbf{x}) = 0$. However, it ensures that the function, on which the exponential operator acts in the third line, which was obtained by an integration by parts with respect to t, has no overlap with the nullspace of L^0 and thus the integral with infinite upper bound is well defined. Note that the upper boundary term vanishes, since the operator L^0 is nonpositive [52]. Inserting (4.74) into (4.12) and (4.15) yields

$$L_{\alpha\beta} = -\frac{1}{k_{\mathrm{B}}} \langle\!\langle \dot{g}_\alpha \delta g_\beta \rangle\!\rangle + \frac{1}{k_{\mathrm{B}}} \int_0^\infty d\tau\; \langle\!\langle \dot{g}_\alpha(0); \delta \dot{g}_\beta(-\tau) \rangle\!\rangle . \tag{4.77}$$

Herein, obviously, $\dot{g}_\alpha(\mathbf{x},t)$ can be replaced by its equilibrium fluctuation $\delta\dot{g}_\alpha(\mathbf{x},t)$ in the first term. Since any constant lies in the left nullspace of L^0 and, hence, is orthogonal to the function $e^{\mathsf{L}^0\tau}\delta\dot{g}_\alpha(\mathbf{x},t-\tau)p^{\mathrm{eq}}(\mathbf{x})$, the same replacement can be carried out in the second term without leading to additional contributions such that (4.39) is, finally, obtained.

4.B Reciprocity Relations

In this appendix, we establish the reciprocity relations (4.41) and (4.42). To this end, we first recall formula (4.39), which becomes

$$L_{\alpha\beta}[H(\mathbf{x},t),T(t),\mathbf{B}] = -\frac{1}{k_{\mathrm{B}}\mathcal{T}}\int_0^{\mathcal{T}} dt \int d^n\mathbf{x}\left(\delta\dot{g}_\alpha(\mathbf{x},t)\delta g_\beta(\mathbf{x},t)p^{\mathrm{eq}}(\mathbf{x}) + \int_0^\infty d\tau\ \delta\dot{g}_\alpha(\mathbf{x},t)e^{\mathsf{L}^0\tau}\delta\dot{g}_\beta(\mathbf{x},t-\tau)p^{\mathrm{eq}}(\mathbf{x})\right), \quad (4.78)$$

using the definitions (4.25) and (4.40). By applying the detailed balance relation (4.32) and changing the integration variable t according to $t \to \mathcal{T} - t$, this expression can be transformed to

$$L_{\alpha\beta}[H(\mathbf{x},t),T(t),\mathbf{B}] = -\frac{1}{k_{\mathrm{B}}\mathcal{T}}\int_0^{\mathcal{T}} dt \int d^n\mathbf{x}\left(-\delta\dot{g}_\alpha(\mathbf{x},-t)\delta g_\beta(\mathbf{x},-t)p^{\mathrm{eq}}(\mathbf{x}) + \int_0^\infty d\tau\ \delta\dot{g}_\beta(\mathbf{x},-t)e^{\tilde{\mathsf{L}}^0\tau}\delta\dot{g}_\alpha(\mathbf{x},\tau-t)p^{\mathrm{eq}}(\mathbf{x})\right), \quad (4.79)$$

where we introduced the shorthand notation $\tilde{\mathsf{L}}^0 \equiv \mathsf{L}^0(\boldsymbol{\varepsilon}\mathbf{x})$. Furthermore, to transfer the variable τ from the argument of $\delta\dot{g}_\beta$ in (4.78) to the argument of $\delta\dot{g}_\alpha$ in (4.79), we used the identity

$$\begin{aligned}\int_0^{\mathcal{T}} dt\ a(t)b(t-\tau) &= \int_{-\tau}^{\mathcal{T}-\tau} dt\ a(t+\tau)b(t)\\ &= \int_0^{\mathcal{T}} dt\ a(t+\tau)b(t) + \int_{-\tau}^{0} dt\ a(t+\tau)b(t) - \int_{\mathcal{T}-\tau}^{\mathcal{T}} dt\ a(t+\tau)b(t)\\ &= \int_0^{\mathcal{T}} dt\ a(t+\tau)b(t), \end{aligned} \quad (4.80)$$

which holds for any two $\mathcal{T}$-periodic functions $a(t)$ and $b(t)$. Finally, we reverse the magnetic field as well as the driving protocols and apply the change of integration variables $\mathbf{x} \to \boldsymbol{\varepsilon}\mathbf{x}$, whose Jacobian is 1. By exploiting the symmetry $\delta g_\alpha(\boldsymbol{\varepsilon}\mathbf{x},t) = \delta g_\alpha(\mathbf{x},t)$, which follows from condition (4.31), and carrying out one integration by parts with respect to t in the first summand, we obtain

$$\begin{aligned}L_{\alpha\beta}[H(\mathbf{x},-t),T(-t),-\mathbf{B}] &= -\frac{1}{k_{\mathrm{B}}\mathcal{T}}\int_0^{\mathcal{T}} dt \int d^n\mathbf{x}\left(\delta\dot{g}_\beta(\mathbf{x},t)\delta g_\alpha(\mathbf{x},t)p^{\mathrm{eq}}(\mathbf{x}) + \int_0^\infty d\tau\ \delta\dot{g}_\beta(\mathbf{x},t)e^{\mathsf{L}^0\tau}\delta\dot{g}_\alpha(\mathbf{x},t-\tau)p^{\mathrm{eq}}(\mathbf{x})\right)\\ &= L_{\beta\alpha}[H(\mathbf{x},t),T(t),\mathbf{B}] \end{aligned} \quad (4.81)$$

thus completing the proof of the reciprocity relation (4.41).

We now turn to the special case where the function $g_w(\mathbf{x},t)$ can be separated in the form

$$g_w(\mathbf{x},t) = g_w(\mathbf{x})\gamma_w(t). \quad (4.82)$$

Plugging this expression into (4.78) and invoking the definition $g_q(\mathbf{x}) \equiv -H_0(\mathbf{x})$ yields the expression

$$L_{\alpha\beta}[\gamma_w(t),\gamma_q(t),\mathbf{B}] = -\frac{1}{k_B\mathcal{T}}\int_0^{\mathcal{T}} dt \int d^n\mathbf{x}\left(\dot\gamma_\alpha(t)\gamma_\beta(t)\delta g_\alpha(\mathbf{x})\delta g_\beta(\mathbf{x})p^{\rm eq}(\mathbf{x}) + \int_0^\infty d\tau\ \dot\gamma_\alpha(t)\dot\gamma_\beta(t-\tau)\delta g_\alpha(\mathbf{x})e^{\mathsf{L}^0\tau}\delta g_\beta(\mathbf{x})p^{\rm eq}(\mathbf{x})\right), \quad (4.83)$$

which, by virtue of the detailed balance relation (4.32), equals

$$L_{\alpha\beta}[\gamma_w(t),\gamma_q(t),\mathbf{B}] = -\frac{1}{k_B\mathcal{T}}\int_0^{\mathcal{T}} dt \int d^n\mathbf{x}\left(\dot\gamma_\alpha(t)\gamma_\beta(t)\delta g_\alpha(\mathbf{x})\delta g_\beta(\mathbf{x})p^{\rm eq}(\mathbf{x}) + \int_0^\infty d\tau\ \dot\gamma_\alpha(t)\dot\gamma_\beta(t-\tau)\delta g_\beta(\mathbf{x})e^{\tilde{\mathsf{L}}^0\tau}\delta g_\alpha(\mathbf{x})p^{\rm eq}(\mathbf{x})\right). \quad (4.84)$$

Relation (4.42) can now be obtained by following the same steps as in the general case, that is, by applying the transformation $\mathbf{x} \to \boldsymbol{\varepsilon}\mathbf{x}$, reversing the magnetic field and interchanging the arguments $\gamma_w(t)$ and $\gamma_q(t)$ of $L_{\alpha\beta}$, using the symmetry $\delta g_\alpha(\mathbf{x}) = \delta g_\alpha(\boldsymbol{\varepsilon}\mathbf{x})$ and performing one integration by parts in the first term.

4.C Positivity of $\mathbb{A}$

The proof that the matrix $\mathbb{A}$ defined in (4.51) is positive semidefinite consists of two major steps. First, for arbitrary numbers $y_w, y_q \in \mathbb{R}$, we consider the quadratic form

$$\begin{aligned}\mathcal{Q}_0(y_w,y_q) &\equiv \sum_{\alpha,\beta=w,q} L_{\alpha\beta}y_\alpha y_\beta, = \frac{1}{k_B}\int_0^\infty d\tau\ \langle\!\langle G(0);G(-\tau)\rangle\!\rangle \\ &= \frac{1}{k_B\mathcal{T}}\int_0^{\mathcal{T}} dt\int_0^\infty d\tau\ \left\langle G(t)e^{\tilde{\mathsf{L}}^{0\dagger}\tau}G(t-\tau)\right\rangle \end{aligned} \quad (4.85)$$

where we used the expression (4.39) for the kinetic coefficients, defined

$$G(\mathbf{x},t) \equiv \sum_{\alpha=w,q} y_\alpha \delta\dot g_\alpha(\mathbf{x},t) \quad (4.86)$$

and applied the detailed balance relation (4.32) to obtain the second line. We recall the definitions (4.25) for the meaning of the angular brackets. The crucial ingredient for this

first step consists of the identity

$$-\frac{1}{2k_{\mathrm{B}}\mathcal{T}}\int_0^{\mathcal{T}}dt\,\left\langle\int_0^{\infty}d\tau\,e^{\tilde{\mathsf{L}}^{0\dagger}\tau}G(t-\tau)\big(\mathsf{L}^{0\dagger}+\tilde{\mathsf{L}}^{0\dagger}\big)\int_0^{\infty}d\tau'\,e^{\tilde{\mathsf{L}}^{0\dagger}\tau'}G(t-\tau')\right\rangle \tag{4.87}$$

$$=-\frac{1}{2k_{\mathrm{B}}\mathcal{T}}\int_0^{\mathcal{T}}dt\int_0^{\infty}d\tau\int_0^{\infty}d\tau'\,\Big\{\Big\langle\Big(\big(\partial_\tau e^{\tilde{\mathsf{L}}^{0\dagger}\tau}\big)G(t-\tau)\Big)e^{\tilde{\mathsf{L}}^{0\dagger}\tau'}G(t-\tau')\Big\rangle + \Big\langle\Big(e^{\tilde{\mathsf{L}}^{0\dagger}\tau}G(t-\tau)\Big)\big(\partial_{\tau'}e^{\tilde{\mathsf{L}}^{0\dagger}\tau'}\big)G(t-\tau')\Big\rangle\Big\} \tag{4.88}$$

$$=\frac{1}{2k_{\mathrm{B}}\mathcal{T}}\int_0^{\mathcal{T}}dt\int_0^{\infty}d\tau\,\Big\{2\Big\langle G(t)e^{\tilde{\mathsf{L}}^{0\dagger}\tau}G(t-\tau)\Big\rangle + \partial_t\int_0^{\infty}d\tau'\,\Big\langle\Big(e^{\tilde{\mathsf{L}}^{0\dagger}\tau}G(t-\tau)\Big)e^{\tilde{\mathsf{L}}^{0\dagger}\tau'}G(t-\tau')\Big\rangle\Big\} \tag{4.89}$$

$$=\frac{1}{k_{\mathrm{B}}\mathcal{T}}\int_0^{\mathcal{T}}dt\int_0^{\infty}d\tau\,\Big\langle G(t)e^{\tilde{\mathsf{L}}^{0\dagger}\tau}G(t-\tau)\Big\rangle=\mathcal{Q}_0(y_w,y_q). \tag{4.90}$$

Here, we used the relation

$$\big\langle A\mathsf{L}^{0\dagger}B\big\rangle=\big\langle B\tilde{\mathsf{L}}^{0\dagger}A\big\rangle, \tag{4.91}$$

which holds for any functions $A(\mathbf{x}),B(\mathbf{x})$ by virtue of the detailed balance condition (4.32), to obtain (4.88) from (4.87). Expression (4.89) follows by applying an integration by parts with respect to τ and τ', respectively, in the first and the second summand of (4.88). Finally, the second contribution in (4.89) vanishes after carrying out the t-integration, since the function $G(\mathbf{x},t)$ is $\mathcal{T}$-periodic in time.

Next, we note that (4.32) implies

$$\begin{aligned}\big\langle A\big(\mathsf{L}^{0\dagger}+\tilde{\mathsf{L}}^{0\dagger}\big)A\big\rangle&=\int d^n\mathbf{x}\,A(\mathbf{x})\big(\mathsf{L}^0p^{\mathrm{eq}}(\mathbf{x})+p^{\mathrm{eq}}(\mathbf{x})\mathsf{L}^{0\dagger}\big)A(\mathbf{x})\\&=\int d^n\mathbf{x}\,(p^{\mathrm{eq}}(\mathbf{x}))^{\frac{1}{2}}A(\mathbf{x})\big(\mathsf{K}^0+\mathsf{K}^{0\dagger}\big)(p^{\mathrm{eq}}(\mathbf{x}))^{\frac{1}{2}}A(\mathbf{x}),\end{aligned} \tag{4.92}$$

where

$$\mathsf{K}^0\equiv(p^{\mathrm{eq}}(\mathbf{x}))^{-\frac{1}{2}}\mathsf{L}^0(p^{\mathrm{eq}}(\mathbf{x}))^{\frac{1}{2}}. \tag{4.93}$$

Since the Hermitian part of this operator is negative semidefinite [52], it follows that (4.92) is non-positive for any $A(\mathbf{x})$. Hence, we can conclude that the quadratic form $\mathcal{Q}_0(y_w,y_q)$ is positive semidefinite, since it can be written in the form (4.87).

For the second step of the proof, we introduce the quadratic form

$$\mathcal{Q}(y_w,y_q,z)\equiv\mathcal{Q}_0(y_w,y_q)+\mathcal{Q}_1(y_w,y_q,z) \tag{4.94}$$

with

$$\begin{aligned}\mathcal{Q}_1(y_w, y_q, z) &\equiv N_{qq} z^2 + 2z \sum_{\alpha=w,q} L_{q\alpha} y_\alpha \\ &= -\frac{1}{k_\mathrm{B}} \left(\left\langle\!\left\langle F \mathsf{L}^{0\dagger} F \right\rangle\!\right\rangle - 2 \left\langle\!\left\langle F G \right\rangle\!\right\rangle - 2 \int_0^\infty d\tau \, \left\langle\!\left\langle \dot{F}(0); G(-\tau) \right\rangle\!\right\rangle \right) \\ &= -\frac{1}{2 k_\mathrm{B} \mathcal{T}} \int_0^\mathcal{T} dt \left\{ 2 \left\langle F(t) \mathsf{L}^{0\dagger} F(t) \right\rangle - 4 \left\langle F(t) G(t) \right\rangle - 4 \int_0^\infty d\tau \, \left\langle \dot{F}(t) e^{\tilde{\mathsf{L}}^{0\dagger} \tau} G(t-\tau) \right\rangle \right\}\end{aligned} \tag{4.95}$$

where $y_w, y_q, z \in \mathbb{R}$ and

$$F(\mathbf{x}, t) \equiv z \delta g_q(\mathbf{x}, t). \tag{4.96}$$

Note that, in (4.95), we used (4.39) and (4.52) as well as the detailed balance condition (4.32). The expression (4.95) can be rewritten as

$$\begin{aligned}\mathcal{Q}_1(y_w, y_q, z) = -\frac{1}{2 k_\mathrm{B} \mathcal{T}} \int_0^\mathcal{T} dt \Bigg\{ &\left\langle F(t) \left(\mathsf{L}^{0\dagger} + \tilde{\mathsf{L}}^{0\dagger} \right) F(t) \right\rangle \\ + \int_0^\infty d\tau \, \left\langle F(t) \left(\mathsf{L}^{0\dagger} + \tilde{\mathsf{L}}^{0\dagger} \right) \left(e^{\tilde{\mathsf{L}}^{0\dagger} \tau} G(t-\tau) \right) \right\rangle &+ \int_0^\infty d\tau \, \left\langle \left(e^{\tilde{\mathsf{L}}^{0\dagger} \tau} G(t-\tau) \right) \left(\mathsf{L}^{0\dagger} + \tilde{\mathsf{L}}^{0\dagger} \right) F(t) \right\rangle \Bigg\}.\end{aligned} \tag{4.97}$$

This assertion can be proven by expanding (4.97), invoking (4.91) as well as the identity

$$\mathsf{L}^{0\dagger} F(\mathbf{x}, t) = z \mathsf{L}^{0\dagger} g_q(\mathbf{x}, t) = -z \gamma_q(t) \mathsf{L}^{0\dagger} H_0(\mathbf{x}) = -z \gamma_q(t) \tilde{\mathsf{L}}^{0\dagger} H_0(\mathbf{x}) = \tilde{\mathsf{L}}^{0\dagger} F(\mathbf{x}, t), \tag{4.98}$$

which is implied by condition (4.35), and integrating by parts, first with respect to τ and then with respect to t, respectively, in the second and third term showing up in (4.97). Finally, putting together (4.87) and (4.97) leads to

$$\begin{aligned}\mathcal{Q}(y_w, y_q, z) = -\frac{1}{2 k_\mathrm{B} \mathcal{T}} \int_0^\mathcal{T} dt \Bigg\langle &\left(F(t) + \int_0^\infty d\tau \, e^{\tilde{\mathsf{L}}^{0\dagger} \tau} G(t-\tau) \right) \left(\mathsf{L}^{0\dagger} + \tilde{\mathsf{L}}^{0\dagger} \right) \\ &\times \left(F(t) + \int_0^\infty d\tau' \, e^{\tilde{\mathsf{L}}^{0\dagger} \tau'} G(t-\tau') \right) \Bigg\rangle.\end{aligned} \tag{4.99}$$

The average showing up in this expression is of the form (4.92) and thus must be non positive. Consequently, we have $\mathcal{Q}(y_w, y_q, z) \geq 0$ for any y_w, y_q, z. Moreover, since

$$\mathcal{Q}(y_w, y_q, z) = \mathbf{y}^t \mathbb{A} \mathbf{y} \tag{4.100}$$

with $\mathbf{y} \equiv (z, y_w, y_q)^t$ it follows that the matrix $\mathbb{A}$ must be positive semidefinite and thus the proof is completed.

4.D Optimal Protocol

The aim is to determine the optimal protocol $\gamma_w^*(t)$, which maximizes the rescaled output power

$$\bar{P} \equiv \frac{P}{T_c \mathcal{F}_q^2} = -(L_{ww}\chi^2 + L_{wq}\chi) \quad \text{with} \quad \chi \equiv \mathcal{F}_w/\mathcal{F}_q \tag{4.101}$$

for given time dependence of the bath temperature $g_q(t)$ and normalized efficiency

$$\bar{\eta} = -\frac{L_{ww}\chi^2 + L_{wq}\chi}{L_{qw}\chi + L_{qq}}. \tag{4.102}$$

This task is captured by the objective functional

$$\mathcal{P}[\gamma_w(t), \gamma_q(t), \lambda] \equiv (\lambda - 1)\chi^2 L_{ww} + (\lambda - 1)\chi L_{wq} + \lambda\bar{\eta}\chi L_{qw} + \lambda\bar{\eta} L_{qq}, \tag{4.103}$$

where the additional constraint (4.102) is taken into account by introducing the Lagrange multiplier λ. By inserting (4.62), (4.103) becomes

$$\mathcal{P}[\gamma_w(t), \gamma_q(t), \lambda] = \frac{1}{\mathcal{T}} \int_0^{\mathcal{T}} dt \sum_{\alpha,\beta=w,q} u_{\alpha\beta} \left\{ \dot{\gamma}_\alpha(t)\gamma_\beta(t) - \int_0^\infty d\tau\, \dot{\gamma}_\alpha(t)\dot{\gamma}_\beta(t-\tau) e^{-2\mu\kappa_0\tau} \right\}. \tag{4.104}$$

Here, we introduced the coefficients

$$\begin{pmatrix} u_{ww} & u_{wq} \\ u_{qw} & u_{qq} \end{pmatrix} \equiv -2k_B T_c^2 \begin{pmatrix} (\lambda-1)\chi^2\xi_w^2 & (\lambda-1)\chi\xi_w\xi_q \\ \lambda\bar{\eta}\chi\xi_w\xi_q & \lambda\bar{\eta}\xi_q^2 \end{pmatrix} \tag{4.105}$$

for notational simplicity. The convolution type structure of (4.104) naturally suggests to solve the variational problem by a Fourier transformation. We expand

$$\gamma_\alpha(t) \equiv \sum_{n\in\mathbb{Z}} c_n^\alpha e^{in\omega t} \quad \text{with} \quad \omega \equiv 2\pi/\mathcal{T} \tag{4.106}$$

and thus obtain

$$\mathcal{P}[\gamma_w(t), \gamma_q(t), \lambda] = (-2\mu\kappa_0) \sum_{\alpha,\beta=w,q} \sum_{n\in\mathbb{Z}} u_{\alpha\beta} c_n^\alpha c_{-n}^\beta \frac{in\omega}{in\omega - 2\mu\kappa_0}. \tag{4.107}$$

Since (4.107) is quadratic in the Fourier coefficients c_n^α, it is straightforward to carry out the optimization with respect to c_n^w. Taking into account that the protocols must be real and therefore $c_{-n}^\alpha = c_n^{\alpha*}$, the conditions

$$\partial_{c_n^w} \mathcal{P}[\gamma_w(t)\gamma_q(t), \lambda] \stackrel{!}{=} 0 \quad \text{and} \quad \partial_{c_n^{w*}} \mathcal{P}[\gamma_w(t), \gamma_q(t), \lambda] \stackrel{!}{=} 0 \tag{4.108}$$

yield

$$c_n^w = -\left(\frac{u_{wq} + u_{qw}}{2u_{ww}} + 2i\mu\kappa_0 \frac{u_{wq} - u_{qw}}{2n\omega u_{ww}} \right) c_n^q \tag{4.109}$$

for $n \neq 0$. Note that (4.107) does not depend on c_0^α and thus the optimal protocol will be unique only up to a trivial offset c_0^w. To comply with the constraint (4.102), the Lagrange multiplier λ must be chosen such that

$$\partial_\lambda \mathcal{P}[\gamma_w(t), \gamma_q(t), \lambda] = 0, \tag{4.110}$$

where the derivative has to be taken before the c_n^w are replaced by the solution (4.109). After some algebra, (4.110) reduces to the simple condition

$$\bar{\eta}^2 - (\lambda - 1)^2(\bar{\eta} - 1)^2 = 0, \tag{4.111}$$

which is fulfilled for

$$\lambda_\pm = (1 - \bar{\eta} \pm \bar{\eta})/(1 - \bar{\eta}). \tag{4.112}$$

Inserting (4.112) and (4.109) into (4.107) yields

$$\bar{P}_+ \equiv \mathcal{P}[\gamma_w(t), \gamma_q(t), \lambda_+] = 0, \tag{4.113}$$

$$\begin{aligned}\bar{P}_- &\equiv \mathcal{P}[\gamma_w(t), \gamma_q(t), \lambda_-] = 8k_\mathrm{B}T_\mathrm{c}^2\mu\kappa_0\xi_q^2\bar{\eta}(1-\bar{\eta})\sum_{n=1}^{\infty}|c_n^q|^2 \\ &= \frac{k_\mathrm{B}T_\mathrm{c}^2\mu\kappa_0}{\mathcal{T}}\bar{\eta}(1-\bar{\eta})\int_0^{\mathcal{T}} dt\ \left(\gamma_q(t) - \bar{\gamma}_q\right)^2,\end{aligned} \tag{4.114}$$

where $\bar{\gamma}_q$ is defined in (4.65). Consequently, the relevant solution for the Lagrange multiplier is given by λ_-. Finally, the optimal protocol $\gamma^*(t,\eta)$ is obtained by summing up the Fourier series (4.106). The explicit result (4.64) can be found by, first, evaluating

$$\begin{aligned}\dot{\gamma}_w^*(t,\eta) &= i\omega\sum_{n\in\mathbb{Z}} n c_n^w e^{in\omega t} = -\sum_{\substack{n\in\mathbb{Z}\\ n\neq 0}}\left(\frac{in\omega(u_{wq}+u_{qw})}{2u_{ww}} - 2\mu\kappa_0\frac{u_{wq}-u_{qw}}{2u_{ww}}\right)c_n^q e^{in\omega t} \\ &= -\frac{u_{wq}+u_{qw}}{2u_{ww}}\dot{\gamma}_q(t) + 2\mu\kappa_0\frac{u_{wq}-u_{qw}}{2u_{ww}}\left(\gamma_q(t)-\bar{\gamma}_q\right) \\ &= -\frac{2k_\mathrm{B}T_\mathrm{c}}{\chi}\Big(2\mu\kappa_0(1-\bar{\eta})\left(\gamma_q(t)-\bar{\gamma}_q\right) - \bar{\eta}\dot{\gamma}_q(t)\Big)\end{aligned} \tag{4.115}$$

and, second, solving the simple differential equation (4.115).

Chapter 5

Bounding the Asymmetry of Positive Semidefinite Matrices

In this chapter, we develop a self-contained algebraic theory on positive semidefinite matrices. Following the spirit of Crouzeix and Gutan [56], we introduce a quantitative measure for the asymmetry of such matrices. We then prove that, for matrices of the special form $\mathbb{D} - \mathbb{T}$, this asymmetry index is subject to a universal bound depending only on the dimension m. Here, $\mathbb{D} \in \mathbb{R}^{m\times m}$ is a diagonal matrix with only non-negative entries chosen such that $\mathbb{D} - \mathbb{T}$ is positive semidefinite and $\mathbb{T} \in \mathbb{R}^{m\times m}$ is either doubly stochastic, doubly substochastic or sum-symmetric. For the second class, we prove additionally a nontrivial bound on the asymmetry index of the corresponding Schur complements [78].

5.1 Quantifying the Asymmetry of Positive Semidefinite Matrices

We first recall the definition (3.38)

$$\mathcal{S}(\mathbb{A}) \equiv \min\left\{ s \in \mathbb{R} |\, \forall \mathbf{z} \in \mathbb{C}^m \quad \mathbf{z}^\dagger \left(s\left(\mathbb{A} + \mathbb{A}^t\right) + i\left(\mathbb{A} - \mathbb{A}^t\right)\right)\mathbf{z} \geq 0. \right\}, \tag{5.1}$$

of the asymmetry index of an arbitrary positive semi-definite matrix $\mathbb{A} \in \mathbb{R}^{m\times m}$. Below, we list some of the basic properties of this quantity, which can be inferred directly from its definition.

Proposition 1 (Basic properties of the asymmetry index)**.** *For any positive semi-definite $\mathbb{A} \in \mathbb{R}^{m\times m}$, any invertible symmetric matrix $\mathbb{U} \in \mathbb{R}^{m\times m}$ and any $\lambda > 0$, we have*

$$\mathcal{S}\left(\mathbb{A}\right) = \mathcal{S}(\mathbb{A}^t) = \mathcal{S}(\mathbb{U}\mathbb{A}\mathbb{U}) = \mathcal{S}\left(\lambda\mathbb{A}\right) \tag{5.2}$$

and

$$\mathcal{S}\left(\mathbb{A}\right) \geq 0 \tag{5.3}$$

with equality if and only if $\mathbb{A}$ is symmetric. If $\mathbb{A}$ is invertible, it holds additionally

$$\mathcal{S}\left(\mathbb{A}\right) = \mathcal{S}(\mathbb{A}^{-1}). \tag{5.4}$$

Furthermore, we can easily prove the following two propositions, which are crucial for the derivation of our main results.

Proposition 2 (Quasiconvexity of the asymmetry index)**.** *Let $\mathbb{A},\mathbb{B} \in \mathbb{R}^{m\times m}$ be positive semi-definite, then*

$$\mathcal{S}\left(\mathbb{A}+\mathbb{B}\right) \leq \max\left\{\mathcal{S}\left(\mathbb{A}\right),\mathcal{S}\left(\mathbb{B}\right)\right\}. \tag{5.5}$$

Proof. By definition 5.1 the matrices

$$\mathbb{J}(s) \equiv s(\mathbb{A}+\mathbb{A}^t)+i(\mathbb{A}-\mathbb{A}^t) \quad \text{and} \quad \mathbb{K}(s) \equiv s(\mathbb{B}+\mathbb{B}^t)+i(\mathbb{B}-\mathbb{B}^t) \tag{5.6}$$

with $s \equiv \max\left\{\mathcal{S}\left(\mathbb{A}\right),\mathcal{S}\left(\mathbb{B}\right)\right\}$ both are positive semi-definite. It follows that

$$\mathbb{J}(s)+\mathbb{K}(s) = s\left(\mathbb{A}+\mathbb{B}\right)+s\left(\mathbb{A}+\mathbb{B}\right)^t+i\left(\mathbb{A}+\mathbb{B}\right)-i\left(\mathbb{A}+\mathbb{B}\right)^t \tag{5.7}$$

is also positive semi-definite and hence $\mathcal{S}\left(\mathbb{A}+\mathbb{B}\right) \leq s$. □

Proposition 3 (Dominance of principal submatrices)**.** *Let $\mathbb{A} \in \mathbb{R}^{m\times m}$ be positive semi-definite and $\bar{\mathbb{A}} \in \mathbb{R}^{p\times p}$ $(p<m)$ a principal submatrix of $\mathbb{A}$, then*

$$\mathcal{S}(\bar{\mathbb{A}}) \leq \mathcal{S}\left(\mathbb{A}\right). \tag{5.8}$$

Proof. By definition 5.1

$$\mathbb{K}(s) \equiv \mathcal{S}\left(\mathbb{A}\right)\left(\mathbb{A}+\mathbb{A}^t\right)+i(\mathbb{A}-\mathbb{A}^t) \tag{5.9}$$

is positive semi-definite. Consequently the matrix

$$\bar{\mathbb{K}}(s) \equiv \mathcal{S}(\mathbb{A})(\bar{\mathbb{A}}+\bar{\mathbb{A}}^t)+i(\bar{\mathbb{A}}-\bar{\mathbb{A}}^t), \tag{5.10}$$

which constitutes a principal submatrix of $\mathbb{K}$, is also positive semi-definite and therefore $\mathcal{S}(\bar{\mathbb{A}}) \leq \mathcal{S}\left(\mathbb{A}\right)$. □

5.2 Bound on the Asymmetry Index for Special Classes of Matrices

5.2.1 Doubly Stochastic Matrices

Definition 1. *A Matrix $\mathbb{P} \in \{0,1\}^{m\times m}$ is a permutation matrix if each row and column of $\mathbb{P}$ contains precisely one non-vanishing entry 1 [57]*

Theorem 1. *Let $\mathbb{P} \in \{0,1\}^{m\times m}$ be a permutation matrix and $\mathbb{1}$ the identity matrix, then the matrix $\mathbb{1}-\mathbb{P}$ is positive semi-definite on $\mathbb{R}^m$ and its asymmetry index fulfils*

$$\mathcal{S}\left(\mathbb{1}-\mathbb{P}\right) \leq \cot\left(\frac{\pi}{m}\right). \tag{5.11}$$

Proof. We first show that $\mathbb{1} - \mathbb{P}$ is positive semi-definite. To this end, we note that the matrix elements of $\mathbb{P}$ are given by $(\mathbb{P})_{ij} = \delta_{i\pi(j)}$, where $\pi \in S_m$ is the unique permutation associated with $\mathbb{P}$ and S_m the symmetric group on the set $\{1, \ldots, m\}$. Now, with $\mathbf{x} \equiv (x_1, \ldots, x_m)^t \in \mathbb{R}^m$ we have

$$\mathbf{x}^t (\mathbb{1} - \mathbb{P}) \mathbf{x} = \sum_{i,j=1}^{m} \left(\delta_{ij} - \delta_{i\pi(j)}\right) x_i x_j = \sum_{i,j=1}^{m} \frac{\delta_{i\pi(j)}}{2} \left(x_i^2 + x_j^2 - 2x_i x_j\right) \tag{5.12}$$

$$= \sum_{i,j=1}^{m} \frac{\delta_{i\pi(j)}}{2} (x_i - x_j)^2 \geq 0. \tag{5.13}$$

We now turn to the second part of Theorem 1. For any $\mathbf{z} \equiv (z_1, \ldots, z_m) \in \mathbb{C}^m$ and $s \geq 0$, we define the quadratic form

$$Q(\mathbf{z}, s) \equiv \mathbf{z}^\dagger \left(s (\mathbb{1} - \mathbb{P}) + s (\mathbb{1} - \mathbb{P})^t + i (\mathbb{1} - \mathbb{P}) - i (\mathbb{1} - \mathbb{P})^t\right) \mathbf{z} \tag{5.14}$$

$$= \mathbf{z}^\dagger \left(2s \cdot \mathbb{1} - (s + i)\mathbb{P} - (s - i)\mathbb{P}^t\right) \mathbf{z}. \tag{5.15}$$

By definition 5.1 the minimum s, for which $Q(\mathbf{z}, s)$ is positive semi-definite, equals the asymmetry index of $\mathbb{1} - \mathbb{P}$. This observation enables us to derive an upper bound for $\mathcal{S}(\mathbb{1} - \mathbb{P})$. To this end, we make use of the cycle decomposition

$$\pi = \left(i_1, \pi(i_1), \ldots, \pi^{n_1 - 1}(i_1)\right) \ldots \left(i_k, \pi(i_k), \ldots, \pi^{n_k - 1}(i_k)\right) \tag{5.16}$$

of π, where $i_1, \ldots, i_k \in \{1, \ldots, m\}$, $\pi^l(i)$ is defined recursively by

$$\pi^l(i) \equiv \pi\left(\pi^{l-1}(i)\right) \qquad \text{and} \qquad \pi^0(i) = i, \tag{5.17}$$

k denotes the number of independent cycles of and n_r the length the r^{th} cycle. By virtue of this decomposition, (5.14) can be rewritten as

$$Q(\mathbf{z}, s) = \sum_{i,j=1}^{m} \left(2s\delta_{ij} - (s + i)\delta_{i\pi(j)} - (s - i)\delta_{\pi(i)j}\right) z_i^* z_j \tag{5.18}$$

$$= \sum_{i=1}^{m} 2s z_i^* z_i - (s + i) z_{\pi(i)}^* z_i - (s - i) z_i^* z_{\pi(i)} \tag{5.19}$$

$$= \sum_{r=1}^{k} \sum_{l_r=0}^{n_r - 1} 2s z^*[\pi^{l_r}(i_r)] z[\pi^{l_r}(i_r)] - (s + i) z^*[\pi^{l_r+1}(i_r)] z[\pi^{l_r}(i_r)] - (s - i) z^*[\pi^{l_r}(i_r)] z[\pi^{l_r+1}(i_r)], \tag{5.20}$$

where, for convenience, we introduced the notation $z[x] \equiv z_x$. Next, we define the vectors $\tilde{\mathbf{z}}_r \in \mathbb{C}^{n_r}$ with elements $(\tilde{\mathbf{z}}_r)_j \equiv z\left[\pi^{j-1}(i_r)\right]$ and the Hermitian matrices $\mathbb{H}_{n_r}(s) \in \mathbb{C}^{n_r \times n_r}$ with matrix elements

$$\left(\mathbb{H}_{n_r}(s)\right)_{ij} \equiv 2s\delta_{ij} - (s + i)\delta_{ij+1} - (s - i)\delta_{i+1j}, \tag{5.21}$$

where periodic boundary conditions $n_r + 1 = 1$ for the indices $i, j = 1, \ldots, n_r$ are understood. These definitions allow us to cast (5.20) in the rather compact form

$$Q(\mathbf{z}, s) = \sum_{r=1}^{k} \tilde{\mathbf{z}}_r^\dagger \mathbb{H}_{n_r}(s) \tilde{\mathbf{z}}_r. \tag{5.22}$$

Obviously, any value of s for which all the $\mathbb{H}_{n_r}(s)$ are positive semi-definite serves as a lower bound for $\mathcal{S}(\mathbb{1}-\mathbb{P})$. Moreover, we can calculate the eigenvalues of $\mathbb{H}_{n_r}(s)$ explicitly. Inserting the Ansatz $\mathbf{v} \equiv (v_1, \ldots, v_{n_r})^t \in \mathbb{C}^{n_r}$ into the eigenvalue equation

$$\mathbb{H}_{n_r}(s)\mathbf{v} = \lambda\mathbf{v} \qquad (\lambda \in \mathbb{R}) \tag{5.23}$$

yields

$$\lambda v_j = 2sv_j - (s+i)v_{j-1} - (s-i)v_{j+1}, \tag{5.24}$$

where again periodic boundary conditions $v_{n_r+1} = v_1$ are understood. This recurrence equation can be solved by standard techniques. We put $v_j \equiv \exp(2\pi i\kappa j/n_r)$ with $(\kappa = 1, \ldots, n_r)$ and obtain the eigenvalues

$$\lambda_\kappa = 2\left(s - s\cos\left(\frac{2\pi\kappa}{n_r}\right) - \sin\left(\frac{2\pi\kappa}{n_r}\right)\right). \tag{5.25}$$

For any fixed $s \geq 0$, the function

$$f(x,s) \equiv s - s\cos x - \sin x \tag{5.26}$$

is non-negative for $x \in [x^*, 2\pi]$ and strictly negative for $x \in (0, x^*)$ with

$$x^* \equiv \arccos\left(\frac{s^2-1}{s^2+1}\right). \tag{5.27}$$

Therefore, all the eigenvalues λ_κ of $\mathbb{H}_{n_r}(s)$ are non-negative, if and only if

$$\frac{2\pi}{n_r} \geq \arccos\left(\frac{s^2-1}{s^2+1}\right). \tag{5.28}$$

Solving (5.28) for s gives the equivalent condition

$$s \geq \cot\left(\frac{\pi}{n_r}\right). \tag{5.29}$$

Since $n_r \leq m$ and therefore $2\pi/n_r \geq 2\pi/m$, we can conclude that any of the $\mathbb{H}_{n_r}(s)$ is positive semi-definite for any

$$s \geq \cot\left(\frac{\pi}{m}\right), \tag{5.30}$$

thus establishing the desired result (5.11).

□

Definition 2. *A matrix $\mathbb{T} \in \mathbb{R}^{m\times m}$ with elements $T_{kl} \equiv (\mathbb{T})_{kl}$ is doubly stochastic if $T_{kl} \geq 0$ and [57]*

$$\sum_{k=1}^{m} T_{kl} = \sum_{l=1}^{m} T_{kl} = 1. \tag{5.31}$$

Corollary 1. *Let $\mathbb{T} \in \mathbb{R}^{m\times m}$ be doubly stochastic, then the matrix $\mathbb{1} - \mathbb{T}$ is positive semi-definite and its asymmetry index fulfils*

$$\mathcal{S}(\mathbb{1} - \mathbb{T}) \leq \cot\left(\frac{\pi}{m}\right). \tag{5.32}$$

Proof. The Birkhoff-theorem (see p. 549 in [57]) states that for any doubly stochastic matrix $\mathbb{T} \in \mathbb{R}^{m\times m}$ there is a finite number of permutation matrices $\mathbb{P}_1, \dots \mathbb{P}_N \in \{0,1\}^{m\times m}$ and positive scalars $\lambda_1, \dots, \lambda_N \in \mathbb{R}$ such that

$$\sum_{k=1}^{N} \lambda_k = 1 \qquad \text{and} \qquad \sum_{k=1}^{N} \lambda_k \mathbb{P}_k = \mathbb{T}. \tag{5.33}$$

Hence, we have

$$\mathbb{1} - \mathbb{T} = \sum_{k=1}^{N} \lambda_k (\mathbb{1} - \mathbb{P}_k) \tag{5.34}$$

and consequently $\mathbb{1} - \mathbb{T}$ must be positive semi-definite by virtue of Theorem 1. Furthermore, using Proposition 2 and again Theorem 1 gives the bound (5.32). □

5.2.2 Doubly Substochastic Matrices

Definition 3. *A matrix $\bar{\mathbb{P}} \in \{0,1\}^{m\times m}$ is a partial permutation matrix if any row and column of $\bar{\mathbb{P}}$ contains at most one non-zero entry and all of these non-zero entries are 1 [79].*

Theorem 2. *Let $\bar{\mathbb{P}} \in \{0,1\}^{m\times m}$ be a partial permutation matrix. Then, the matrix $\mathbb{1} - \bar{\mathbb{P}}$ is positive semi-definite and its asymmetry index fulfils*

$$\mathcal{S}\left(\mathbb{1} - \bar{\mathbb{P}}\right) \leq \cot\left(\frac{\pi}{m+1}\right). \tag{5.35}$$

Proof. Let q be the number of non-vanishing entries of $\bar{\mathbb{P}}$. If $q = 0$, $\bar{\mathbb{P}}$ equals the zero matrix and there is nothing to prove. If $q = m$, $\bar{\mathbb{P}}$ itself must be a permutation matrix and Lemma 1 provides that $\mathbb{1} - \bar{\mathbb{P}}$ is positive semi-definite as well as the bound

$$\mathcal{S}\left(\mathbb{1} - \bar{\mathbb{P}}\right) \leq \cot\left(\frac{\pi}{m}\right), \tag{5.36}$$

which is even stronger than (5.35). If $0 < q < m$, there are two index sets $A \subset \{1, \dots, m\}$ and $B \subset \{1, \dots, m\}$ of equal cardinality $m - q$, such that the rows of $\bar{\mathbb{P}}$ indexed by A and the columns of $\bar{\mathbb{P}}$ indexed by B contain only zero entries. Clearly, in this case, $\bar{\mathbb{P}}$ is not a permutation matrix. Nevertheless, we can define a bijective map

$$\bar{\pi} : \{1, \dots, m\} \setminus B \to \{1, \dots, m\} \setminus A \tag{5.37}$$

in such a way that $\bar{\mathbb{P}}$ can be regarded as a representation of $\bar{\pi}$. To this end, we denote by $\{\mathbf{e}_1, \dots, \mathbf{e}_m\}$ the canonical basis of $\mathbb{R}^m$ and define $\bar{\pi} : i \mapsto \bar{\pi}(i)$ such that

$$\bar{\mathbb{P}}\mathbf{e}_i \equiv \mathbf{e}_{\bar{\pi}(i)}. \tag{5.38}$$

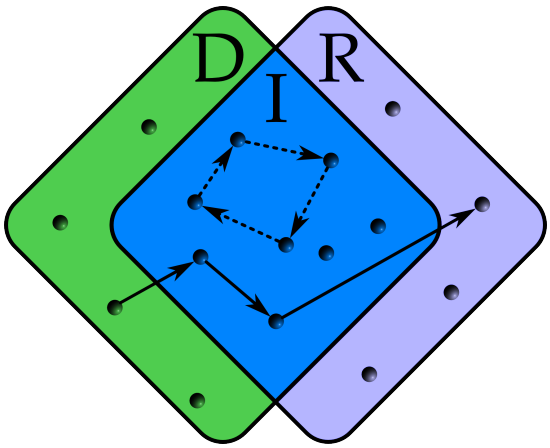

Figure 5.1: Schematic illustration of the cycle decomposition (5.39). The green square represents the set $\{1,\dots,m\}\setminus B$, the blue one the set $\{1,\dots,m\}\setminus A$. The black dots symbolize the elements of the respective sets and the arrows show the action of the map $\bar{\pi}$. While the dashed arrows form a complete cycle, the solid ones combine to an incomplete cycle.

This definition naturally leads to the cycle decomposition

$$\begin{aligned}\bar{\pi} = \quad & (i_1, \bar{\pi}(i_1), \dots, \bar{\pi}^{n_1-1}(i_1)) \cdots (i_k, \bar{\pi}(i_k), \dots, \bar{\pi}^{n_k-1}(i_k)) \\ & [j_1, \bar{\pi}(j_1), \dots, \bar{\pi}^{\bar{n}_1-1}(j_1)] \cdots [j_{\bar{k}}, \bar{\pi}(j_{\bar{k}}), \dots, \bar{\pi}^{\bar{n}_{\bar{k}}-1}(j_{\bar{k}})]\,. \end{aligned} \tag{5.39}$$

Here, we introduced two types of cycles. The ones in round brackets, which we will term complete, are just ordinary permutation cycles, which close by virtue of the condition $\bar{\pi}^{n_r}(i_r) = i_r$ and therefore must be contained completely in the set

$$I \equiv (\{1,\dots,m\}\setminus B) \cap (\{1,\dots,m\}\setminus A) = \{1,\dots,m\}\setminus(A\cup B)\,. \tag{5.40}$$

The cycles in rectangular brackets, which will be termed incomplete, do not close, but begin with a certain $j_{\bar{r}}$ taken from the set

$$D \equiv (\{1,\dots,m\}\setminus B)\setminus(\{1,\dots,m\}\setminus A) = A\setminus B \tag{5.41}$$

and terminate after $\bar{n}_{\bar{r}} - 1$ iterations with $\bar{\pi}^{\bar{n}_{\bar{r}}-1}(j_{\bar{r}})$, which is contained in

$$R \equiv (\{1,\dots,m\}\setminus A)\setminus(\{1,\dots,m\}\setminus B) = B\setminus A. \tag{5.42}$$

Figure 5.1 shows a schematic visualization of the two different types of cycles. We note that, since the map $\bar{\pi}$ is bijective, the cycle decomposition (5.39) is unique up to the choice of the i_r and any element of

$$J \equiv (\{1,\dots,m\}\setminus B)\cup(\{1,\dots,m\}\setminus A) = \{1,\dots,m\}\setminus(A\cap B) \tag{5.43}$$

shows up exactly once.

For the next step, we introduce the vectors

$$\mathbf{a} \equiv \sum_{i\in A} \mathbf{e}_i \qquad \text{and} \qquad \mathbf{b} \equiv \sum_{i\in B} \mathbf{e}_i, \tag{5.44}$$

as well as the bordered matrix

$$\mathbb{B} \equiv \begin{pmatrix} \bar{\mathbb{P}} & \mathbf{a} \\ \mathbf{b}^t & 1-m+q \end{pmatrix}. \tag{5.45}$$

Obviously, all rows and columns of $\mathbb{B}$ sum up to 1 and all off-diagonal entries are non-negative. Hence, with $B_{ij} \equiv (\mathbb{B})_{ij}$, we have for any $\mathbf{x} \in \mathbb{R}^m$

$$\begin{aligned}\mathbf{x}^t (\mathbb{1} - \mathbb{B}) \mathbf{x} &= \sum_{i,j=1}^{m} (\delta_{ij} - B_{ij}) x_i x_j = \sum_{i,j=1}^{m} \frac{B_{ij}}{2} \left(x_i^2 + x_j^2 - 2x_i x_j\right) \\ &= \sum_{i,j=1,\, i\neq j}^{m} \frac{B_{ij}}{2} (x_i - x_j)^2 \geq 0, \end{aligned} \tag{5.46}$$

i.e., the matrix $\mathbb{1} - \mathbb{B}$ is positive semi-definite. Since $\mathbb{1} - \bar{\mathbb{P}}$ is a principal submatrix of $\mathbb{1} - \mathbb{B}$, (5.46) implies in particular that $\mathbb{1} - \bar{\mathbb{P}}$ is positive semi-definite, thus establishing the first part of Lemma 2.

We will now prove the bound (5.35) on the asymmetry index of $\mathbb{1} - \bar{\mathbb{P}}$. To this end, for any $\mathbf{z} \in \mathbb{C}^{m+1}$ we associate the matrix $\mathbb{B}$ with the quadratic form

$$\bar{Q}(\mathbf{z}, s) \equiv \mathbf{z}^\dagger \left(s(\mathbb{1} - \mathbb{B}) + s(\mathbb{1} - \mathbb{B})^t + i(\mathbb{1} - \mathbb{B}) - i(\mathbb{1} - \mathbb{B})^t\right) \mathbf{z} \tag{5.47}$$

$$= \mathbf{z}^\dagger \left(2s \cdot \mathbb{1} - (s + i)\mathbb{B} - (s - i)\mathbb{B}^t\right) \mathbf{z}. \tag{5.48}$$

and notice that the minimum s for which $\bar{Q}(\mathbf{z}, s)$ is positive semi-definite equals the asymmetry index of $\mathbb{1} - \mathbb{B}$. Furthermore, since $\mathbb{1} - \bar{\mathbb{P}}$ is a principal submatrix of $\mathbb{1} - \mathbb{B}$, Proposition 3 implies that this particular value of s is also an upper bound on the asymmetry index of $\mathbb{1} - \bar{\mathbb{P}}$. Now, by inserting the decomposition

$$\mathbf{z} \equiv \sum_{i=1}^{m+1} z_i \mathbf{e}_i \tag{5.49}$$

into (5.48) while keeping in mind the definition (5.38), we obtain

$$\begin{aligned}\bar{Q}(\mathbf{z}, s) = {} & 2s \sum_{i=1}^{m} z_i^* z_i + 2s(m - q) z_{m+1}^* z_{m+1} \\ & - (s + i) \left(\sum_{i \in \{1,\ldots,m\} \setminus B} z_{\bar{\pi}(i)}^* z_i + \sum_{i \in A} z_i^* z_{m+1} + \sum_{i \in B} z_{m+1}^* z_i \right) \\ & - (s - i) \left(\sum_{i \in \{1,\ldots,m\} \setminus B} z_i^* z_{\bar{\pi}(i)} + \sum_{i \in A} z_{m+1}^* z_i + \sum_{i \in B} z_i^* z_{m+1} \right). \end{aligned} \tag{5.50}$$

By realizing

$$A = D \cup (A \cap B), \quad B = R \cup (A \cap B), \quad \{1, \ldots, m\} = J \cup (A \cap B) \tag{5.51}$$

and making use of the cycle decomposition (5.39), we can rewrite (5.50) as

$$\begin{aligned}\bar{Q}(\mathbf{z},s) &= 2s\sum_{r=1}^{k}\sum_{l_r=0}^{n_r-1} z^*[\bar{\pi}^{l_r}(i_r)]z[\bar{\pi}^{l_r}(i_r)] + 2s\sum_{\bar{r}=1}^{\bar{k}}\sum_{l_{\bar{r}}=0}^{n_{\bar{r}}-1} z^*[\bar{\pi}^{l_{\bar{r}}}(j_{\bar{r}})]z[\bar{\pi}^{l_{\bar{r}}}(j_{\bar{r}})] \\ &+ 2s\sum_{i\in A\cap B} z_i^* z_i + 2s(m-q)z_{m+1}^* z_{m+1} \\ &- (s+i)\Bigg(\sum_{r=1}^{k}\sum_{l_r=0}^{n_r-1} z^*[\bar{\pi}^{l_r+1}(i_r)]z[\bar{\pi}^{l_r}(i_r)] + \sum_{\bar{r}=1}^{\bar{k}}\sum_{l_{\bar{r}}=0}^{n_{\bar{r}}-2} z^*[\bar{\pi}^{l_{\bar{r}}+1}(j_{\bar{r}})]z[\bar{\pi}^{l_{\bar{r}}}(j_{\bar{r}})] \\ &\qquad + \sum_{i\in D} z_i^* z_{m+1} + \sum_{i\in R} z_{m+1}^* z_i + \sum_{i\in A\cap B}(z_i^* z_{m+1} + z_{m+1}^* z_i)\Bigg) \\ &- (s-i)\Bigg(\sum_{r=1}^{k}\sum_{l_r=0}^{n_r-1} z^*[\bar{\pi}^{l_r}(i_r)]z[\bar{\pi}^{l_r+1}(i_r)] + \sum_{\bar{r}=1}^{\bar{k}}\sum_{l_{\bar{r}}=0}^{n_{\bar{r}}-2} z^*[\bar{\pi}^{l_{\bar{r}}}(j_{\bar{r}})]z[\bar{\pi}^{l_{\bar{r}}+1}(j_{\bar{r}})] \\ &\qquad + \sum_{i\in D} z_{m+1}^* z_i + \sum_{i\in R} z_i^* z_{m+1} + \sum_{i\in A\cap B}(z_{m+1}^* z_i + z_i^* z_{m+1})\Bigg),\end{aligned} \tag{5.52}$$

thus explicitly separating contributions from complete and incomplete cycles. Finally, since we have

$$\sum_{i\in D} z_i^* z_{m+1} = \sum_{\bar{r}=1}^{\bar{k}} z^*[j_{\bar{r}}]z_{m+1}, \qquad \sum_{i\in R} z_{m+1}^* z_i = \sum_{\bar{r}=1}^{\bar{k}} z_{m+1}^* z[\bar{\pi}^{n_{\bar{r}}-1}(j_{\bar{r}})], \tag{5.53}$$

$$\sum_{i\in D} z_{m+1}^* z_i = \sum_{\bar{r}=1}^{\bar{k}} z_{m+1}^* z[j_{\bar{r}}], \qquad \sum_{i\in R} z_i^* z_{m+1} = \sum_{\bar{r}=1}^{\bar{k}} z^*[\bar{\pi}_{\bar{r}}^{n_{\bar{r}}-1}(j_{\bar{r}})]z_{m+1}, \tag{5.54}$$

by employing the definitions

$$\tilde{\mathbf{z}}_r \equiv \left(z[i_r], z[\bar{\pi}(i_r)], \ldots, z[\bar{\pi}^{n_r-1}(i_r)]\right)^t \in \mathbb{C}^{n_r\times n_r} \qquad \text{and} \tag{5.55}$$

$$\tilde{\tilde{\mathbf{z}}}_{\bar{r}} \equiv \left(z[j_{\bar{r}}], z[\bar{\pi}(j_{\bar{r}})], \ldots, z[\bar{\pi}^{n_{\bar{r}}-1}(j_{\bar{r}})], z_{m+1}\right)^t \in \mathbb{C}^{(n_{\bar{r}}+1)\times(n_{\bar{r}}+1)}, \tag{5.56}$$

(5.52) can be written as

$$\bar{Q}(\mathbf{z},s) = \sum_{r=1}^{k} \tilde{\mathbf{z}}_r^\dagger \mathbb{H}_{n_r}(s)\tilde{\mathbf{z}}_r + \sum_{\bar{r}=1}^{\bar{k}} \tilde{\tilde{\mathbf{z}}}_{\bar{r}}^\dagger \mathbb{H}_{n_{\bar{r}}+1}(s)\tilde{\tilde{\mathbf{z}}}_{\bar{r}} + 2s\sum_{i\in A\cap B}|z_i - z_{m+1}|^2, \tag{5.57}$$

where the matrices $\mathbb{H}_n(s)$ are defined in (5.21). Since we have already shown for the proof of Lemma 1 that $\mathbb{H}_n(s)$ is positive semi-definite for any $s \geq \cot(\pi/n)$, we immediately infer from (5.57) that $\bar{Q}(\mathbf{z},s)$ is positive semi-definite for any

$$s \geq \cot\left(\frac{\pi}{\max\{n_r, n_{\bar{r}}+1\}}\right). \tag{5.58}$$

Since $\max\{n_r, n_{\bar{r}}+1\} \leq m+1$, we finally end up with

$$\mathcal{S}\left(\mathbb{1}-\bar{\mathbb{P}}\right) \leq \mathcal{S}\left(\mathbb{1}-\mathbb{B}\right) \leq \cot\left(\frac{\pi}{m+1}\right). \tag{5.59}$$

□

Definition 4. *A matrix* $\bar{\mathbb{T}} \in \mathbb{R}^{m\times m}$ *with elements* $\bar{T}_{kl} \equiv (\mathbb{T})_{kl}$ *is doubly substochastic if* $\bar{T}_{kl} \geq 0$ *and [79]*

$$\sum_{k=1}^{m} \bar{T}_{kl} \leq 1 \quad \textit{and} \quad \sum_{l=1}^{m} \bar{T}_{kl} \leq 1. \tag{5.60}$$

Corollary 2. *Let* $\bar{\mathbb{T}} \in \mathbb{R}^{m\times m}$ *be doubly substochastic, then the matrix* $\mathbb{1} - \bar{\mathbb{T}}$ *is positive semi-definite and its asymmetry index fulfils*

$$\mathcal{S}\left(\mathbb{1} - \bar{\mathbb{T}}\right) \leq \cot\left(\frac{\pi}{m+1}\right). \tag{5.61}$$

Proof. It can be shown that any doubly substochastic matrix is the convex combination of a finite number of partial permutation matrices $\bar{\mathbb{P}}_k$ (see p. 165 in [79]), i.e., we have

$$\bar{\mathbb{T}} = \sum_{k=1}^{N} \lambda_k \bar{\mathbb{P}}_k \tag{5.62}$$

with

$$\lambda_k > 0 \qquad \text{and} \qquad \sum_{k=1}^{N} \lambda_k = 1. \tag{5.63}$$

Consequently, it follows

$$\mathbb{1} - \bar{\mathbb{T}} = \sum_{k=1}^{N} \lambda_k \left(\mathbb{1} - \bar{\mathbb{P}}\right). \tag{5.64}$$

Using the same argument with Lemma 2 instead of Lemma 1 in the proof of Corollary 1 completes the proof of Corollary 2 . □

5.2.3 Sum-symmetric Matrices

Definition 5. *Let* $A \subseteq \{1, \ldots, m\}$ *be an index set and denote by* S_A *the symmetric group on* A*. For any fixed-point free permutation* $\pi \in S_A$*, the matrix* $\mathbb{X}(A) \in \{0,1\}^{m\times m}$ *with elements*

$$(\mathbb{X}(A))_{kl} \equiv \begin{cases} 1 & \text{for} \quad k, l \in A \text{ and } l = \pi(k) \\ 0 & \text{else} \end{cases} \tag{5.65}$$

is a circuit matrix [80].

Theorem 3. *For* A *like in Definition 5, let* $\mathbb{E}(A) \in \{0,1\}^{m\times m}$ *be a matrix with elements* $E_{kl}(A) \equiv (\mathbb{E}(A))_{kl}$ *such that* $E_{kl} = 1$ *for* $k = l \in A$ *and* $E_{kl} = 0$ *otherwise. Then, for any circuit matrix* $\mathbb{X}(A)$*, the matrix* $\mathbb{E}(A) - \mathbb{X}(A)$ *is positive semi-definite and its asymmetry index fulfills*

$$\mathcal{S}(\mathbb{E}(A)) - \mathbb{X}(A)) \leq \cot\left(\frac{\pi}{|A|}\right), \tag{5.66}$$

where $|A|$ *denotes the cardinality of* A*.*

Proof. Let $\mathbb{Q} \in \{0,1\}^{n\times n}$ be a symmetric permutation matrix such that $\mathbb{Q}\mathbb{E}(A)\mathbb{Q} = \mathbb{1} \oplus \mathbb{O}_{m-|A|}$, where $\mathbb{O}_m$ denotes the $m \times m$ matrix with only zero entries. Since the rows and columns of $\mathbb{X}(A)$ indexed by A contain precisely one entry 1, while the remaining rows and columns contain only zero entries, we have $\mathbb{Q}(\mathbb{E}(A) - \mathbb{X}(A))\mathbb{Q} = (\mathbb{1} - \mathbb{P}) \oplus \mathbb{O}_{m-|A|}$, where $\mathbb{P} \in \{0,1\}^{|A|\times|A|}$ is a permutation matrix. The matrix $\mathbb{1} - \mathbb{P}$ is positive semi-definite by virtue of Theorem 1. Consequently, we have proven the first assertion of Theorem 3. Now, by recalling Proposition 1, we find

$$\begin{aligned} \mathcal{S}\left(\mathbb{E}(A) - \mathbb{X}(A)\right) &= \mathcal{S}\left(\mathbb{Q}(\mathbb{E}(A) - \mathbb{X}(A))\mathbb{Q}\right) = \mathcal{S}\left((\mathbb{1} - \mathbb{P}) \oplus \mathbb{O}_{n-|A|}\right) \\ &= \mathcal{S}\left(\mathbb{1} - \mathbb{P}\right) \leq \cot\left(\frac{\pi}{|A|}\right), \end{aligned} \tag{5.67}$$

where the last inequality again follows from Theorem 1. □

Definition 6. *Let $\tilde{\mathbb{T}} \in \mathbb{R}^{m\times m}$ be a matrix with elements $\tilde{T}_{kl} \equiv (\tilde{\mathbb{T}})_{kl} \geq 0$, then $\tilde{\mathbb{T}}$ is sum-symmetric if [80]*

$$\sum_{k=1}^{m} \tilde{T}_{kl} = \sum_{l=1}^{m} \tilde{T}_{kl}. \tag{5.68}$$

Corollary 3. *Let $\tilde{\mathbb{T}} \in \mathbb{R}^{n\times n}$ be sum-symmetric with row sums $r_i \geq 0$ and $\mathbb{D} \in \mathbb{R}^{m\times m}$ a diagonal matrix with entries $(\mathbb{D})_{kl} \equiv r_k\delta_{kl}$. Then the matrix $\mathbb{D} - \tilde{\mathbb{T}}$ is positive semi-definite and its asymmetry index fulfills*

$$\mathcal{S}\left(\mathbb{D} - \tilde{\mathbb{T}}\right) \leq \cot\left(\frac{\pi}{n}\right). \tag{5.69}$$

Proof. It can be shown that for any sum-symmetric matrix $\tilde{\mathbb{T}}$ there is a set of N circuit matrices $\mathbb{X}_k(A_k)$ such that

$$\tilde{\mathbb{T}} = \sum_{k=1}^{N} \lambda_k \mathbb{X}_k(A_k), \tag{5.70}$$

where the λ_k are positive real numbers [80]. Accordingly, the matrix $\mathbb{D} - \tilde{\mathbb{T}}$ can be rewritten as

$$\mathbb{D} - \tilde{\mathbb{T}} = \sum_{k=1}^{N} \lambda_k \left(\mathbb{E}(A_k) - \mathbb{X}(A_k)\right) \tag{5.71}$$

with $\mathbb{E}(A_k)$ like in Theorem 3. From Theorem 3, it follows that $\mathbb{D} - \tilde{\mathbb{T}}$ is positive semi-definite. By using the quasiconvexity of the asymmetry index, proven in Proposition 2, and again Theorem 3, we infer

$$\mathcal{S}\left(\mathbb{D} - \tilde{\mathbb{T}}\right) \leq \max\left\{\mathcal{S}\left(\mathbb{E}(A_k) - \mathbb{X}_k(A_k)\right)\right\} \leq \max\left\{\cot\left(\frac{\pi}{|A_k|}\right)\right\} \leq \cot\left(\frac{\pi}{n}\right). \tag{5.72}$$

□

5.3 Bound on the Asymmetry Index of Schur Complements

For $\mathbb{A} \in \mathbb{C}^{m\times m}$ partitioned as

$$\mathbb{A} \equiv \begin{pmatrix} \mathbb{A}_{11} & \mathbb{A}_{12} \\ \mathbb{A}_{21} & \mathbb{A}_{22} \end{pmatrix} \tag{5.73}$$

with non-singular $\mathbb{A}_{22} \in \mathbb{R}^{p\times p}$, the Schur complement of $\mathbb{A}_{22}$ in $\mathbb{A}$ is defined by (see p. 18 in [78])

$$\mathbb{A}/\mathbb{A}_{22} = \mathbb{A}_{11} - \mathbb{A}_{12}\mathbb{A}_{22}^{-1}\mathbb{A}_{21}. \tag{5.74}$$

Regarding the asymmetry index, we have the following proposition.

Proposition 4 (Dominance of the Schur complement)**.** *Let $\mathbb{A} \in \mathbb{R}^{m\times m}$ be a positive semi-definite matrix partitioned as in (5.73), where $\mathbb{A}_{22} \in \mathbb{R}^{p\times p}$ is non-singular, then the matrix $\mathbb{A}/\mathbb{A}_{22}$ is positive semi-definite and its asymmetry index fulfils*

$$\mathcal{S}\left(\mathbb{A}/\mathbb{A}_{22}\right) \leq \mathcal{S}\left(\mathbb{A}\right). \tag{5.75}$$

Proof. By assumption and by definition 5.1, we have for any $\mathbf{z} \in \mathbb{C}^m$

$$\mathbf{z}^\dagger \mathbb{A}\mathbf{z} \geq 0 \qquad \text{and} \qquad \mathbf{z}^\dagger \left(\mathcal{S}\left(\mathbb{A}\right)\left(\mathbb{A} + \mathbb{A}^t\right) + i(\mathbb{A} - \mathbb{A}^t)\right)\mathbf{z} \geq 0. \tag{5.76}$$

Putting

$$\mathbf{z} \equiv \begin{pmatrix} \mathbf{z}_p \\ -\mathbb{A}_{22}^{-1}\mathbb{A}_{21}\mathbf{z}_p \end{pmatrix} \qquad \text{with} \qquad \mathbf{z}_p \in \mathbb{C}^p \tag{5.77}$$

yields

$$\mathbf{z}_p^\dagger \left(\mathbb{A}/\mathbb{A}_{22}\right)\mathbf{z}_p \geq 0 \tag{5.78}$$

and

$$\mathbf{z}_p^\dagger \left(\mathcal{S}\left(\mathbb{A}\right)\left(\mathbb{A}/\mathbb{A}_{22} + (\mathbb{A}/\mathbb{A}_{22})^t\right) + i(\mathbb{A}/\mathbb{A}_{22} - (\mathbb{A}/\mathbb{A}_{22})^t)\right)\mathbf{z}_p \geq 0. \tag{5.79}$$

□

For the special class of matrices considered in Corollary 2, the assertion of Proposition 4 can be even strengthened. Before being able to state this stronger result, we need to prove the following Lemma.

Lemma 1. *Let $\bar{\mathbb{T}} \in \mathbb{R}^{m\times m}$ be a doubly substochastic matrix and $\mathbb{S} \equiv \mathbb{1} - \bar{\mathbb{T}}$ be partitioned as*

$$\mathbb{S} \equiv \begin{pmatrix} \mathbb{S}_{11} & \mathbb{S}_{12} \\ \mathbb{S}_{21} & \mathbb{S}_{22} \end{pmatrix}, \tag{5.80}$$

where $\mathbb{S}_{22} \in \mathbb{R}^{p\times p}$ is non-singular, then there is a doubly substochastic matrix $\bar{\mathbb{T}}_{m-p} \in \mathbb{R}^{(m-p)\times(m-p)}$, such that

$$\mathbb{S}/\mathbb{S}_{22} = \mathbb{1} - \bar{\mathbb{T}}_{m-p}. \tag{5.81}$$

Proof. We start with the case $p = 1$. Let $\bar{T}_{ij}$ be the matrix elements of $\bar{\mathbb{T}}$, then the matrix elements of $\mathbb{S}/\mathbb{S}_{22}$ are given by

$$(\mathbb{S}/\mathbb{S}_{22})_{kl} \equiv \delta_{kl} - \bar{T}_{kl} - \frac{\bar{T}_{km}\bar{T}_{ml}}{1-\bar{T}_{mm}} \tag{5.82}$$

with $k, l = 1, \ldots, m-1$. Obviously, we have

$$\sum_{k=1}^{m-1} (\mathbb{S}/\mathbb{S}_{22})_{kl} = 1 - \sum_{k=1}^{m-1} \bar{T}_{kl} - \frac{\bar{T}_{ml}}{1-\bar{T}_{mm}} \sum_{k=1}^{m-1} \bar{T}_{km} \leq 1. \tag{5.83}$$

Furthermore, since by assumption

$$\sum_{i=1}^{m} \bar{T}_{ij} \leq 1 \tag{5.84}$$

it follows

$$\sum_{k=1}^{m-1} (\mathbb{S}/\mathbb{S}_{22})_{kl} \geq 1 - (1-\bar{T}_{ml}) - \frac{\bar{T}_{ml}(1-\bar{T}_{mm})}{1-\bar{T}_{mm}} = 0. \tag{5.85}$$

Analogously, we find

$$0 \leq \sum_{l=1}^{m-1} (\mathbb{S}/\mathbb{S}_{22})_{kl} \leq 1. \tag{5.86}$$

Next, we investigate the sign pattern of the $(\mathbb{S}/\mathbb{S}_{22})_{kl}$. First, for $k \neq l$, we have

$$(\mathbb{S}/\mathbb{S}_{22})_{kl} = -\bar{T}_{kl} - \frac{\bar{T}_{km}\bar{T}_{ml}}{1-\bar{T}_{mm}} \leq 0. \tag{5.87}$$

Second, we rewrite the $(\mathbb{S}/\mathbb{S}_{22})_{kk}$ as

$$(\mathbb{S}/\mathbb{S}_{22})_{kk} = 1 - \bar{T}_{kk} - \frac{\bar{T}_{km}\bar{T}_{mk}}{1-\bar{T}_{mm}} = \frac{(1-\bar{T}_{kk})(1-\bar{T}_{mm}) - \bar{T}_{km}\bar{T}_{mk}}{1-\bar{T}_{mm}} \tag{5.88}$$

The numerator appearing on the right hand side can be written as

$$(1-\bar{T}_{kk})(1-\bar{T}_{mm}) - \bar{T}_{km}\bar{T}_{mk} = \mathrm{Det}\begin{pmatrix} 1-\bar{T}_{kk} & -\bar{T}_{km} \\ -\bar{T}_{mk} & 1-\bar{T}_{mm} \end{pmatrix}, \tag{5.89}$$

which is a principal minor of $\mathbb{1} - \bar{\mathbb{T}}$. Since, by Corollary 2, $\mathbb{1} - \bar{\mathbb{T}}$ is positive semi-definite, we end up with

$$0 \leq (\mathbb{S}/\mathbb{S}_{22})_{kk} \leq 1. \tag{5.90}$$

From the sum rules (5.83), (5.85) and (5.86) and the constraints (5.87) and (5.90), we deduce that $\mathbb{1} - \mathbb{S}/\mathbb{S}_{22}$ is doubly substochastic and thus we have proven Lemma 1 for $p = 1$. We now continue by induction. To this end, we assume that Lemma 1 is true for $p = q$. For $p = q + 1$ the matrix $\mathbb{S}_{22} \in \mathbb{R}^{(q+1)\times(q+1)}$ can be partitioned as

$$\mathbb{S}_{22} \equiv \begin{pmatrix} W_{11} & \mathbf{W}_{12}^t \\ \mathbf{W}_{21} & \mathbb{W}_{22} \end{pmatrix} \tag{5.91}$$

with $\mathbb{W}_{22} \in \mathbb{R}^{q\times q}$, $W_{11} \in \mathbb{R}$ and accordingly $\mathbf{W}_{12}, \mathbf{W}_{21} \in \mathbb{R}^{q}$. The Crabtree-Haynsworth quotient formula (see p. 25 in [78]), allows us to rewrite $\mathbb{S}/\mathbb{S}_{22}$ as

$$\mathbb{S}/\mathbb{S}_{22} = (\mathbb{S}/\mathbb{W}_{22}) \,/\, (\mathbb{S}_{22}/\mathbb{W}_{22})\,. \tag{5.92}$$

A direct calculation shows that $\mathbb{S}_{22}/\mathbb{W}_{22} \in \mathbb{R}$ is the lower right diagonal entry of $\mathbb{S}/\mathbb{W}_{22}$ (see p. 25 in [78] for details). Furthermore, by the induction hypothesis, there is a doubly substochastic matrix $\bar{\mathbb{T}}_{m-q} \in \mathbb{R}^{(m-q)\times(m-q)}$, such that

$$\mathbb{S}/\mathbb{W}_{22} = \mathbb{1} - \bar{\mathbb{T}}_{m-q}. \tag{5.93}$$

Thus, (5.92) reduces to the case $p = 1$, for which we have already proven Lemma 1. □

From Lemma 1 and Corollary 2, we immediately deduce

Corollary 4. *Let $\bar{\mathbb{T}}$, $\mathbb{S}$ and $\mathbb{S}_{22}$ be as in Lemma 1, then*

$$\mathcal{S}\,(\mathbb{S}/\mathbb{S}_{22}) \leq \cot\left(\frac{\pi}{m-p+1}\right). \tag{5.94}$$

5.4 Conclusion

We have proven a universal bound on the asymmetry index of three classes of positive semidefinite matrices, which can be parameterized as $\mathbb{D} - \mathbb{T} \in \mathbb{R}^{m\times m}$ with Δ being diagonal and the non-negative elements of $\mathbb{T}$ fulfilling certain sum rules. Matrices of this type are typically involved in the expressions for the kinetic coefficients obtained in the scattering approach to quantum transport. As we have shown in Ch. 3, the mathematical results derived here can be used to constrain these coefficients and thus to derive bounds on the efficiency of a general class of thermoelectric heat engines. Apart from this important application, the theory developed in this chapter constitutes an independent and original contribution to the mathematical field of matrix algebra.

Chapter 6

Concluding Perspectives

The fundamental question raised by the intriguing work of Benenti *et al.* [27] whether heat engines with broken microscopic time-reversal symmetry, at least if operated in linear response, might be able to deliver finite power at Carnot efficiency was starting point for the investigations outlined in this thesis.

6.1 Strong Bounds

In retrospect, we have obtained three major results. First, for a large class of models for thermoelectric heat engines, we have proven two independent constraints on the kinetic coefficients that are both stronger than the ones imposed by the second law and Onsager's reciprocal relations. Ultimately, they follow from current conservation. The first of these constraints implies a universal bound on the efficiency of multi-terminal thermoelectric generators, which depends only on the number of involved terminals and becomes successively weaker as this number increases. The second constraint leads to a universal relation between power and efficiency, which depends neither on the number of terminals nor on other microscopic details of the model and bounds power to vanish at least linearly when the Carnot efficiency is approached.

As our second main result, we have shown that the notions of irreversible thermodynamics can be naturally transferred to periodically driven systems. In particular, our new framework permits a consistent definition of a linear response regime for such systems, within which model-specific properties are encoded in a set of four kinetic coefficients. Since the external driving breaks the internal time-reversal symmetry of the system, even in the absence of magnetic fields, these coefficients do typically not fulfill a symmetric reciprocal relation. Consequently, the option of reversible power generation arises also for cyclic heat engines. However, by using a general Fokker-Planck equation to describe the micro-dynamics of the system, we have established the aforementioned relation between power and efficiency also for periodically operating heat engines. Due to this bound, which constitutes our third main result, power output must vanish at least linearly in the vicinity of the Carnot efficiency.

6.2 Microscopic Models

Despite the achievements summarized above, there is still plenty of room for future investigations. From a practical point of view, a question of particular interest is how the general bounds derived here can be saturated in specific models for thermoelectric or cyclic heat engines. Some progress towards this direction was already made. Specifically, within a quite involved numerical study, Balachandran *et al.* showed that our three-terminal bound on thermoelectric efficiency, in principle, can be saturated [81]. This result, however, follows by optimizing general transmission probabilities rather than designing a specific single-particle Hamiltonian to determine the time evolution inside the central region.

The first truly microscopic realization of a multi-terminal model, within which the corresponding upper bound on efficiency could be reached was the classical Nernst engine studied by Stark in his master thesis [62]. For this setup, it turned out that, in the limit of a strong magnetic field, a characteristic transmission pattern allowing the exchange of particles only between adjacent reservoirs leads to maximal efficiency. Recently, it has been pointed out that the same mechanism can be utilized for efficient power generation in the quantum realm [82,83], where the bouncing orbits of the classical system become quantum Hall edge states. In particular, these studies suggest that quantum Nernst engines might outperform their classical counterparts. Further investigations in this direction appear especially interesting given recent experiments showing the accessibility of magnetic field effects in nanostructures even at low and moderate field strengths [28, 84, 85].

Inelastic scattering events and interactions between particles are incorporated in the multi-terminal model only on a phenomenological level. On the basis of the non-equilibrium Green's function method, formally exact expressions for the heat and matter current through regions of genuinely interacting particles can be obtained from first principles [86–88]. These expressions are indeed reminiscent of the Landauer-Büttiker formula. However, the corresponding generalized transmission coefficients do not necessarily fulfill the crucial sum rules all bounds derived in Ch. 3 technically rely on. Therefore, it remains unclear at this point, whether these bounds also apply to intrinsically interacting systems. Models, which explicitly take into account particle-particle interactions, like for example the ones considered in [89–91], might thus be used to challenge our bounds on the efficiency and power of thermoelectric heat engines.

In the last part of Ch. 4, we have discussed a simple but instructive model for a cyclic Brownian heat engine operating in linear response. It turned out that, within this setup, the previously derived bound on the output power of such devices can be reached asymptotically. Saturation can, however, only be achieved in the rather artificial limit, where the system is coupled only to the cold heat bath such that both, the power output and its upper bound, vanish. The question, whether our general bound can be attained at finite power in more complex systems, operating for example in the underdamped regime and in the presence of a magnetic field, should therefore constitute an interesting subject for future investigations.

6.3 Universality

Our analysis has revealed remarkable similarities between thermoelectric and cyclic heat engines. In particular, the respective relations between power and efficiency, which we

have proven here for rather general classes of systems, are identical up to the normalization factor. Whether this intriguing analogy suggests the existence of a so far undiscovered universal principle that applies to periodic as well as to steady states leading to a bound on power for any type of heat engine that operates in the linear regime remains an exciting topic for future research.

A promising starting point for investigations in this directions might be found in the Green-Kubo relations, which follow from first principles and provide general expressions for the conventional kinetic coefficients in terms of equilibrium correlation functions [69]. Using a Fokker-Planck approach, we have shown that an analogous representation for the kinetic coefficients exists in periodically driven systems. The quantities related by the relevant correlation functions are, however, well defined irrespective of specific dynamics governing the time evolution of the phase space density. It might therefore be possible to obtain Hamiltonian-based expressions also for the periodic kinetic coefficients introduced in this work. Finding a proper way to take the time dependence of temperature into account is arguably the major challenge here.

This problem also prevents an immediate extension of our formalism to periodically driven quantum systems. While the first part of our analysis, the identification of proper fluxes and affinities, carries over to quantum mechanics line by line, it is not clear at the moment whether the constraints on the kinetic coefficients obtained here classically can be likewise transferred or properly generalized. This topic appears all the more urgent in the light of recent developments showing that the emerging field of quantum thermodynamics nowadays comes within the range of experiments [33, 92–94]. Moreover, there is currently a growing evidence that genuine quantum effects like coherence might help to enhance the performance of thermal machines [95–98]. Whether or not such phenomena can be exploited to lift the classical bounds derived here is still an open question. In any case, our results provide valuable benchmarks for future studies.

Bibliography

[1] Curzon F.L. and Ahlborn B., Efficiency of a Carnot Engine at Maximum Power Output, *Am. J. Phys.* **43**, 22 (1975).

[2] Takaishi T., Nakano R., Numata A. and Sakaguchi K., Approach to High Efficiency Diesel and Gas Engines, *Mitsubishi Heavy Ind. Ltd. Tech. Rev.* **45**, 21 (2008).

[3] Esposito M., Kawai R., Lindenberg K. and Van den Broeck C., Efficiency at Maximum Power of Low-Dissipation Carnot Engines, *Phys. Rev. Lett.* **105**, 150603 (2010).

[4] Allahverdyan A.E., Hovhannisyan K.V., Melkikh A.V. and Gevorkian S.G., Carnot Cycle at Finite Power: Attainability of Maximal Efficiency, *Phys. Rev. Lett.* **111**, 050601 (2013).

[5] Callen H.B., *Thermodynamics and an Introduction to Thermostatics*, 2nd ed., John Wiley & Sons, New York (1985).

[6] Van den Broeck C., Thermodynamic Efficiency at Maximum Power, *Phys. Rev. Lett.* **95**, 190602 (2005).

[7] Schmiedl T. and Seifert U., Efficiency at maximum power: An analytically solvable model for stochastic heat engines, *Europhys. Lett.* **81**, 20003 (2008).

[8] Esposito M., Lindenberg K. and Van den Broeck C., Universality of Efficiency at Maximum Power, *Phys. Rev. Lett.* **102**, 130602 (2009).

[9] Nakpathomkun N., Xu H.Q. and Linke H., Thermoelectric efficiency at maximum power in low-dimensional systems, *Phys. Rev. B* **82**, 235428 (2010).

[10] Seifert U., Stochastic thermodynamics, fluctuation theorems and molecular machines., *Rep. Prog. Phys.* **75**, 126001 (2012).

[11] Humphrey T.E. and Linke H., Quantum, cyclic, and particle-exchange heat engines, *Physica E* **29**, 390 (2005).

[12] Matsubara K., Development of a High Efficient Thermoelectric Stack for a Waste Exhaust Heat Recovery of Vehicles, in *Int. Conf. Thermoelectr.*, 418 (2002).

[13] Mahan G., Sales B. and Sharp J., Thermoelectric Materials: New Approaches to an Old Problem, *Phys. Today* **50**, 42 (1997).

[14] Dresselhaus M.S., Chen G., Tang M.Y., Yang R., Lee H., Wang D., Ren Z., Fleurial J.P. and Gogna P., New Directions for Low-Dimensional Thermoelectric Materials, *Adv. Mat.* **19**, 1043 (2007).

[15] Bell L.E., Cooling, Heating, Generating Power, and Recovering Waste Heat with Thermoelectric Systems, *Science* **321**, 1457 (2008).

[16] Snyder G.J. and Toberer S., Complex thermoelectric materials, *Nat. Mater.* **7**, 105 (2008).

[17] Vineis C.J., Shakouri A., Majumdar A. and Kanatzidis M.G., Nanostructured Thermoelectrics: Big Efficiency Gains from Small Features., *Adv. Mat.* **22**, 3970 (2010).

[18] Heremans J.P., Dresselhaus M.S., Bell L.E. and Morelli D.T., When thermoelectrics reached the nanoscale., *Nat. Nanotechnol.* **8**, 471 (2013).

[19] Mahan G.D. and Sofo J.O., The best thermoelectric, *Proc. Natl. Acad. Sci. USA* **93**, 7436 (1996).

[20] Humphrey T.E., Newbury R., Taylor R.P. and Linke H., Reversible Quantum Brownian Heat Engines for Electrons, *Phys. Rev. Lett.* **89**, 116801 (2002).

[21] Humphrey T.E. and Linke H., Reversible Thermoelectric Nanomaterials, *Phys. Rev. Lett.* **94**, 096601 (2005).

[22] Izumida Y. and Okuda K., Onsager coefficients of a finite-time Carnot cycle, *Phys. Rev. E* **80**, 021121 (2009).

[23] Izumida Y. and Okuda K., Onsager coefficients of a Brownian Carnot cycle, *Eur. Phys. J. B* **77**, 499 (2010).

[24] Izumida Y. and Okuda K., Linear irreversible heat engines based on the local equilibrium assumptions (2015), `arXiv:1501.03987`.

[25] Goldsmid H.J., *Introduction to Thermoelectricity*, 1st ed., Springer Series in Material Science (2009).

[26] Goupil C., Seifert W., Zabrocki K., Müller E. and Snyder G.J., Thermodynamics of Thermoelectric Phenomena and Applications, *Entropy* **13**, 1481 (2011).

[27] Benenti G., Saito K. and Casati G., Thermodynamic Bounds on Efficiency for Systems with Broken Time-Reversal Symmetry, *Phys. Rev. Lett.* **106**, 230602 (2011).

[28] Matthews J., Battista F., Sánchez D., Samuelsson P. and Linke H., Experimental verification of reciprocity relations in quantum thermoelectric transport, *Phys. Rev. B* **90**, 165428 (2014).

[29] Steeneken P.G., Le Phan K., Goossens M.J., Koops G.E.J., Brom G.J.A.M., van der Avoort C. and van Beek J.T.M., Piezoresistive heat engine and refrigerator, *Nat. Phys.* **7**, 354 (2011).

[30] Blickle V. and Bechinger C., Realization of a micrometer-sized stochastic heat engine, *Nat. Phys.* **8**, 143 (2011).

[31] Ribezzi-Crivellari M. and Ritort F., Free-energy inference from partial work measurements in small systems., *Proc. Natl. Acad. Sci. USA* **111**, E3386 (2014).

[32] Koski J.V., Maisi V.F., Pekola J.P. and Averin D.V., Experimental realization of a Szilard engine with a single electron, *Proc. Natl. Acad. Sci. USA* **111**, 13786 (2014).

[33] Pekola J.P., Towards quantum thermodynamics in electronic circuits, *Nat. Phys.* **11**, 118 (2015).

[34] Martínez I.A., Roldán E., Dinis L., Petrov D. and Rica R.A., Adiabatic Processes Realized with a Trapped Brownian Particle, *Phys. Rev. Lett.* **114**, 120601 (2015).

[35] Landauer R., Spatial Variations of Currents and Fields Due to Localized Scatterers in Metallic Conduction, *IBM J. Res. Dev.* **1**, 223 (1957).

[36] Büttiker M., Imry Y., Landauer R. and Pinhas S., Generalized many-channel conductance formula with application to small rings, *Phys. Rev. B* **31**, 6207 (1985).

[37] Büttiker M., Role of quantum coherence in series resistors, *Phys. Rev. B* **33**, 3020 (1986).

[38] Sivan U. and Imry Y., Multichannel Landauer formula for thermoelectric transport with application to thermopower near the mobility edge, *Phys. Rev. B* **33**, 551 (1986).

[39] Büttiker M., Four-Terminal Phase-Coherent Conductance, *Phys. Rev. Lett.* **57**, 1761 (1986).

[40] Büttiker M., Coherent and sequential tunneling in series barriers, *IBM J. Res. Dev.* **32**, 63 (1988).

[41] Butcher P.N., Thermal and electrical transport formalism for electronic microstructures with many terminals, *J. Phys. Condens. Matter* **2**, 4869 (1990).

[42] Büttiker M., Symmetry of electrical conduction, *IBM J. Res. Dev.* **32**, 317 (1988).

[43] Mahan G.D., *Many-Particle Physics*, 2nd ed., Plenum Press (1990).

[44] Langreth D.C. and Abrahams E., Derivation of the Landauer conductance formula, *Phys. Rev. B* **24**, 2978 (1981).

[45] Fisher D.S. and Lee P.A., Relation between conductivity and transmission matrix, *Phys. Rev. B* **23**, 6851 (1981).

[46] Stone A.D. and Szafer A., What is measured when you measure a resistance? - The Landauer formula revisited, *IBM J. Res. Dev.* **32**, 384 (1988).

[47] Baranger H.U. and Stone A.D., Electrical linear-response theory in an arbitrary magnetic field: A new Fermi-surface formation, *Phys. Rev. B* **40**, 8169 (1989).

[48] Viehweger O., Dissipation coefficients and conductances in mesoscopic systems without time reversal invariance, *Z. Phys. B* **77**, 135 (1989).

[49] Janssen M., Conductance coefficients for multi-probe conductors, *Solid State Commun.* **79**, 1073 (1991).

[50] Shepard K., Multichannel, multiprobe Landauer formula in the presence of a uniform magnetic field, *Phys. Rev. B* **43**, 623 (1991).

[51] Büttiker M., Prêtre A. and Thomas H., Dynamic Conductance and the Scattering Matrix of Small Conductors, *Phys. Rev. Lett.* **70**, 4114 (1993).

[52] Risken H., *The Fokker-Planck Equation*, 2nd ed., Springer (1996).

[53] Spinney R.E. and Ford I.J., Entropy production in full phase space for continuous stochastic dynamics, *Phys. Rev. E* **85**, 051113 (2012).

[54] Jung P., Periodically driven stochastic systems, *Phys. Rep.* **234**, 175 (1993).

[55] Ballentine L.E., *Quantum Mechanics: A Modern Developement*, 1st ed., World Scientific (1998).

[56] Crouzeix J.P. and Gutan C., A Measure Of Asymmetry For Positive Semidefinite Matrices, *Optimization* **52**, 251 (2003).

[57] Horn R.A. and Johnson C.R., *Matrix Analysis*, 2nd ed., Cambridge University Press (2013).

[58] Elliott J.F., Thermomagnetic Generator, *J. Appl. Phys.* **30**, 1774 (1959).

[59] Wright D.A., Theory of the Nernst-Ettingshausen generator, *Brit. J. Appl. Phys.* **13**, 583 (1962).

[60] Norwood M.H., Theory of Nernst Generators and Refrigerators, *J. Appl. Phys.* **34**, 594 (1963).

[61] Harman T.C. and Honig J.M., Theory of Galvano-Thermomagnetic Energy Conversion Devices. III. Generators Constructed from Anisotropic Materials, *J. Appl. Phys.* **34**, 189 (1963).

[62] Stark J., *Influence of broken time-reversal symmetry on the efficiency of thermal machines*, Master thesis, Universität Stuttgart (2013).

[63] Larralde H., Leyvraz F. and Mejía-Monasterio C., Transport Properties of a Modified Lorentz Gas, *J. Stat. Phys.* **113**, 197 (2003).

[64] Whitney R.S., Most Efficient Quantum Thermoelectric at Finite Power Output, *Phys. Rev. Lett.* **112**, 130601 (2014).

[65] Whitney R.S., Finding the quantum thermoelectric with maximal efficiency and minimal entropy production at given power output, *Phys. Rev. B* **91**, 115425 (2015).

[66] Ott E., *Chaos in dynamical systems*, 2nd ed., Cambridge University Press (2009).

[67] Kohn W., Periodic thermodynamics, *J. Stat. Phys.* **103**, 417 (2001).

[68] Owedyk J. and Kociszewski A., On the Fokker-Planck equation with time-dependent drift and diffusion coefficients and its exponential solution, *Z. Phys. B* **59**, 69 (1985).

[69] Kubo R., Toda M. and Hashitsume N., *Statistical Physics II - Nonequilibrium Statistical Mechanics*, 2nd ed., Springer Series in Solid-State Sciences (1998).

[70] Machura L., Kostur M., Marchesoni F., Talkner P., Hänggi P. and Luczka J., Optimal strategy for controlling transport in inertial Brownian motors, *J. Phys. Condens. Matter* **17**, S3741 (2005).

[71] Onsager L., Reciprocal Relations in Irreversible Processes II, *Phys. Rev.* **38**, 2265 (1931).

[72] Onsager L., Reciprocal Relations in Irreversible Processes I, *Phys. Rev.* **37**, 405 (1931).

[73] Abreu D. and Seifert U., Extracting work from a single heat bath through feedback, *Europhys. Lett.* **94**, 10001 (2011).

[74] Bauer M., Abreu D. and Seifert U., Efficiency of a Brownian information machine, *J. Phys. A: Math. Theor.* **45**, 162001 (2012).

[75] Tu Z.C., Stochastic heat engine with the consideration of inertial effects and shortcuts to adiabaticity, *Phys. Rev. E* **89**, 052148 (2014).

[76] Berger F., Schmiedl T. and Seifert U., Optimal potentials for temperature ratchets, *Phys. Rev. E* **79**, 031118 (2009).

[77] Schmiedl T. and Seifert U., Optimal finite-time processes in stochastic thermodynamics, *Phys. Rev. Lett.* **98**, 108301 (2007).

[78] Zhang F., *The Schur Complement and its Applications*, 1st ed., Springer (2005).

[79] Horn R.A. and Johnson C.R., *Topics in Matrix Analysis*, 1st ed., Cambridge University Press (1991).

[80] Bapat R.B. and Raghavan T.E.S., *Nonnegative Matrices and Applications*, 1st ed., Cambridge University Press (2009).

[81] Balachandran V., Benenti G. and Casati G., Efficiency of three-terminal thermoelectric transport under broken time-reversal symmetry, *Phys. Rev. B* **87**, 165419 (2013).

[82] Sothmann B., Sánchez R. and Jordan A.N., Quantum Nernst engines, *Europhys. Lett.* **107**, 47003 (2014).

[83] Sánchez R., Sothmann B. and Jordan A.N., Chiral Thermoelectrics with Quantum Hall Edge States, *Phys. Rev. Lett.* **114**, 146801 (2015).

[84] Pogosov A.G., Budantsev M.V., Uzur D., Nogaret A., Plotnikov A.E., Bakarov A.K. and Toropov A.I., Thermopower of a multiprobe ballistic conductor, *Phys. Rev. B* **66**, 201303 (2002).

[85] Maximov S., Gbordzoe M., Buhmann H., Molenkamp L. and Reuter D., Low-field diffusion magnetothermopower of a high-mobility two-dimensional electron gas, *Phys. Rev. B* **70**, 121308 (2004).

[86] Meir Y. and Wingreen N.S., Landauer Formula for the Current through an Interacting Electron Region, *Phys. Rev. Lett.* **68**, 2512 (1992).

[87] Zak R. and Flensberg K., Coulomb blockade of a three-terminal quantum dot, *Phys. Rev. B* **77**, 045329 (2008).

[88] Liu J., Sun Q. and Xie X.C., Enhancement of the thermoelectric figure of merit in a quantum dot due to the Coulomb blockade effect, *Phys. Rev. B* **81**, 245323 (2010).

[89] Sánchez R. and Büttiker M., Optimal energy quanta to current conversion, *Phys. Rev. B* **83**, 085428 (2011).

[90] Sothmann B., Sánchez R., Jordan A.N. and Büttiker M., Rectification of thermal fluctuations in a chaotic cavity heat engine, *Phys. Rev. B* **85**, 205301 (2012).

[91] Kennes D.M., Schuricht D. and Meden V., Efficiency and power of a thermoelectric quantum dot device, *Europhys. Lett.* **102**, 57003 (2013).

[92] Abah O., Rossnagel J., Jacob G., Deffner S., Schmidt-Kaler F., Singer K. and Lutz E., Single-ion heat engine at maximum power, *Phys. Rev. Lett.* **109**, 203006 (2012).

[93] An S., Zhang J.N., Um M., Lv D., Lu Y., Zhang J., Yin Z.Q., Quan H.T. and Kim K., Experimental test of the quantum Jarzynski equality with a trapped-ion system, *Nat. Phys.* **11**, 193 (2015).

[94] Dechant A., Kiesel N. and Lutz E., All-Optical Nanomechanical Heat Engine, *Phys. Rev. Lett.* **114**, 183602 (2015).

[95] Correa L.A., Palao J.P., Alonso D. and Adesso G., Quantum-enhanced absorption refrigerators., *Sci. Rep.* **4**, 3949 (2014).

[96] Brandner K., Bauer M., Schmid M.T. and Seifert U., Coherence-enhanced efficiency of feedback-driven quantum engines (2015), `arXiv:1503.04865v1`.

[97] Mitchison M.T., Woods M.P., Prior J. and Huber M., Coherence-assisted single-shot cooling by quantum absorption refrigerators (2015), `arXiv:1504.01593v1`.

[98] Rossnagel J., Abah O., Schmidt-Kaler F., Singer K. and Lutz E., Nanoscale heat engine beyond the carnot limit, *Phys. Rev. Lett.* **112**, 030602 (2014).

Danksagung

Zum Ende dieser Arbeit möchte ich mich herzlich bei allen bedanken, die ihr Entstehen ermöglicht und unterstützt haben.

Zunächst geht hierbei natürlich ein großer Dank an Herrn Professor Seifert, der mich nicht nur an seinem Institut aufgenommen und mir damit die Bearbeitung eines spannenden Themas ermöglicht hat, sondern es auch geschafft hat, in unzähligen Diskussionen immer wieder aufs Neue meine Begeisterung für die Wissenschaft zu wecken und zu bestärken.

Außerdem möchte ich mich sehr bei Herrn Professor Saito bedanken, der mir viele wichtige Impulse für meine Arbeit gab und mir eine wunderbare und wissenschaftlich erfolgreiche Zeit in Japan ermöglicht hat.

Weiterhin danke ich Herrn Professor Dietrich und Herrn Professor Lutz für die Übernahme und schnelle Anfertigung der Mitberichte.

Ein weiteres Dankeschön geht an Frau Steinhauser für die liebevolle Unterstützung in allen organisatorischen Belangen, sowie an alle Mitarbeiter des II. Instituts für Theoretische Physik für eine stets angenehme und kollegiale Arbeitsatmosphäre.

Schließlich gilt mein ganz besonderer Dank meinen Eltern, die mich über viele Jahre hinweg moralisch und materiell unterstützt haben, mir mein Studium ermöglichten und mir in jeder Lebenslage sicher und bedingungslos zur Seite standen. Auch möchte ich meinen Großeltern sehr für Ihre jahrelange und großzügige Unterstützung danken.

Ehrenwörtliche Erklärung

Ich erkläre, dass ich diese Arbeit selbstständig verfasst und keine anderen als die angegebenen Quellen und Hilfsmittel benutzt habe.

Stuttgart, 22. Juli 2015 Kay Brandner